AN INTEGRATED GEOCHEMICAL APPROACH FOR DEFINING SOURCES OF GROUNDWATER SALINITY IN THE SOUTHERN RIO GRANDE VALLEY OF THE MESILLA BASIN, NEW MEXICO AND WEST TEXAS, USA

BY

Christopher Kubicki B.S.

A dissertation submitted to the Graduate School

in partial fulfillment of the requirements

for the degree

Masters of Science

Major Subject: Water Science and Management

Concentration: Watershed, Riparian, and Aquatic Systems

NEW MEXICO STATE UNIVERSITY

LAS CRUCES, NEW MEXICO

May 2019

Christopher W. Kubicki

Candidate

Water Science and Management

Major

This Thesis is approved on behalf of the faculty of New Mexico State University, and it is acceptable in quality and form for publication:

Approved by the thesis Committee:

Dr. Kenneth C. Carroll

Chairperson

Dr. Frank Ramos

Committee Member

James C. Witcher

Committee Member

DEDICATION

I would like to dedicate this thesis to my family.

ACKNOWLEDGEMENTS

The New Mexico Water Resource Research Institute and U. S. Bureau of Reclamation are gratefully acknowledged for their support and funding of this project. I would also like to thank Dr. Shari Kelley (NMTech), Dr. Virgil Lueth (NMTech), Dr. Laura Crossey (UNM), and Dr. John Hawley for their contributions. I would like to thank Andrew Robertson of the USGS and the USGS personnel who helped with the collection and interpretation of data. I would like to thank Dr. Jeff Pepin (USGS) for his assistance in sampling and the interpretation of temperature logs. Thank you, James C. Witcher, for your guidance throughout my graduate studies, you have been an invaluable resource for this project. Thank you, Dr. Frank Ramos, for deepening my understanding of isotopes and geology. Thank you, Dr. Kenneth C. Carroll, for your substantial investment of time and resources into this project and myself, I am grateful to have been given the opportunity to work on this project. Also thank you to my research cohort, it's been a pleasure working with each of you.

VITA

Education

New Mexico State University, Las Cruces, NM

Master of Science, Water Science and Management, August 2019

Montana State University, Bozeman, MT
Bachelor of Science, Environmental Science, May 2016

Employment Information

Research Assistant- June 2017 to Present
New Mexico State University— Las Cruces, NM and Oak Ridge, TN

-Sampling groundwater and analyzing noble gas isotopes in groundwater to determine residence times

-Collaborating with the USGS and Argonne National Laboratory

-Conducting tracer tests at a field site in eastern Tennessee under the supervision of Oak Ridge National Laboratory

Teaching Assistant for SOIL 477, Soil 472, and ES 110- August 2017 to December 2018
New Mexico State University— Las Cruces, NM

-Taught an Environmental Soil Physics (477) laboratory section to seniors and graduate students

-Improved students understanding of darcy's law, soil water content, wilting point, etc. through guided labs

-Assisted in the instruction of Soil Morphology (472) by helping students characterize soil pits
-Taught a laboratory section of Introduction to Environmental Science (110) to freshman and sophomores

Clinical Technician- September 2016 to May 2017
BioScience Laboratories —Bozeman, MT

-Conducted clinical studies which test antimicrobial products seeking FDA approval

-Guided subjects through study procedures

Wetland Soils and Hydrology Technician- May 2016 to August 2016
Montana DEQ – Helena, MT

-Preformed rapid and intensive wetlands assessments based on the Army Corps of Engineers protocol

-Utilized GPS and GIS technology

Soil Science Intern GS-4- May 2015 to Aug 2015
NRCS – Sonora, CA

-Entered pedon data into a national soils data base (Pedon PC)

-Classified pedons in the field

-Colored, measured pH, and weighed soil samples in the laboratory

Laboratory Assistant- May 2013 to Aug 2013
Montana State University – Bozeman, MT

-Collected soil and wheat samples in the field

-Tested samples for nitrate and phosphate levels

Abstract

Spatial variability in sources of groundwater salinity may exist due to stratigraphic, geochemical, and hydrologic processes even in an integrated and relatively homogeneous aquifer system. For this reason, characterization methods are needed to determine salinity sources, flow, and transport in alluvial/fluvial groundwater basins. Geochemical tracers analyzed from groundwater samples were used to determine the sources of salt contributing to groundwater beneath the southern Rio Grande flood plain of the Mesilla basin located in southern New Mexico and west Texas. Results from southern Mesilla Valley groundwaters show a localized plume of saline groundwater (10,000-29,700 mg/L total dissolved solids) near Sunland Park, NM. $\delta^{34}S$ signatures of groundwater within the plume (+12.36 to +12.46‰) are comparable to $\delta^{34}S$ signatures of Permian gypsum (+12.5‰) suggesting prolonged contact between groundwater and underlying Paleozoic bedrock. Above atmospheric concentrations of ^{39}Ar (132-134% pM) and ^{4}He (10^{-6} to 10^{-7} ccSTP/g(H_2O)) in groundwater from the plume, confirm a significant fraction of the groundwater is old (>1,000 years). North of Sunland Park, NM, decreasing groundwater salinity is coexists with a spatial transition from sedimentary to volcanic rock underlying the alluvial aquifer, increasing alluvial sediment thickness, and $\delta^{34}S$ signatures of groundwater (+2.28 to +5.76‰) which cannot originate from Paleozoic bedrock. These results suggest a decreased influence of upward flow from sedimentary bedrock and increased dilution of brackish groundwater within the lower salinity alluvial aquifer in the central and northern Mesilla Valley. This study illustrates how nested well clusters and geochemical tracers can be used to identify salinity sources and processes in geochemical investigations.

Key-Words: Age Dating, Aqueous Geochemistry, Argon, Evaporite Minerals, Groundwater.

TABLE OF CONTENTS

LIST OF TABLES

LIST OF FIGURES

1.0 Introduction

Salinization of aquifers in arid regions is a growing issue due to increased water use as a result of population growth and increased agricultural demands (Szynkiewicz et al., 2011). Salinization studies typically address the location of high salinity areas, changes in salinity through time and space, and the sources of salinity identified using isotopic and geochemical tracers (Moyer et al., 2013). Salinization is generally attributed to solute additions from anthropogenic or lithologic sources and/or evaporative processes in arid environments (Hogan et al., 2007). While temporal increases in groundwater salinity are easily observable, characterizing the sources of salinity and the spatial distribution of salinity sources across an aquifer system proves more difficult (Szynkiewicz et al., 2015; Teeple, 2017). Issues arise due to (1) data gaps caused by the irregular distribution of wells throughout an aquifer and (2) difficulty discerning between sources of groundwater salinity, which often overlap in geochemical signatures (Land, 2016; Witcher et al., 2004). Geophysical approaches, which attempt to map salinity in groundwater with electrical resistivity or electro-magnetic methods in areas where groundwater data is unavailable, often fail to differentiate between high salinity groundwater and high electrical conductivity subsurface materials such as clay and evaporites (Teeple, 2017) or are unsuitable to use due to electrical interference in highly developed urban areas. Uncertainty over groundwater salinity sources, distribution of salt in groundwater, and groundwater flow/transfer processes can interfere with mitigation efforts to prevent continued salinization of useable and available ground and surface water (CH2MHill, 2013). In addition, mixing between groundwater, geothermal waters, and surface water, can lead to further uncertainty when attempting to quantify the sources of salt in groundwater (Hogan et al., 2007; Moyer et al., 2013; Szynkiewicz et al., 2011; Witcher et al., 2004).

Commonly, lithological chemical analysis is not done in conjunction with geochemical investigations of groundwater (e.g., Hiebing et al., 2018; King and Hawley, 1975; Teeple, 2017; Williams et al., 2013; 2015). As a result, the mass transfer of salt between lithology and groundwater is poorly defined. Assumptions regarding groundwater-rock interactions tend to dictate conclusions regarding dissolution of minerals, mixing, and groundwater flow paths of high salinity groundwater. In order to prevent further salinization of valuable arid water resources and to validate groundwater salinization processes, the characterization of salt in groundwater and lithology is necessary.

2.0 Problem

Anomalously high salinity groundwaters have been identified near the Paso Del Norte at the southern end of the Mesilla Valley (CH2MHill, 2013; Teeple, 2017). A distribution of wells concentrated within the shallow alluvial aquifer has resulted in data gaps throughout the deeper components of the southern Mesilla Valley (Land, 2016). Consequently, the source(s), flow path(s), and mixing relationships of high salinity groundwater near the Paso Del Norte is not well understood. Recharge to-and-from the Rio Grande has resulted in additional uncertainty when accessing flow paths and sources of these high salinity groundwaters. A series of well nests or piezometers allow for the documentation and evaluation of water quality, flow path(s), and source(s) of salinity of waters located beneath the Rio Grande. This is a unique opportunity to document groundwater salinization processes near the Rio Grande proper in the Mesilla basin from north to south.

Sources of salinity and mixing of groundwaters were observed using $\delta^{34}S$ isotopes, major cation and anion data, and stable hydrogen and oxygen data for water ($\delta^{18}O$, $\delta^{2}D$). Then analysis

for $\delta^{34}S$ isotopes from various rock formations, X-Ray Diffraction (XRD) of well cuttings, and past research on the Mesilla basin stratigraphy were used to formulate a more comprehensive understating of the relationship between salt dissolution and groundwater flow. Plausible dissolution scenarios between salinity sources and groundwater were evaluated using age dating isotopes (^{85}Kr, ^{81}Kr, ^{39}Ar, ^{3}H, ^{3}He, ^{4}He, and ^{14}C), geochemical modeling, and temperature logs.

3.0 Previous Studies

Sources of groundwater salinity in the southern Mesilla Valley have been examined using geochemical tracers (CH2MHill, 2013; Hiebing et al., 2018; Szynkiewicz et al., 2011; Teeple, 2017; Witcher et al., 2004) and geophysics (Teeple, 2017). Major salinity sources have been attributed to irrigation (Sheng, 2013), evaporite minerals in the lower and middle Santa Fe Group (Hiebing et al., 2018), and shallow evaporite brines (Szynkiewicz et al., 2015). Others have suggested topographically driven groundwater flow, a concept originally described by Toth (1963), is responsible for the higher salinity groundwater located near the Paso Del Norte (Hawley and Kennedy, 2004; Hogan et al., 2007; Phillips et al., 2003; Witcher et al., 2004). In this hypothesis, deep regional flow sweeps up or accumulates ions and increases in temperature along its flowpath and is forced into the shallow alluvial aquifer at the topographically lowest point and discharge location in a groundwater basin. A subset of this concept includes inputs from outflow of structurally-controlled geothermal systems that provide recharge to Mesilla Basin groundwater (Witcher et al., 2004). The Paso Del Norte is the discharge location for most groundwater in the Mesilla basin alluvial aquifer (Hawley and Kennedy, 2004; Teeple, 2017; Witcher et al., 2004). Topographically-driven groundwater flow has been shown to be representative of groundwater flow in other Rio Grande rift basins where terminal bedrock

constrictions force deep groundwater towards the surface and Rio Grande (Phillips et al., 2003; Williams et al., 2013). Previous research is unclear whether fluid migration through rift-bounding faults (Williams et al., 2013) or basin aquifers dominate the salinity input process (Phillips et al., 2003). Tracers commonly utilized for groundwater age dating (Tritium and carbon-14 (^{14}C)) within the Mesilla basin ha been unable to characterize flow paths due to short half-lives (Tritium) or carbonate interference (^{14}C; Teeple, 2017).

Noble gas radioisotopes can provide complementary chronometric and geochemical source and mixing information to groundwater investigations, but have not been previously explored in the Mesilla basin (Yokochi et al., 2013). Because noble gases are inert, corrections for geochemical processes are generally not necessary (Clark and Fritz, 1997). The noble gas isotopes krypton-81 (^{81}Kr), krypton-85 (^{85}Kr), and argon-39 (^{39}Ar) have been shown to be effective in determining flow paths of groundwater in other arid regions (Mace et al., 2017; Zappala, 2017).

4.0 Geologic and Hydrogeologic Setting

Designated well categories are north, central, and southern. North wells are located within the Mesilla Valley north of Vado, NM. Central wells are located in the Mesilla Valley between Anthony, NM and Vado, NM. Wells located to the south of Anthony, NM in the Mesilla Valley are identified as southern wells. Wells located outside the Mesilla Valley are labeled according to their geographical location (Fig. 1). For example, the Afton Power Plant well is located on the West Mesa of the Mesilla Basin and Well 68 is located in the Jornada Del Muerto Basin (Fig. 1). Additional references are made to the ISC-4 plume, an area of high salinity groundwater encountered by the ISC-4 well cluster near the Paso Del Norte. References to the “alluvial aquifer”

are used for the Santa Fe Group aquifer and inset Rio Grande fluvial deposits within the Mesilla Valley when discussing both aquifers as a composite or single integrated aquifer system.

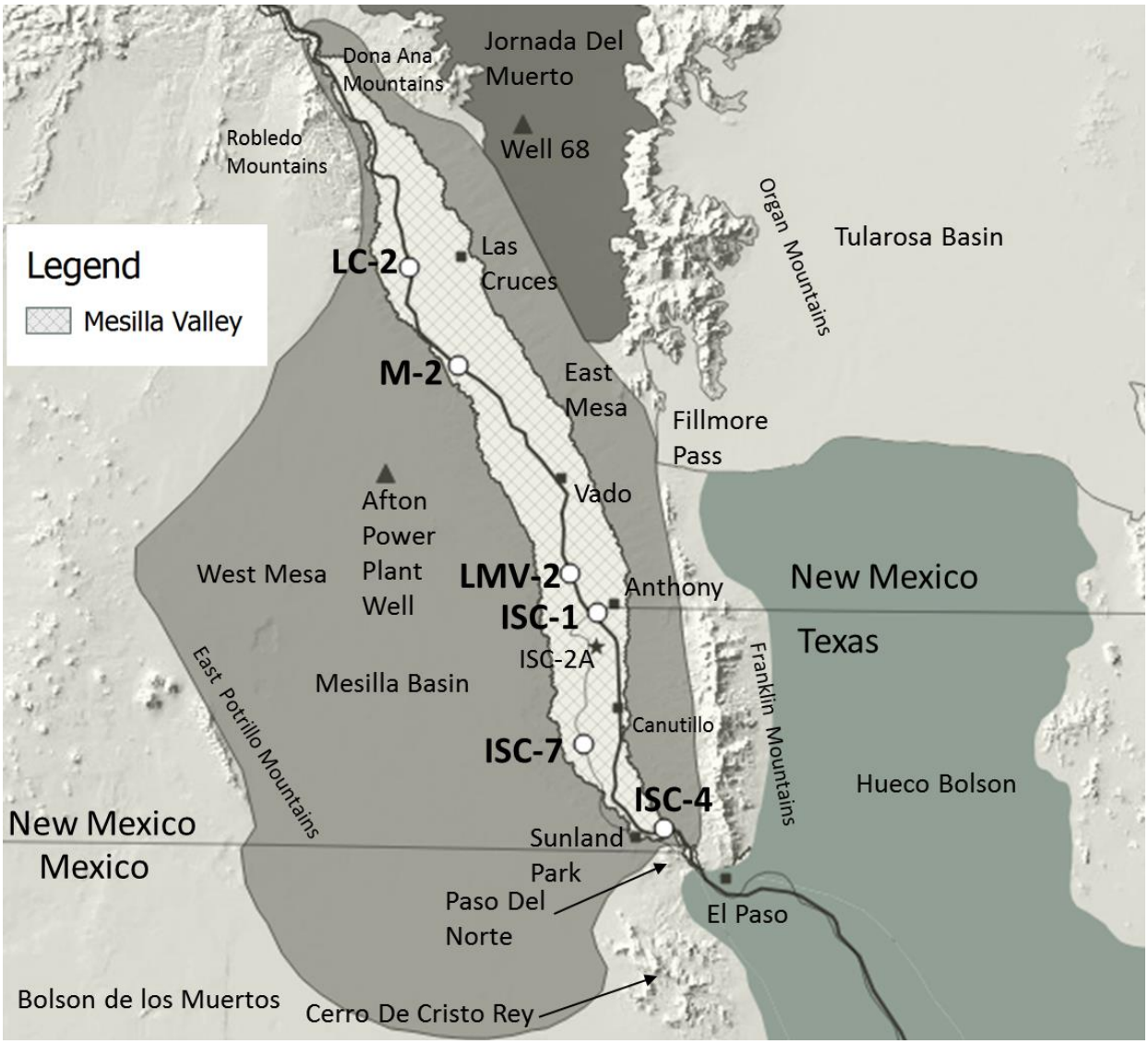

Figure 1. Study area showing sampling locations. Well clusters (shown as white circles) were sampled for ^{39}Ar ,^{81}Kr, and ^{85}Kr, temperature logs, and standard USGS water chemistry parameters (Appendix A). Individual wells sampled for ^{39}Ar ,^{81}Kr, and ^{85}Kr and standard USGS water chemistry parameters marked by black triangles. Individual wells sampled only using temperature logs are shown as black stars.

The Mesilla Valley, the flood plain of the present-day Rio Grande and its inset fluvial sediments, are hydrologically connected to the Santa Fe Group aquifer system in the surrounding Mesilla basin. Santa Fe Group deposition in the Mesilla basin is defined by local structure of the Rio Grande rift. The Mesilla basin is located in the southern Rio Grande rift. The Rio Grande rift extends from central Colorado across central New Mexico into west Texas and northern Chihuahua, Mexico (Hawley et al., 2001). Like other Rio Grande rift basins, the Mesilla basin trends from north to south and mountains flanking the east and west sides act as structural and hydrologic boundaries (Hawley et al., 2001). Major structural components include large subbasins to the east, southwest, and northwest, a buried mid-basin uplift, and a south-central basin that extends into northern Mexico west of the Cerro De Cristo Rey uplift (Hawley and Lozinsky, 1992). High-angle normal faults block out the various subbasins and uplifts (Hawley and Kennedy, 2004). Faulting of the Mesilla basin began during the Oligocene and continues into the present (Hawley and Kennedy, 2004). This deformation along with glacial-interglacial cycles have played an important role in sedimentation processes within the Mesilla basin (Hawley and Lozinsky, 1992; Witcher et al., 2004).

Tertiary to Quaternary sands and gravels of the Santa Fe Group form the primary basin-fill aquifer of the Mesilla basin (Hawley et al., 2001). The Santa Fe Group is generally semi-confined, but in some locations unconfined (Nickerson and Myers, 1992). Hawley and Kennedy (2004) informally subdivide the Santa Fe Group into lower, middle, and upper hydrostratigraphic units or aquifers, which consist of up to 762 m of alluvial and fluvial sediments overlying bedrock (defined as basal rock formations with low permeability; Hawley and Kennedy, 2004). Groundwater production potential and hydraulic conductivity generally decrease with depth within Santa Fe subgroups (Hawley et al., 2001). Most upper Santa Fe lithofacies have horizontal hydraulic

conductivities between 5 and 30 m/day. In comparison, lower Santa Fe lithofacies have horizontal hydraulic conductivities of less than 1 m/day (Hawley et al., 2001). Flow is generally horizontal within the Santa Fe Group due to low vertical hydraulic conductivities (ranging from less than 0.1 m/day to 1 m/day; Frenzel and Kaheler, 1992). Santa Fe Group subdivisions approximately correspond with transitions between formally designated formations and depth. For example, the Camp Rice Formation is considered the predominant lithofacies of the Upper Santa Fe, the Fort Hancock Formation and Rincon Valley Formations are the predominant lithofacies of the middle Santa Fe, and the Hayner Ranch Formation is the main lithofacies of the lower Santa Fe (Hawley et al., 2001; Hawley and Kennedy, 2004; Witcher et al., 2004).

Late Pleistocene to recent fluvial inset Rio Grande deposits, 15 m to 38 m in thickness, form a smaller alluvial aquifer that overlies the Santa Fe Group within the Mesilla Valley (Hawley, 1984; Land, 2016; Wilson et al., 1981). High energy fluvial systems during the late Pleistocence glacial episodes caused valley entrenchment (Hawley and Kennedy, 2004). Successive backfilling during inter-glacial episodes by the Rio Grande provide the shallow fluvial aquifer beneath the valley flood plain (Hawley and Kennedy, 2004). Inset Rio Grande fluvial deposits are largely unconfined and recharged by the Rio Grande and underlying Santa Fe Group (Nickerson and Myers, 1993).

Pre-Santa Fe Group rock formations define aquifer boundaries, but may transmit water through deep regional flow paths (Hawley and Kennedy, 2004). Generally, low permeability Eocene and Oligocene volcanic and volcaniclastic rocks underlie the Santa Fe Group throughout the central and northern Mesilla basin. Near the town of Canutillo, Texas, Tertiary volcanic and volcaniclastic rocks are missing and Santa Fe Group sediments overlie Eocene-Paleocene sedimentary rocks, sandstones, mudstones and conglomerates (Hawley et al., 2018). An additional

transition is observed just south of Canutillo, Texas where Santa Fe Group sediments rest unconformably on Cretaceous limestone, shales, and sandstones (Hawley et al., 2018). The Cretaceous formations rise to the land surface effectively pinching out the Santa Fe Group just south of Sunland Park, NM (Hawley et al., 2018). Several andesite intrusions rupture Cretaceous units in the southern Mesilla Valley. The largest of these andesite intrusions is Cerro de Cristo Rey (Lovejoy, 1976; Lucas et al., 2010). A smaller andesite intrusion sits below Sunland Park, NM (Hawley et al., 2018). Andesite intrusions and Cretaceous units may be highly fractured and provide possible conduits for upward leakage of deep regional flow (Witcher et al., 2004).

Groundwater within the alluvial aquifer of the Mesilla basin primarily flows from northwest to south-southeast where it is discharged at the Paso Del Norte into the Rio Grande (Hawley et al., 2001; Teeple, 2017). Increased Rio Grande salinity near the Paso Del Norte suggests higher salinity groundwater at the Paso Del Norte is discharged into the river where Cretaceous bedrock rises to the land surface (Hogan et al., 2007). Groundwater elevation contour maps suggest some flow may originate from the Conejos-Medanos subbasin of the Mesilla basin in northern Mexico and flow northwest into the southern Mesilla Valley (Hawley and Kennedy, 2004; IBWC, 2011).

Groundwater geochemically evolves between recharge and discharge in the Mesilla basin (Witcher et al., 2004). Recharge to the Mesilla basin aquifer system primarily occurs in the Mesilla Valley along losing reaches of the Rio Grande and irrigation canals, with smaller contributions of water from mountain front recharge (Frenzel and Kaehler, 1992; Teeple, 2017; Witcher et al., 2004). In mountain front recharge areas, TDS is low (<250 mg/L) and characterized by dominate ions of Ca, Mg, and HCO_3 (Witcher et al., 2004). Recharge from the reach of the Rio Grande within the study area has a slightly greater TDS (400-1,200 mg/L) and retains an Na-Cl-SO_4 water

type (Moyer et al., 2013). Evaporative processes and upwelling of geothermal water can lead to elevated concentrations of dissolved solids (>2,000 mg/L) along agricultural drains; recharge from these drains often leads to elevated concentrations of dissolved ions in the shallow subsurface (Witcher et al., 2004; CH2MHill, 2013).

Once surface water has infiltrated, water-rock interactions and/or mixing may change the chemical composition of the water (Faure, 1998). Evaporative minerals gypsum and anhydrite are present in sediments within the alluvial aquifer and contribute Na, Cl, SO_4, and Ca into solution (Witcher et al., 2004). When halite dissolves, Na and Cl are released in a 1:1 manner. Generally southern Mesilla basin groundwaters are enriched in Na in comparison to Cl, suggesting additional processes are contributing Na. Cation exchange and/or dissolution of feldspars are also likely responsible for the addition of Na to groundwater (Plummer et al., 2004; Teeple, 2017; Witcher, et al., 2004). Elevated concentrations of trace ions, Cl, K, and SiO_2 are often associated with geothermal water, although elevated concentrations of these ions are also reported in evaporate mineral deposits (Witcher et al., 2004). Waters with elevated concentrations of trace ions are observed in the southern Mesilla basin, near the East Potrillo Mountains, and along the Mesilla Valley fault zone near Tortugas mountain (Anderholm, 1992; Doremus and Michelsen 2008; Witcher et al., 2004). It should be noted that cold water dissolution of feldspars may also add K and SiO_2 into solution (Witcher et al., 2004).

5.0 Methods and Approach

Groundwater samples were collected from nested wells; characterized by negligible lateral distance between boreholes and significant vertical variation between screen elevations. Selected well nests represent local piezometers along the Rio Grande in the Mesilla Valley and

offer insight into hydrogeochemical and hydraulic head changes vertically in the subsurface at each nest. Comparisons between the isotopic and geochemical composition of Mesilla Valley groundwaters in the well or piezometer nests provide a basis to identify and interpret flow paths, mixing, and salinity variations. Known sources of salinity (rock formations, surface water, other groundwater) were used to characterize sources, flow paths, and mixing relationships of these high salinity groundwaters. Several samples were collected from wells located on the West Mesa and the Jornada del Muerto basin to supplement data interpretation (Fig. 1).

A suite of groundwater parameters was measured from select wells (Fig. 1; Table 1.; Appendix A). Field sampling techniques were completed in accordance to the methodology described in the USGS field manual (U.S. Geological Survey, variously dated; Appendix C.). Dissolved gas samples were also collected from select wells and analyzed for radionuclides ^{39}Ar, ^{85}Kr, and ^{81}Kr (Fig. 1; Table 1.; Appendix C.).

Table 1. Table showing sample parameter and analytical methods used.

Parameter	**Analytical Method**
Major Ions	Fishman and Friedman (1989) and Fishman (1993)
Trace Ions	Fishman and Friedman (1989), Garbarino (1999), and Garbarino et al. (2006)
$\delta^{2}D$	Révész and Coplen (2008A)
$\delta^{18}O$	Révész and Coplen (2008B)
$\delta^{13}C$	Vogel et al. (1987)
^{14}C	Roberts et al. (2010)
$^{87}Sr/^{86}Sr$	Kendall and McDonnell (1998)
^{3}H	Östlund et al. (1969) and Östlund et al. (1974)
Uranium Isotopes (^{238}U, ^{234}U, ^{235}U)	Section on Alpha Spectrometry (Tucker and Workman, 2013)
Dissolved Gas Concentrations (O_2, CO_2, Methane, and N_2)	Hunt (2015)
Noble Gas Concentrations (Kr, Xe, N_2, ^{4}He, Ne, Ar)	Hunt (2015)
Noble Gas Isotope Ratios ($^{3}He/^{4}He$, $^{20}Ne/^{22}Ne$, $^{40}Ar/^{36}Ar$, $^{86}Kr/^{84}Kr$, $^{130}Xe/^{132}Xe$)	Hunt (2015)
^{85}Kr	Atom Trap Trace Analysis (ATTA; Argonne National Lab) reported in Jiang et al. (2012) and Zappala (2017). Low Level Counting (LLC; University of Bern) reported in Du et al. (2003)
^{81}Kr	ATTA in Jiang et al. (2012) and Zappala (2017).
^{39}Ar	LLC in Loosli (1983)
$\delta^{34}S$ of Gypsum	Preparation of $BaSO_4$ covered in Szynkiewicz et al. (2011). Analysis of $BaSO_4$ covered in Kelly et al. (2018)
X-Ray Diffraction	Medville (2018)

The USGS PHREEQC speciation program version 3.3.12 (Parkhurst and Appelo, 2013) allowed speciation of saturation indices between water solutions and solid minerals and was used to interpret water-rock interactions along groundwater flow paths. Results were compared to geochemical analysis techniques including Piper diagrams (Piper, 1944) and isometric log ratios (Engle and Rowan, 2012). These results were used to determine sources of groundwater salinity and/or salinization processes within nested well clusters throughout the Mesilla Valley.

X-Ray Diffraction (XRD) analyses of gypsum and halite were used to evaluate the presence of evaporite minerals near screened intervals of two well nests (Appendix C.). Two samples were selected from well cuttings of a central Mesilla Valley borehole (LMV-2), and five samples were selected from well cuttings from a southern Mesilla Valley well (ISC-4B). Other minerals were also identified, but not quantified.

To identify sources of dissolved sulfate in groundwater, $\delta^{34}S$ of gypsum was sampled and analyzed from the Miocene Rincon Valley Formation, Cretaceous Mesilla Valley Formation, and Lake Lucero. Gypsum samples are representative or originate from several hydrogeological units within the Mesilla basin: the Santa Fe Group basin fill (the Miocene Rincon Valley Formation), Cretaceous Shales, Sandstones, and Limestones (Mesilla Valley Formation), and deeper Paleozoic units (Lake Lucero). Results were compared to previously collected $\delta^{34}S$ of dissolved sulfate in Mesilla basin groundwaters and surface waters; initially collected to investigate anthropogenic sources of dissolved sulfate within the Rio Grande (Szynkiewcz et al., 2011).

The vertical component of local groundwater flow within well nests was observed using temperature logs. A vertically flowing groundwater component may systematically change the conductive temperature gradient via convective heat transport (Bredehoeft and Papadopulos, 1965). These changes in the natural temperature gradient can be observed and quantified to

determine velocities of vertical groundwater flow as upflow (discharge) or as downflow (recharge). Temperature profiles were measured from the deepest well within the various well clusters and also ISC-2A to determine vertical direction of flow (Appendix B). Detailed methods and data analysis techniques are reported in Appendix C.

6.0 Results

6.1 Sources of Recharge

Groundwater recharge is characterized with $\delta^{18}O$ and $\delta^{2}D$ by comparing to the Global Meteoric Water Line (GMWL; Craig, 1961) and the Rio Grande Evaporation Line (RGEL; Phillips et al., 2003). The RGEL relationship indicates evaporation processes such as pooling of water behind the Elephant Butte and Caballo Dams, evapotranspiration in the floodplain and return flows of drainage canals, and a warmer and dryer Holocene climate, resulting in a heavy $\delta^{18}O$ isotopic signature of the modern Rio Grande (Phillips et al.,2003; Teeple, 2017; Witcher et al., 2004; Fig. 2.). Nearly all of the groundwater samples from the Mesilla Valley fall along the RGEL and indicate that infiltration of river water as the predominant source of recharge for groundwater. Wells screened at lengths below land surface elevation (BLS) between 0 and 45 m have significantly heavier $\delta^{18}O$ (-7.7 to -8.47) than wells screened below 122 m (-11.29 to -11.83). The heavier signature from wells screened between 0 and 45 m implies more recent recharge from the Rio Grande. Wells screened below 122 m have lighter δD and $\delta^{18}O$ and plot between -12.5 and -10.5 $\delta^{18}O$ and may indicate the aquifer below 122 m depth has a high component of recharge from the Rio Grande during the cooler periods of the Pleistocene (Teeple, 2017). Wells screened between 45-122 m have intermediate signatures (-7.69 to –11.96 $\delta^{18}O$) and may indicate mixing between old and young groundwaters. Teeple (2017) noted that

precipitation in Santa Fe, NM; El Paso TX; and Ciudad Juárez, Chihuahua plot along the GMWL. Samples, ISC-7B and ISC-4A, which plot closer to the GMWL, may indicate a component of storm or arroyo runoff into the Rio Grande.

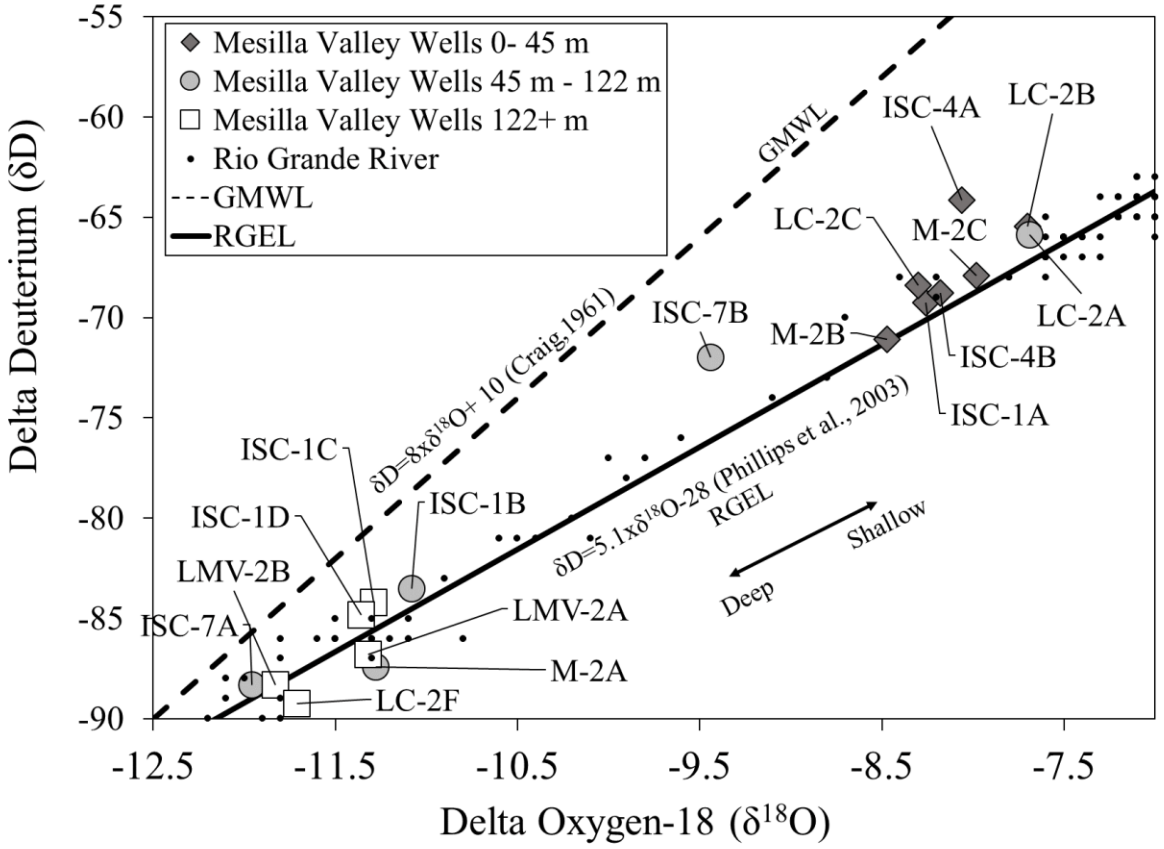

Figure 2. $\delta^{18}O$- $\delta^{2}D$ diagram showing the stable isotope composition of groundwater and the Rio Grande in the Mesilla Valley.

6.2 Sources of Groundwater Salinity

Isometric log ratios (ILR; See Appendix C. for a short discussion on ILR) for the molar compositions of Ca, Cl, Na, and SO_4 (Fig. 3) show southern Mesilla Valley groundwaters trend towards evaporite mineral equilibrium with increasing salinity and also exhibit Na-Ca cation exchange in groundwater. In northern Mesilla Valley groundwaters, there is a similar shift

towards evaporate mineral equilibrium in higher TDS groundwater, but the overall TDS of northern Mesilla Valley waters is much lower (< 1,000 mg/L). Most groundwater samples are enriched in Na relative to Cl, shown by a positive ILR balance on the X-axis in Fig. 3. Significant increases in Na are often associated with dissolution of silicate minerals, calcite dissolution, and/or cation-exchange (Teeple, 2017; Witcher et al., 2004). Such processes may be occurring within groundwaters screened at ISC-7A, which plots furthest to the right (Fig. 3).

Southern and central Mesilla Valley groundwaters are enriched in SO_4 in relation to Ca as shown by negative ILR balance of the Y-axis in Figure 3. Witcher et al. (2004) noted the enrichment of SO_4 in relation to Ca is probably caused by the common ion affect, where dissolution of gypsum results in the precipitation of calcite ($CaCO_3$), removing excess Ca from solution. Dissolution of gypsum in southern Mesilla Valley waters probably results in precipitation of calcite and saturation indices indicate most groundwaters throughout the Mesilla Valley are oversaturated with respect to calcite (Table 2.). Ca is enriched in relation to SO_4 in northern Mesilla Valley groundwaters, which is likely due to the waters being undersaturated with gypsum.

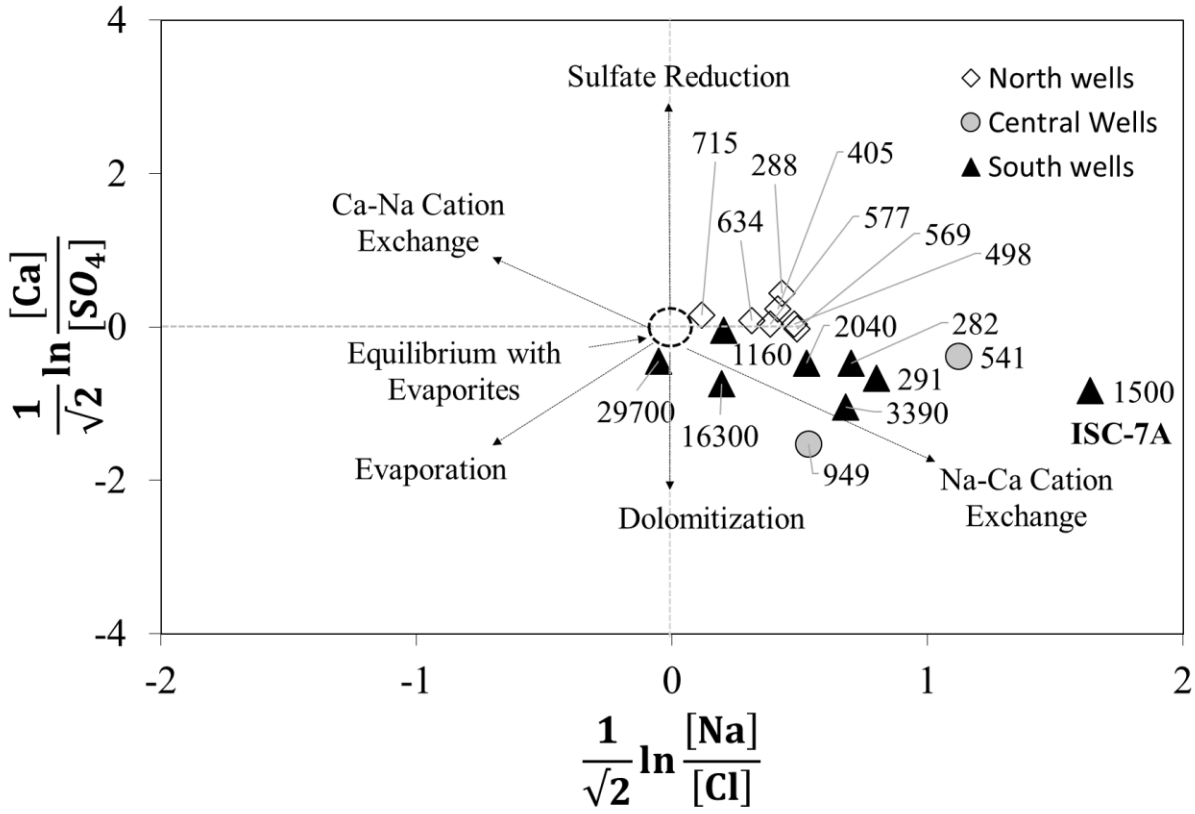

Figure 3. Isometric log ratio (ILR) diagram showing the molar compositions of Ca, Cl, Na, and SO_4 (Engle and Rowan, 2012). Increasing proximity towards the center of the diagram indicates groundwater equilibrium with evaporate minerals. Values indicate total dissolved solids (TDS) in mg/L.

An ILR plot of the molar compositions Ca, Cl, Na, and Br (Fig. 4) shows similar results as Figure 3. Southern Mesilla Valley groundwaters are enriched in Na and Cl relative to Br shown by a positive ILR balance on the X-axis (Fig. 4). Significant enrichments in Na and Cl in relation to Br indicate contribution from halite dissolution (Engle and Rowan, 2012; Figure 4.). Northern Mesilla Valley waters are less enriched in Cl and Na relation to Br in comparison to southern wells, indicating less influence from evaporate mineral dissolution (Fig. 4). As noted by Davis et al. (1998), Br ions are too large to fit within the crystal lattice of halite; consequently, dissolution of halite will not contribute Br into solution (Davis et al., 1998).

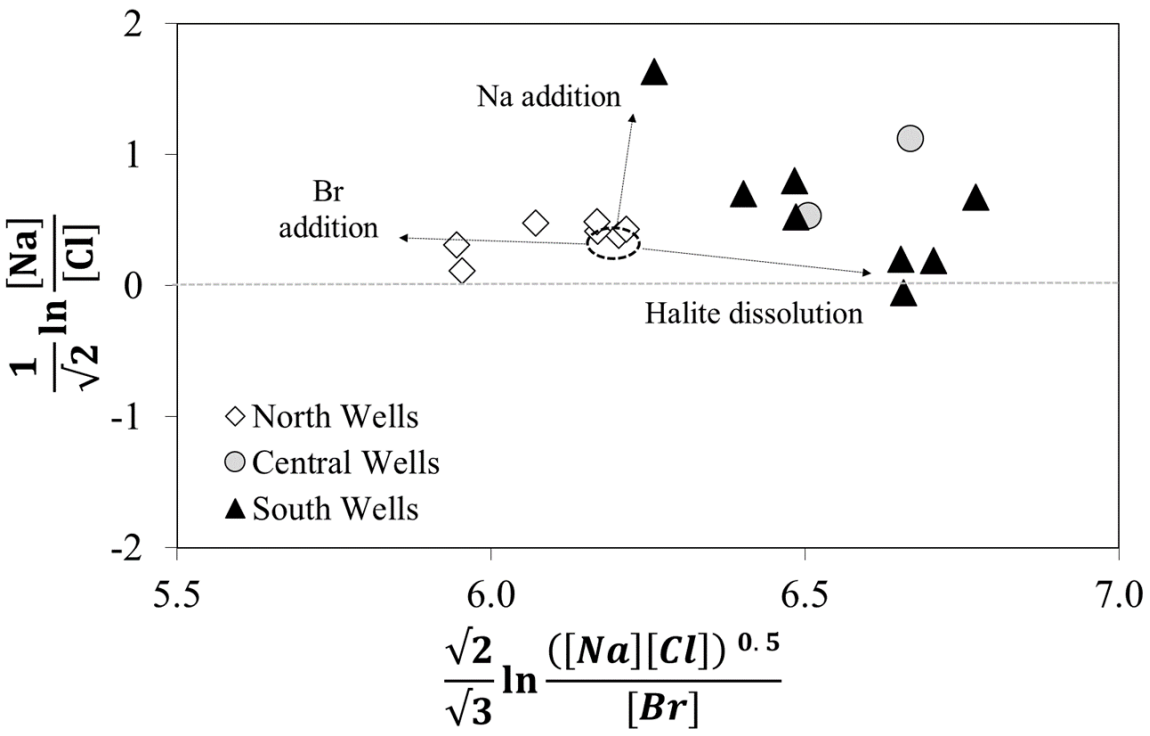

Figure 4. Isometric log ratio (ILR) diagrams (Engle and Rowan, 2012) illustrating halite dissolution in southern Mesilla Valley groundwaters. Northern Mesilla Valley groundwaters are less influenced by halite than southern Mesilla Valley groundwaters, shown by lower ILR balance values on the X-axis.

$^{3}He/^{4}He$ signature of groundwater (R) in ISC-7 wells are elevated relative to the $^{3}He/^{4}He$ fraction of the atmosphere (Ra) indicating leakage from the mantle (R/Ra ratio greater than 1; Williams et al., 2013; Fig. 5). Elevated R/Ra ratios are observed near fault zones that are sometimes associated with thermal waters in the Albuquerque Basin of central New Mexico, supporting a fault zone in the vicinity of the ISC-7 wells (R/Ra values >1 of ISC-7 groundwater samples; Williams et al., 2013). Elevated He/Ne ratios likely indicate older ages in the ISC-7 wells. He concentrations accumulates over time in the subsurface due to magmatic derived He and more importantly radiogenic decay of U and Th in various rock formations, while Ne does

not (Kendall and McDonnell, 1998; Williams et al., 2013). In wells ISC-4A, ISC-4B, and LMV-2B, R/Ra ratios less than 1 and elevated He concentrations compared to Ne indicate prolonged contact between groundwater and rocks rich in U, Th, and K (Clark and Fritz, 1997).

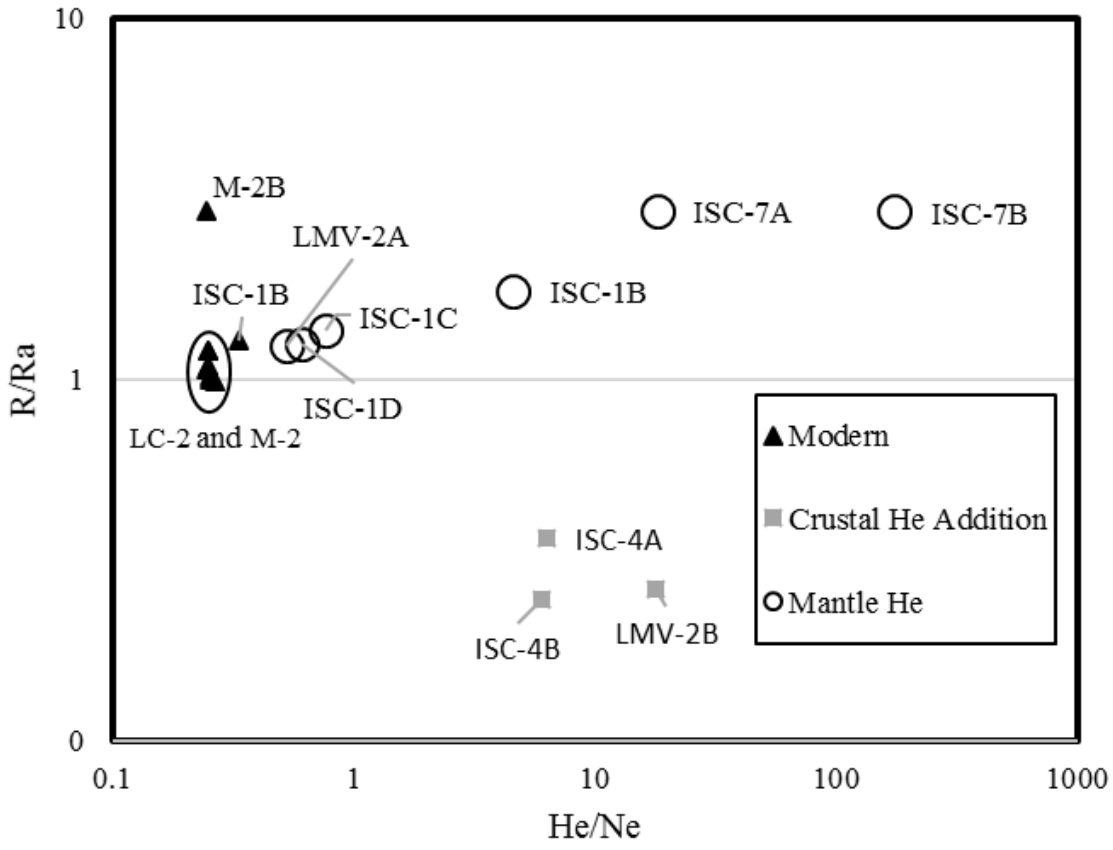

Figure 5. Diagram showing helium ratios of Mesilla Valley wells compared to He/Ne ratios. Elevated $^{3}He/^{4}He$ ratios indicate connections to the mantle in ISC-7 and ISC-1 wells. Crustal decay (U, Th, and K decay within sedimentary rocks) which is the predominant source of He within the subsurface, is observed in other groundwater samples ISC-4A, ISC-4B, and LMV-2B.

A Piper diagram (Fig. 6) shows similar results as Figures 3 and 4, with southern and central Mesilla Valley groundwaters exhibiting Na-Cl-SO_4 dominant water types, likely an

indicator of gypsum and halite dissolution. Northern Mesilla Valley groundwaters have a Ca-Na-HCO_3-Cl water type. Mixing between water types is apparent in the cation triangle of the Piper diagram where water type shifts linearly from Ca dominant waters in northern Mesilla Valley groundwaters towards Na-dominant water in the central and southern Mesilla Valley. Results for anions in the Piper diagram is more ambiguous, although there appears to be a general shift from HCO_3 waters in the northern Mesilla Valley groundwater towards Cl-SO_4 waters in the southern Mesilla Valley. The transition occurs from north to south, suggesting increased influence from halite and gypsum dissolution and/or cation exchange in southern groundwaters.

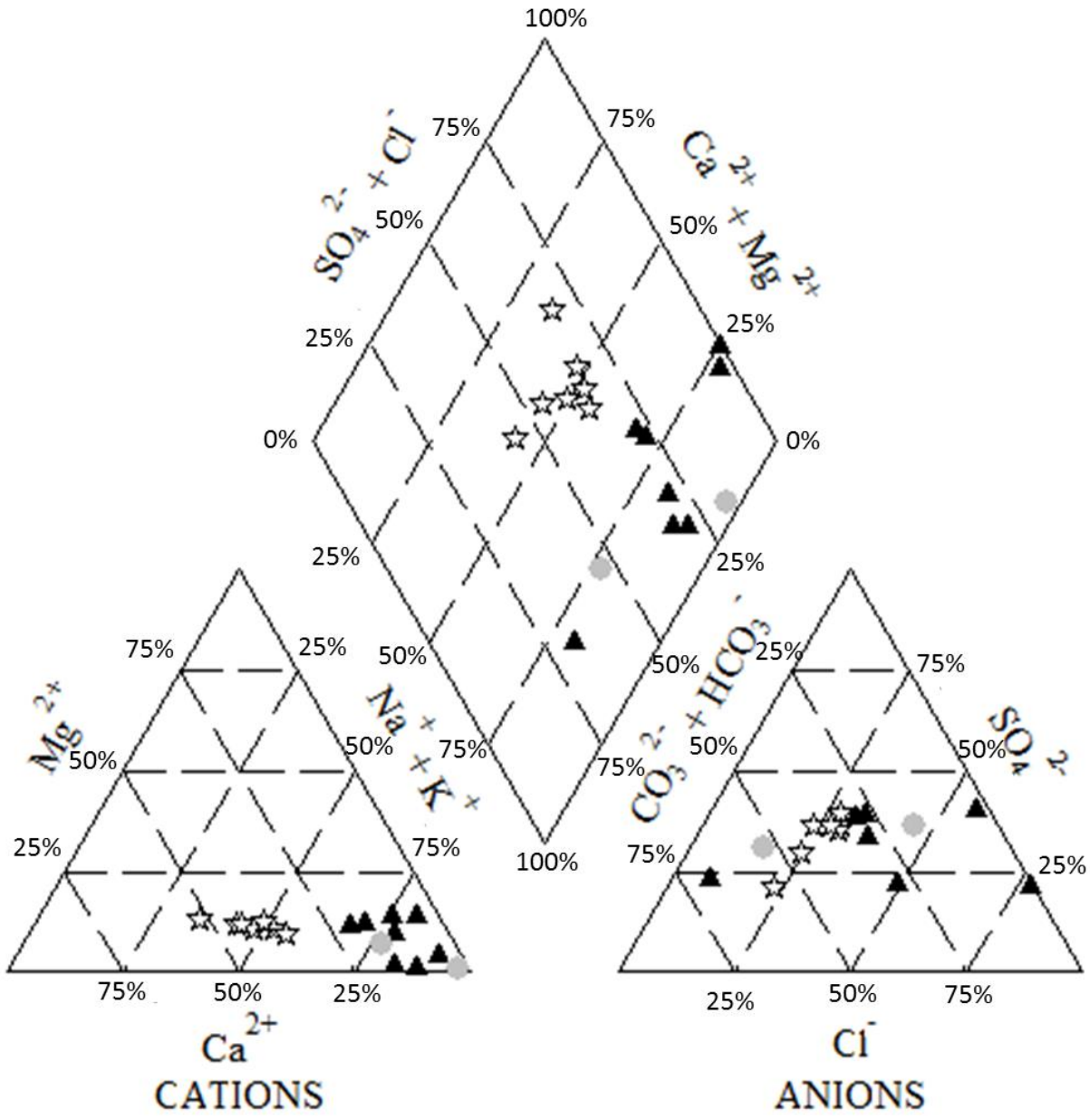

Figure 6. Piper diagram showing Mesilla Valley groundwaters. Open stars indicate northern wells, grey circles indicate central wells, and black triangles indicate southern wells.

Mineral saturation indices show equilibrium with gypsum in southern Mesilla Valley groundwater wells ISC-4A and ISC-4B (SI of 0 and 0.6), and undersaturation of gypsum (SI less

than -1) for central and northern Mesilla Valley groundwater (Table 2.). Southern Mesilla Valley wells are generally closer to equilibrium with halite than central or northern Mesilla Valley wells. There is a large range of halite saturation indexes of southern Mesilla Valley waters (-7.03 to -2.74); however, ISC-4A and ISC-4B are the closest to equilibrium with halite (-3.4 and -2.74). Evidence shows that groundwater salinity in the Mesilla Valley is increasingly derived from evaporate mineral dissolution and/or cation exchange as water flows southward. Except for ISC-1C and ISC-1D, all water samples were oversaturated with calcite suggesting precipitation of calcite is and/or has been occurring throughout the Mesilla Valley.

Table 2. Table showing saturation indices (SI) of evaporate minerals and calcite in Mesilla Valley groundwater. A SI value at zero represent equilibrium, negative indexes represent under saturation, and positive numbers represent oversaturation.

Well	Gypsum	Halite	Anhydrite	Calcite
ISC-1A	-0.97	-5.32	-1.2	0.46
ISC-1B	-1.44	-5.62	-1.66	0.17
ISC-1C	-2.34	-7.03	-2.56	-0.08
ISC-1D	-2.44	-6.97	-2.67	-0.05
ISC-4A	0	-3.4	-0.22	0.58
ISC-4B	0.06	-2.74	-0.16	0.43
ISC-7A	-1.84	-6.08	-2.06	0.03
ISC-7B	-1.23	-4.78	-1.43	0.05
LC-2A	-1.35	-6.51	-1.59	0.11
LC-2B	-1.47	-6.56	-1.7	0.15
LC-2C	-1.55	-6.81	-1.77	0.14
LC-2F	-2.08	-7.32	-2.31	0.02
LMV-2A	-1.94	-6.72	-2.17	0.26
LMV-2B	-2.26	-5.7	-2.49	0.1
M-2A	-1.7	-6.98	-1.95	0.31
M-2B	-1.15	-6.57	-1.39	0.26
M-2C	-1.49	-6.58	-1.73	0.3

6.3 Spatial Distribution and Sources of Evaporite Minerals in the Subsurface

X-ray diffraction (XRD) analysis of high salinity well cuttings from ISC-4B and LMV-2 only tested positive for gypsum in the deepest 6 m of ISC-4B (Fig. 7). These well cuttings are from a light greenish-grey Cretaceous silty shale at 46.77 m to 54.86 m depth. These results confirm that gypsum occurs in Cretaceous bedrock in the southern Mesilla Valley. It is unclear from XRD analysis alone whether gypusm deposits originate from primary deposition or secondary minerals filling fractures and bedding planes.

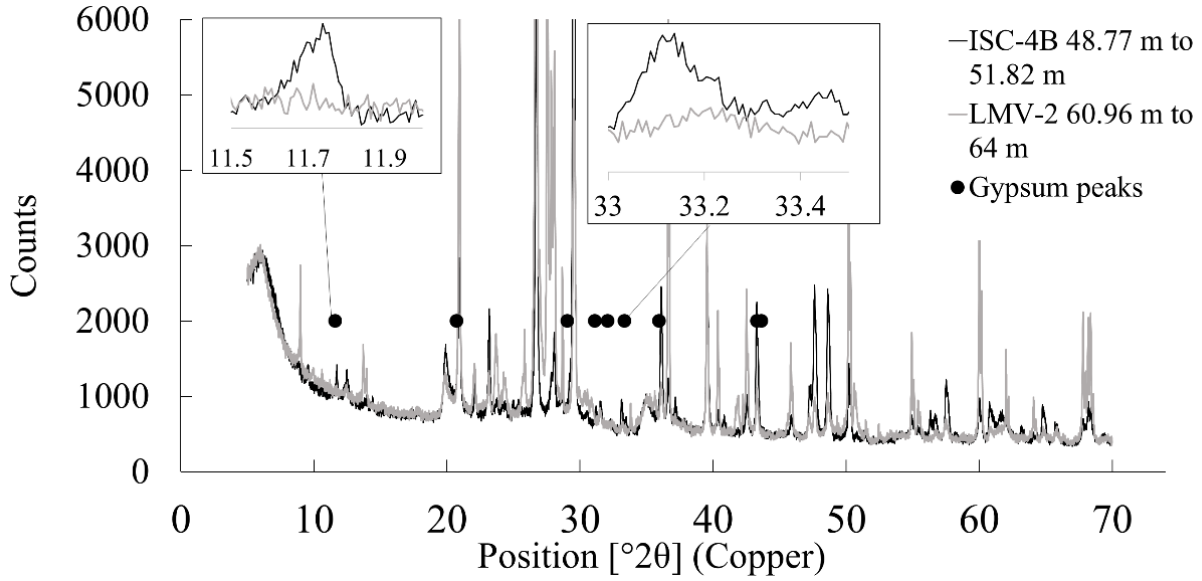

Figure 7. XRD profiles results showing select cuttings for ISC-4B and LMV-2. Gypsum was identified in the well cuttings for ISC-4B (black), but was not identified in well cuttings for LMV-2 (light grey). Peaks for calcite, quartz, albite, illite, and clinochlore also present, but not labeled in the figure. Gypsum peaks noted by black dots.

Gypsum $\delta^{34}S$ values from important regional stratigraphic units vary greatly and allow identification of possible groundwater salinity endmembers. Gypsum $\delta^{34}S$ values are -24.1 for the Cretaceous Mesilla Valley Formation, +7.9 for the Miocene playa deposits of the Rincon Valley

Formation, and +12.5 for the modern Lake Lucero playa in the Tularosa basin (Appendix A; Table 10.). The distinctly negative $\delta^{34}S$ signature observed in the Mesilla Valley Formation is common for many non-magmatic sulfide minerals and sulfate that has formed from oxidation of these sulfides (Kirkland, 1982; Szynkiewicz et al., 2011; Szynkiewicz et al., 2012). Black shale (Member C in Lucas et al., 2010) within the upper Mesilla Valley Formation is rich in organic matter and probably formed in a poorly-oxygenated marine environment, an ideal setting for the formation of pyrite (Lucas et al., 2010). When pyrite is oxidized, sulfuric acid is formed and may react with calcite to form gypsum with a depleted $\delta^{34}S$ signature (Kirkland, 1982). Sulfuric acid may also form when microbes interact with hydrocarbons, which may then interact with calcite to form gypsum; such a process has been hypothesized to be the cause of depleted $\delta^{34}S$ in gypsum deposits in Carlsbad Caverns, NM (Hill, 2000; Kirkland, 1982).

Additionally, pyrite is a common accessory mineral in igneous intrusions. Pyrite may be present as a trace mineral in andesite intrusions located near Sunland Park, NM and at Cerro De Cristo Rey. Pyrite in the andesite intrusions could have interacted with meteoric water resulting in oxidization and release of sulfate. However, magmatic sulfur in pyrite generally shows a narrow range $\delta^{34}S$ just above the standard Vienna Cañon Diablo Troilite standard (0‰ VCDT; Clark and Fritz, 1997).

The $\delta^{34}S$ signature of Lake Lucero playa gypsum matched Permian anhydrite/gypsum sampled from the Yeso and San Andres Formations in the nearby southern Sacramento and San Andres Mountains, New Mexico (+12.3‰ to +13.4‰) and gypsum sand of the White Sands dune field, New Mexico (+12.1 to +13.9‰; Szynkiewicz et al., 2012; Szynkiewicz et al., 2010). Similarities in $\delta^{34}S$ of gypsum from the Permian/Pennsylvanian throughout southern New Mexico, central New Mexico, and west Texas suggest the $\delta^{34}S$ of Permian/Pennsylvanian formations in the

Mesilla basin would also have similar $\delta^{34}S$ signatures (Szynkiewicz et al. 2012; Szynkiewicz et al., 2010; Kirkland, 1982). Szynkiewicz et al. (2010) showed a range of +10.9 to +15.1‰ (n=23) for $\delta^{34}S$ in Permian gypsum/anhydrite deposits throughout southern and central New Mexico. These results are in good agreement with $\delta^{34}S$ of seawater during the Permian Period, which ranged from +9.5 to +12.5‰ (Kirkland et al., 2000). Although no samples were collected from Permian/Pennsylvanian sediments in the Mesilla basin, a likely formation of matching $\delta^{34}S$ signatures would be the gypsum deposits of the Pennsylvanian Panther Seep Formation in the Franklin Mountains (Kottlowski et al., 1956). A $\delta^{34}S$ signature of the Miocene Rincon Valley Formation (+7.9‰) was lower than $\delta^{34}S$ signatures observed in Permian/Pennsylvanian age formations, and suggests gypsum from Rincon Valley playa deposits may originate primarily from the deeper older Permian/Pennsylvanian aged formations which had mixed with a smaller component of a lighter endmember.

6.4 Groundwater Flow Paths and Mixing of High Salinity Groundwater

Sulfate $\delta^{34}S$ of groundwater samples in comparison with TDS from southern Mesilla Valley groundwater indicates mixing between the alluvial aquifer and upper Paleozoic sourced water (Fig. 8). A significant component of groundwater SO_4 from the ISC-1 wells (+2.28 to +5.76‰ $\delta^{34}S$ signatures) are recharged from the Rio Grande (-1.6 to +0.9 ‰) or Mesilla Valley drainage canals with a fertilizer component (-2.1 to +1.6 ‰; Szynkiewcz et al., 2011). ISC-7 water samples have slightly higher $\delta^{34}S$ signatures (+8.01 to +9.52 ‰) than the Rincon Valley Formation (+7.9 ‰) and suggest some influences from deeper Paleozoic units. ISC-4 wells have $\delta^{34}S$ values (+12.36 to +12.46‰) matching Paleozoic $\delta^{34}S$ sulfate (Kirkland, 1982; Szynkiewcz et al., 2011; Szynkiewcz et al., 2010; Szynkiewcz et al., 2012).

PHREEQC equilibrium phases show that when halite is fully dissolved in fresh water (TDS of 0 mg/L, pH of 7, and temperature of 25°C) specific conductance is 451,009 uS/Cm. When gypsum is fully dissolved in fresh water, specific conductance is 2,160 uS/Cm. Approximate conversions from specific conductance to TDS can be calculated using the equation TDS=specific conductance*0.66 (Witcher et al., 2004). Results from this equation suggest gypsum equilibrium occurs near 1,426 mg/L Ca^{2+} plus SO_4^{2-} and halite equilibrium occurs near 297,665 mg/L Na^{+} plus Cl^{-}. Results show several groundwater samples from wells that are oversaturated with gypsum in the southern Mesilla Valley (Fig. 8), but undersaturated with halite; which was also supported by PHREEQC saturation indices (Table 2.).

Anoxic environments such as wetland, riparian areas, and oxbow lakes existed in the Mesilla Valley prior to agricultural development (Hawley et al., 2001; Lee, 1907; Witcher et al., 2004). Sulfate reduction occurs in such environments and can decrease $\delta^{34}S$ by about 7‰. Such processes are thought to be negligible in groundwater in this study area due to the lack of soil organic matter necessary for reduction to occur (Szynkiewicz et al., 2011). Additionally, ILR balances do not indicate sulfate reduction is occurring in any of the groundwaters sampled (Fig. 3).

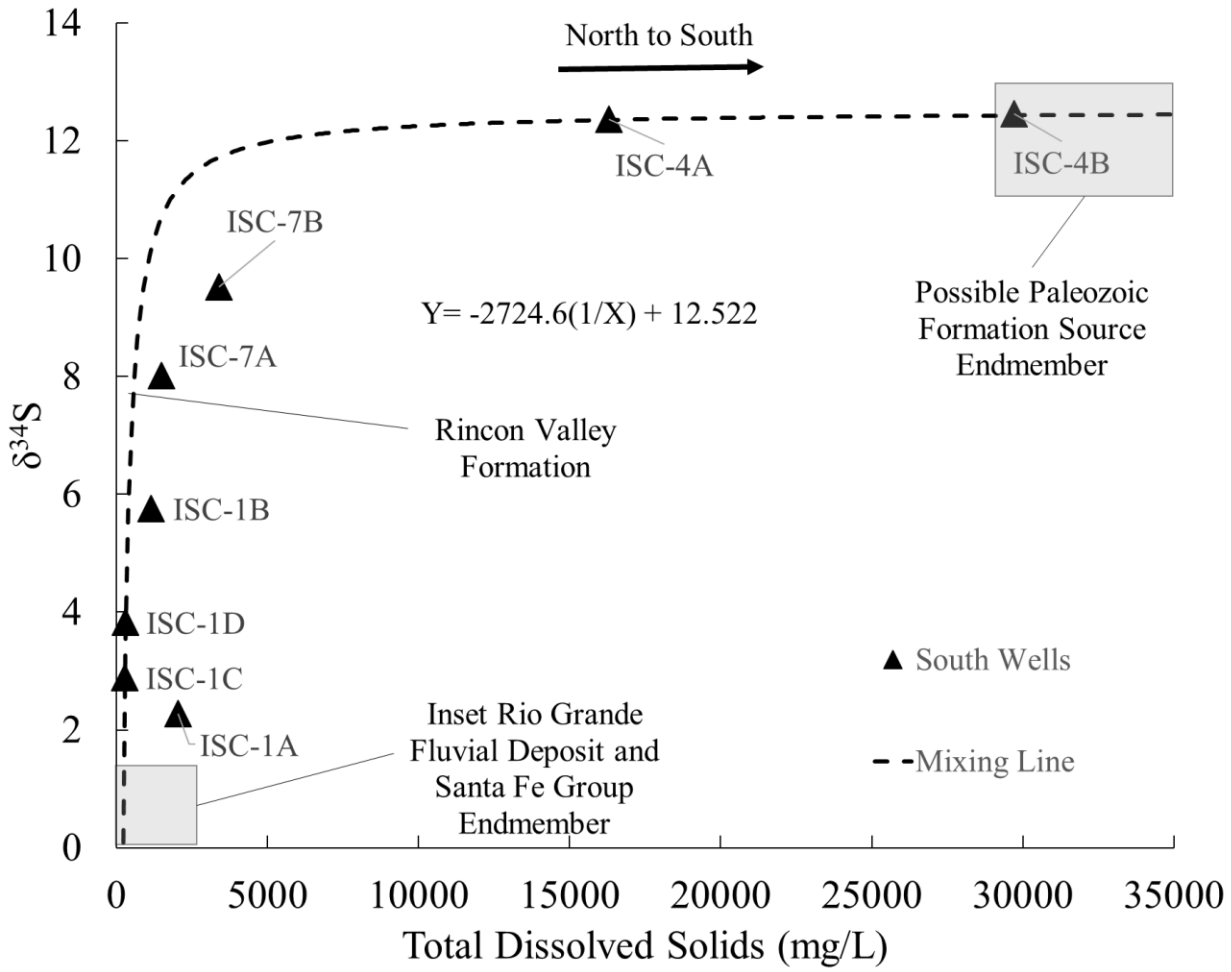

Figure 8. Diagram comparing groundwater $\delta^{34}S$ (data from Szynkiewcz et al., 2011) to TDS. A binary mixing line between the inset Rio Grande fluvial deposit and Santa Fe group endmember and a possible Paleozoic formation endmember is presented (dashed line). Inset Rio Grande Fluvial Deposit and Santa Fe Group Endmember refer to the $\delta^{34}S$ of the Rio Grande and Mesilla Valley irrigation canals, predominant sources of recharge to the alluvial aquifer.

A similar binary mixing relationship between alluvial aquifer groundwater and Paleozoic bedrock derived water can also be observed using trace ions (Fig. 9). Trace ions Li and K appear to increase southward within the Mesilla Valley: the highest concentrations are observed in the ISC-4 well cluster followed by ISC-1 wells and ISC-7 wells. Both Li and K can be geothermal

indicators (Witcher et al., 2004). High concentrations of these ions in southern Mesilla Valley support the hypothesis that a regional flow path is discharging into the alluvial aquifer (higher temperatures are associated with deeper flow paths).

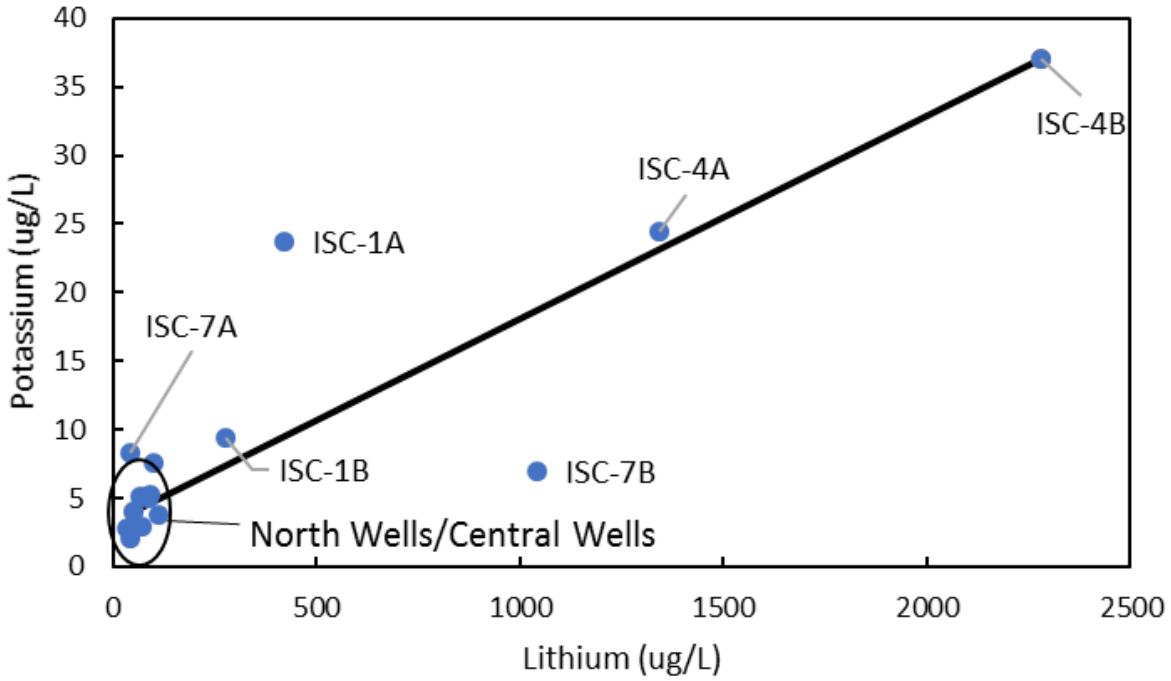

Figure 9. Diagram showing Li concentrations compared to K concentrations in Mesilla Valley groundwater. Mixing is shown between north and south Mesilla Valley groundwater.

Groundwater salinity increases with decreasing thickness of the Santa Fe Group in the southern Mesilla Valley, and a significant salinity increase is coincident with the Santa Fe Group subcrop from volcanic to sedimentary rock. (Fig. 10). A cross-section with well locations shows notable faults and transitions in Santa Fe Group subcrop lithology (Fig. 10). High salinity groundwater sulfate $\delta^{34}S$ matches Paleozoic $\delta^{34}S$ sulfate, but not Cretaceous $\delta^{34}S$ sulfate. This observation indicates the groundwater is not interacting with the Cretaceous units along its flow path out of deeper Paleozoic units. The close proximity of ISC-4 to the andesite intrusions shown

in the Hawley (2018) cross sections may provide a vertical pathway across the Cretaceous units through fractures within the andesite or in fractures along the contact between the andesite and the untruded Cretaceous units. Fault zones can also provide vertical permeability to allow flow across the Cretaceous confining units.

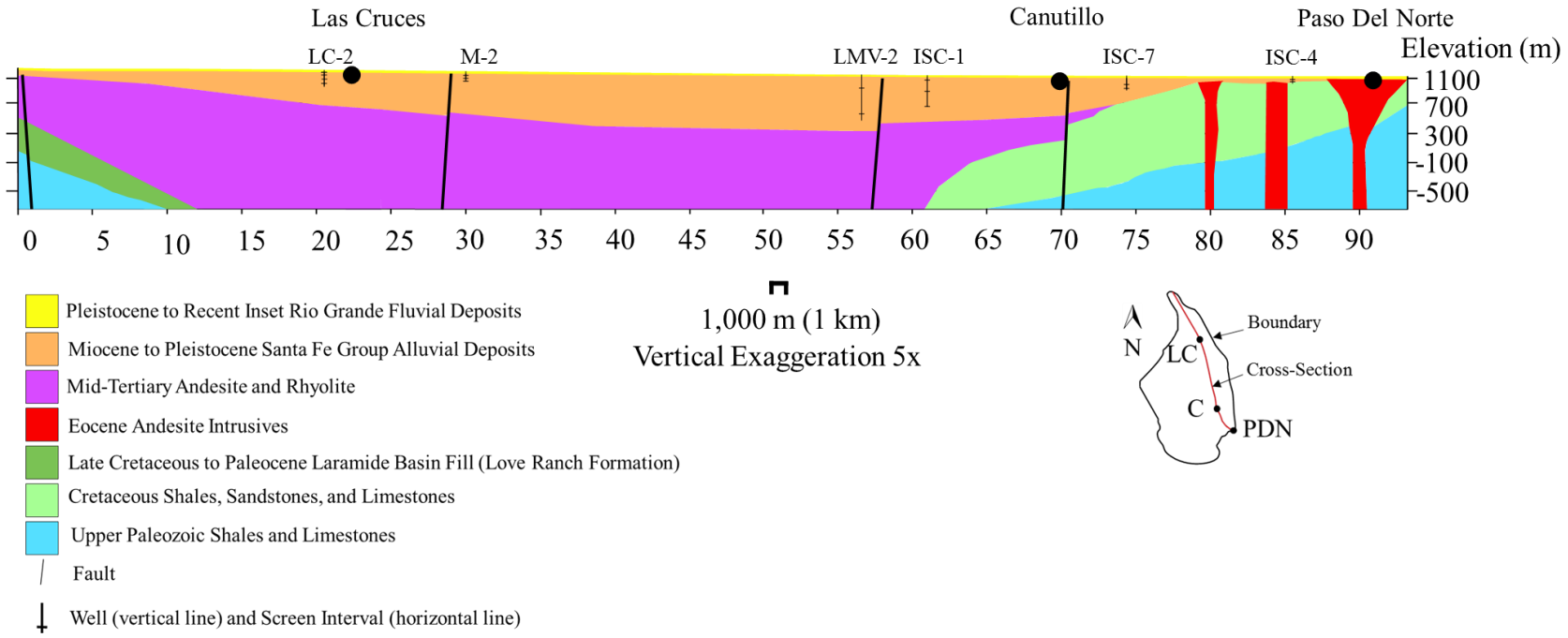

Figure 10. Geologic north-south cross section of the Mesilla Valley showing interpolated well locations and screen depths. Acronyms shown on small location map represent towns shown on the cross section: Las Cruces, NM (LC), Canutillo, TX (C), and the Paso Del Norte, Texas (PDN; modified from Hawley et al., 2018).

A notably thicker alluvial aquifer relative to the thin alluvial aquifer of the southern Mesilla Valley overlies the bedrock aquifer throughout most of the study area (Fig. 10). If groundwater were upwelling from bedrock units throughout the Mesilla Valley, the thick alluvial aquifer located throughout much of the northern and central Mesilla Valley may dilute high salinity groundwater derived from bedrock. Regional flow systems described by Hawley and Kennedy (2004) suggest vertical groundwater flow from bedrock occurs at the southern end of the Mesilla Valley within sedimentary units, and along faults in northern and central volcanic units. The Santa Fe Group subcrop north of Canutillo, Texas consists of middle Tertiary (Eocene to Oligocene) volcanic rocks that do not contain significant amounts of gypsum (Hawley and Kennedy, 2004). A correlation between increased TDS and decreasing distance from well screen is observed in southern Mesilla Valley groundwaters, but not in central or northern wells. Results suggest bedrock is a significant source of salinity in southern wells (Fig. 11). Comparing TDS to alluvial thickness shows that decreases in alluvial thickness are not correlated with increasing salinity in northern groundwaters, suggesting bedrock is a less significant source of groundwater salinity in northern Mesilla Valley compared to the southern Mesilla Valley (Fig. 11).

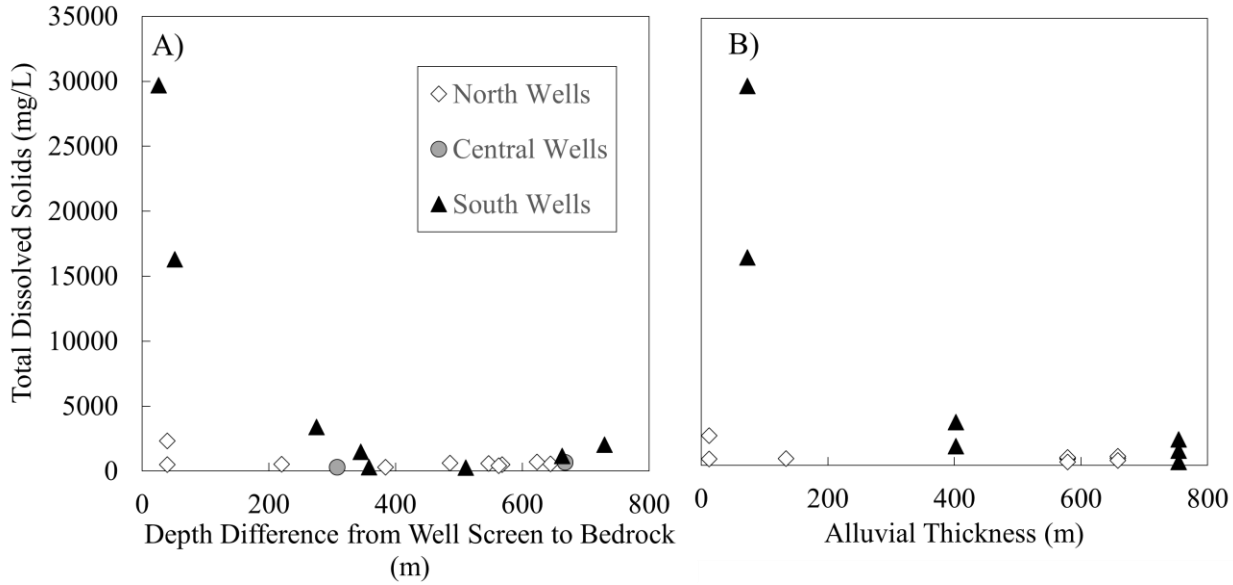

Figure 11. Diagrams comparing A) TDS to depth difference from well screen to bedrock and B) alluvial thickness of northern, central, and southern Mesilla Valley groundwater samples. Additional groundwater samples shown in Table 9 of Appendix A was used to supplement northern groundwater well data.

In addition to increasing TDS, $\delta^{34}S$ values mirror Paleozoic $\delta^{34}S$ sulfate as the depth differences between well screen to the Santa Fe Group subcrop decreases in southern Mesilla Valley wells (Fig. 12). The roughly linear systematic increase in $\delta^{34}S$ with decreasing depth difference from well screen to the Santa Fe Group subcrop supports a binary mixing model between a Santa Fe Group alluvial/Rio Grande fluvial sand inset endmember sulfate and a Paleozoic bedrock derived sulfate. Additionally, $\delta^{34}S$ increases in a near linear fashion with decreasing alluvial thickness, suggesting decreases in dilution of bedrock derived groundwater from north to south in the Mesilla Valley (Fig. 12).

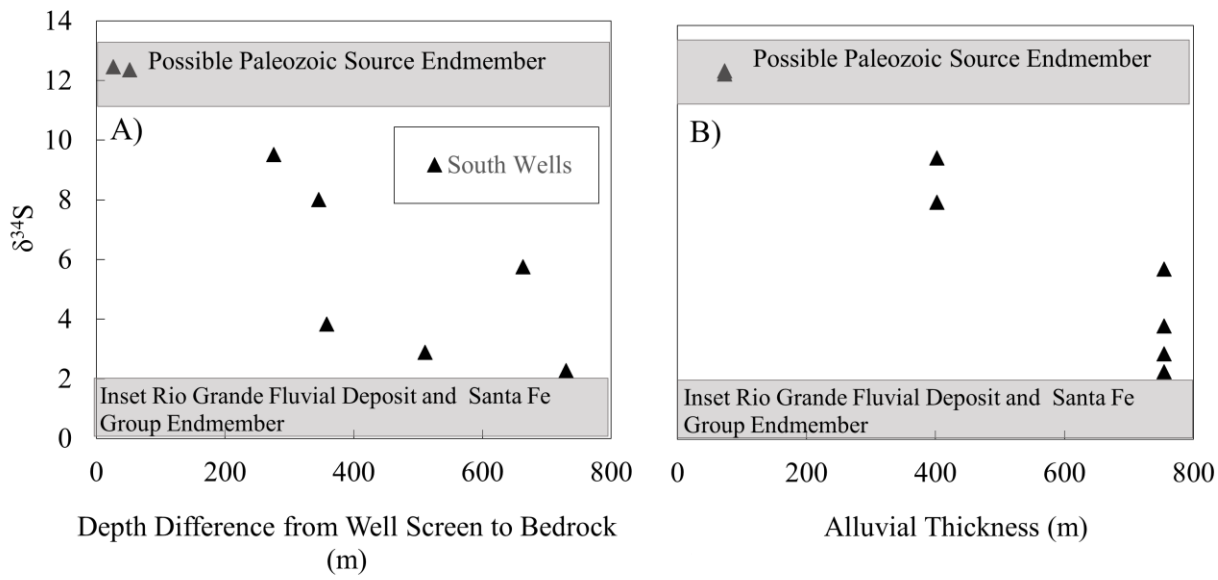

Figure 12. Diagram showing A) $\delta^{34}S$ (Szynkiewcz et al., 2011) compared to depth distance from well screen to bedrock and B) alluvial thickness of southern Mesilla Valley groundwater samples. Data shown in Table 7 of Appendix A.

A contour plot of groundwater TDS sampled throughout the southern Mesilla Valley shows a plume of high-salinity groundwater localized around the ISC-4 groundwater cluster (center of plume). The plume (>9,000 mg/L TDS) is ~5 km long by ~2 km wide (Fig. 13). The I-10 and the Three sisters' faults terminate within the plume. The increased vertical hydraulic conductivity within and immediately adjacent the faults relative to the host lithology may provide a pathway for upward flow.

If deep groundwater was flowing into the shallow alluvial aquifer and mixing, it is assumed that the geochemical plume would have a thermal signature. Both ISC-4 wells sampled have temperatures several degrees cooler (21.5 °C) than thermally anomalous waters in the Mesilla basin (>26 °C). Even so, ISC-4 wells water have elevated concentrations of probable geothermal chemical indicators Li and B suggesting a geothermal component (Witcher et al.,

2004). These results suggest that deep groundwater is upwelling upgradient of the ISC-4 well cluster and cooling as it flows laterally downstream and south to the ISC-4 well screens. Sparse groundwater data south of the ISC-4 wells and Cerro De Cristo Rey do not effectively show where the southern boundary of the plume is located. Other lower salinity plumes (<3,000 mg/L) appear to be generally located along other faults in the area.

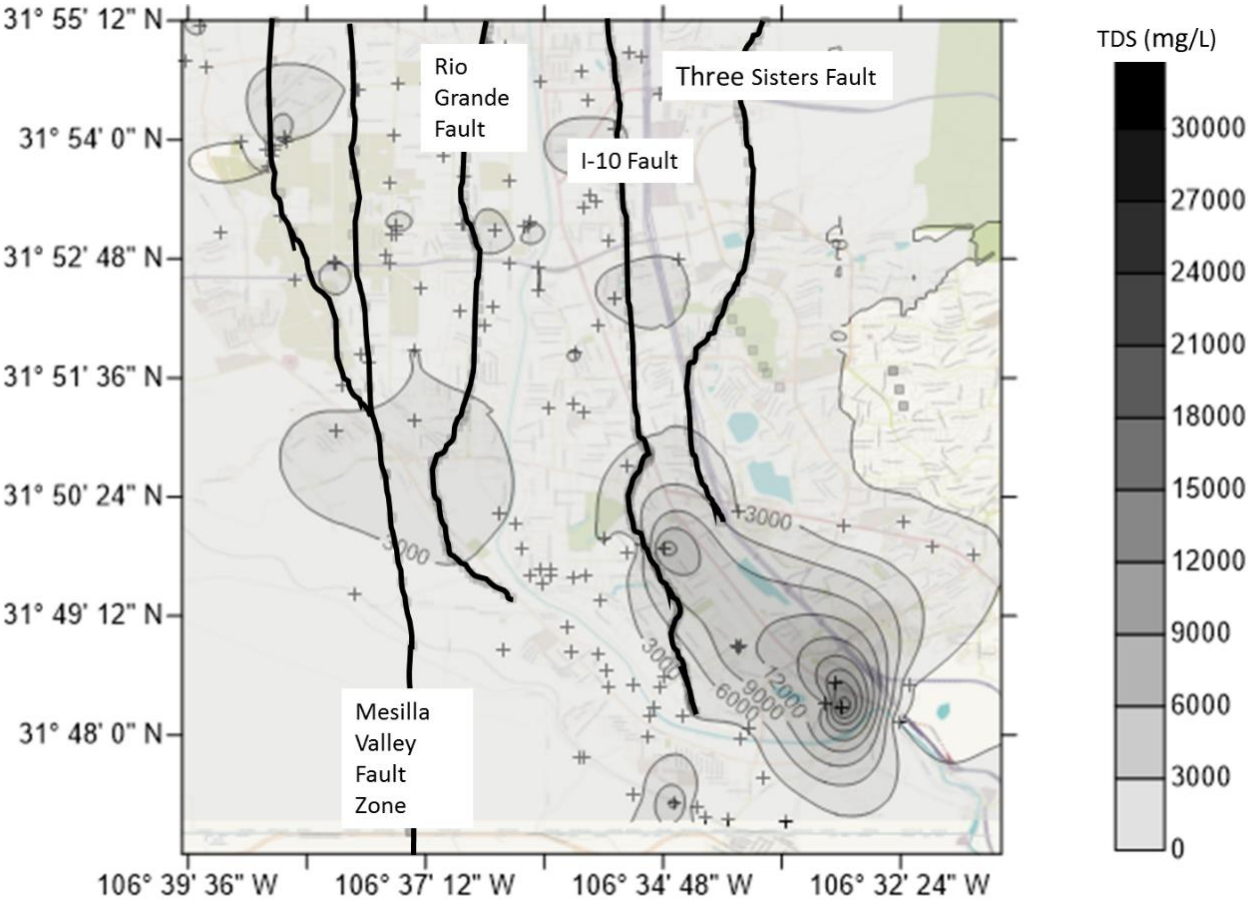

Figure 13. Contour map showing TDS compared to major fault locations (Sweetkind, 2017). Data for TDS and well locations provided by Hiebing et al. (2018). Legend is TDS is in mg/L.

6.5 Vertical Direction of Flow in the ISC-4 Plume

Although thermally anomalous (>26 °C) waters were not observed in the ISC-4 wells, vertical temperature profiles may contain information related to the vertical upward or downward movement of water within the aquifer. To test this hypothesis, temperature profiles were recorded in both wells in the ISC-4 well cluster and the deepest wells of all other well clusters. Appendix B shows temperature logs and their temperature gradient for each of the well clusters in the Mesilla Basin with an additional well from ISC-2A. Temperature profiles fell into several categories: 1) wells with conductive profiles (no vertical flow) indicated by a linear temperature increase with depth, 2) recharging conditions or downward flow indicated by concave upward profiles, and 3) discharging or upward flow shown by convex upward profiles. The significant difference in thermal conductivity between clays and rock is also observed (ISC-7B; Appendix B Fig. 23) as shown by a decrease in geothermal gradient corresponding with a transition from clay to silty sand at ~35 m depth. Wells with recharge temperature profiles include well cluster ISC-4 (Fig. 14) and ISC-2A (Appendix B Fig. 22). Transport of heat downward downward cause the concave upward temperature profile shown in ISC-4 and ISC-2A (Reiter, 2001).

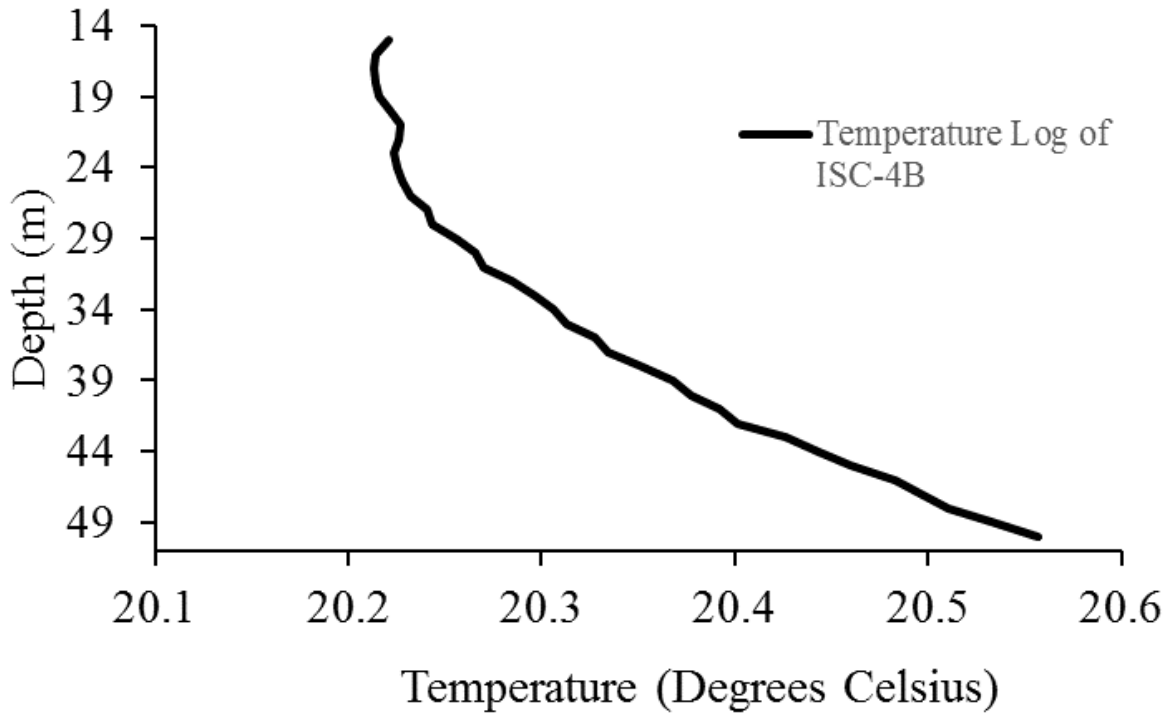

Figure 14. Temperature log of ISC-4B showing recharge from shallow sources (black line) indicated by the concave upward shape.

6.6 Groundwater Age Results

Groundwater age data is consistent with variations in flow paths between various groundwaters. ISC-4A and ISC-4B exhibited ^{39}Ar percent modern values greater than 100% (atmospheric ratio of $^{39}Ar/^{40}Ar$) suggesting subsurface production of Ar (Fig. 15); a phenomenon typically observed in sandstone aquifers, crystalline basement rocks, and occasionally sandy sediments (Ritterbusch et al., 2014; Mei et al., 2010). Subsurface production occurs due to i) in-situ neutron flux from nucleogenic reactions (produced by terrestrial processes) and/or ii) cosmic ray negative muon interactions (Mei et al., 2010; Šrámek et al., 2017). Potential nucleonic sources of Ar production within the Mesilla Valley include alluvial aquifer sands, Precambrian granite, and Thunderbird Rhyolite found in the Franklin Mountains; all of which contain higher

concentrations of potassium, thorium, and uranium than surrounding host rock. For groundwater to accumulate ^{39}Ar from these nucleonic sources, prolonged contact must occur. One possibility may be regional flows paths of ISC-4 groundwaters extend deeper into Precambrian units where ^{39}Ar production takes place. Cosmogenic production of ^{39}Ar is also possible. ISC-4A and ISC-4B well screens are close enough to the land surface that negative muon capture on ^{39}K produces ^{39}Ar ($\mu^- + {}^{39}K \rightarrow \nu\mu + {}^{39}Ar$; μ^- represents a muon and $\nu\mu$ represents a muon neutrino; Šrámek et al., 2017). If muon capture is the dominant source ^{39}Ar production in ISC-4 waters, values at/or near atmosphere in other shallow wells (ISC-7A and LC-2A) cannot be readily explained.

Regardless of the mechanism of ^{39}Ar production, above atmospheric concentrations of ^{39}Ar suggest old groundwater is present. A study by Mei et al. (2010) show uranium rich granites produce $<10^{-3}$ atoms ^{39}Ar /year per gram of rock. Loosli et al. (1991) has suggested that if ^{39}Ar activities of groundwater are controlled solely from release of atoms by rocks, groundwater that has reached equilibrium with those rocks would be at least 1,000 years old suggesting ISC-4 wells contain a significant component of old water. Until, subsurface Ar production is characterized, interpretation of ^{39}Ar groundwater age in wells other than ISC-4A and ISC-4B is not appropriate.

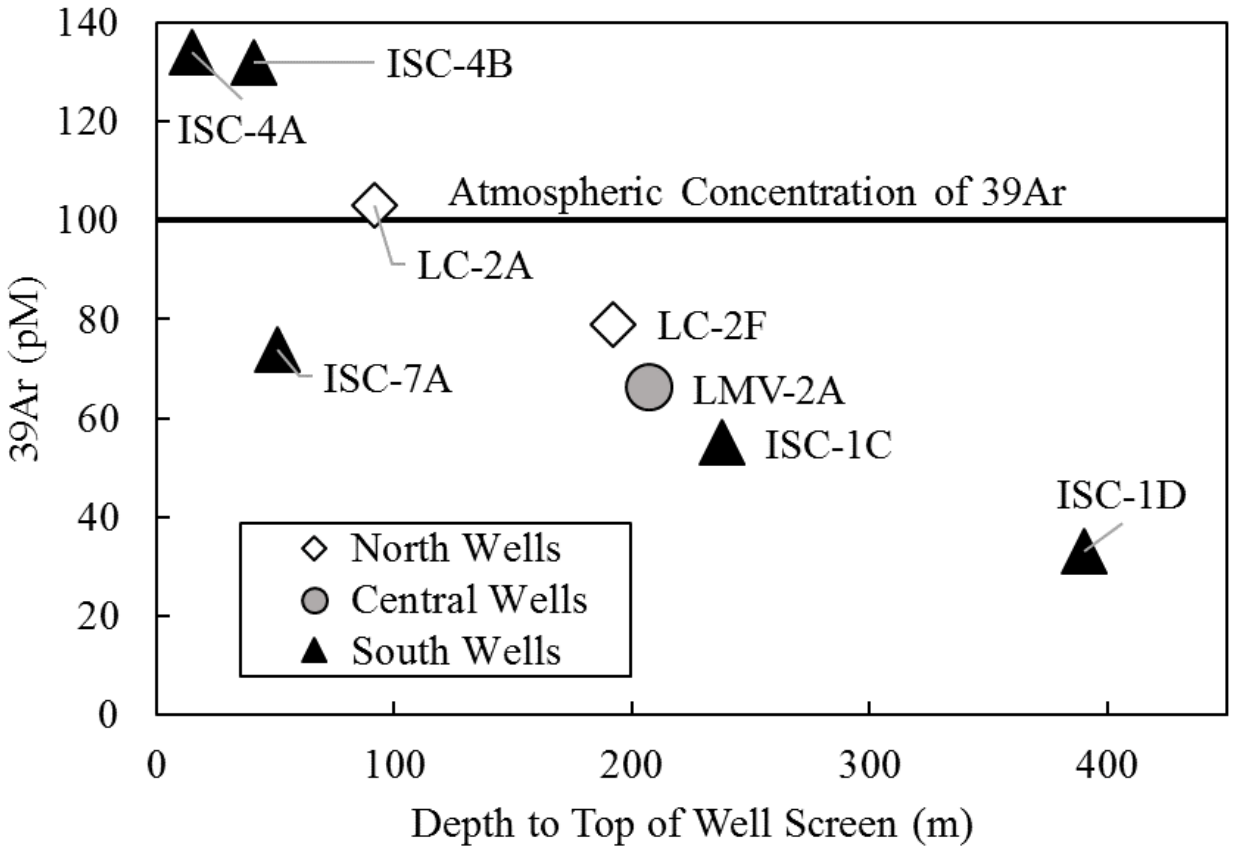

Figure 15. Diagram showing ^{39}Ar compared to depth to top of well screen for Mesilla Valley wells.

Groundwater samples from southern wells ISC-4A, ISC-4B, and ISC-7A, all have low concentrations of tritium (<3 TU) when compared to wells that have well screens less than 60 m (an arbitrary depth representative of the transition from high tritium concentrations to low tritium concentrations) below land surface (Fig. 16). These results suggest that older, tritium-depleted groundwaters are mixing with younger, tritium-rich recharge in the southern Mesilla Valley. In the north, LC-2A has an elevated concentration of tritium when considering the well was screened below 60 m; this may suggest a preferential flow path between the Rio Grande recharge and the LC-2 well cluster. Although, the temperature profile of LC-2F of the same well cluster does not clearly show an expected concave upward profile indicative of recharging groundwater.

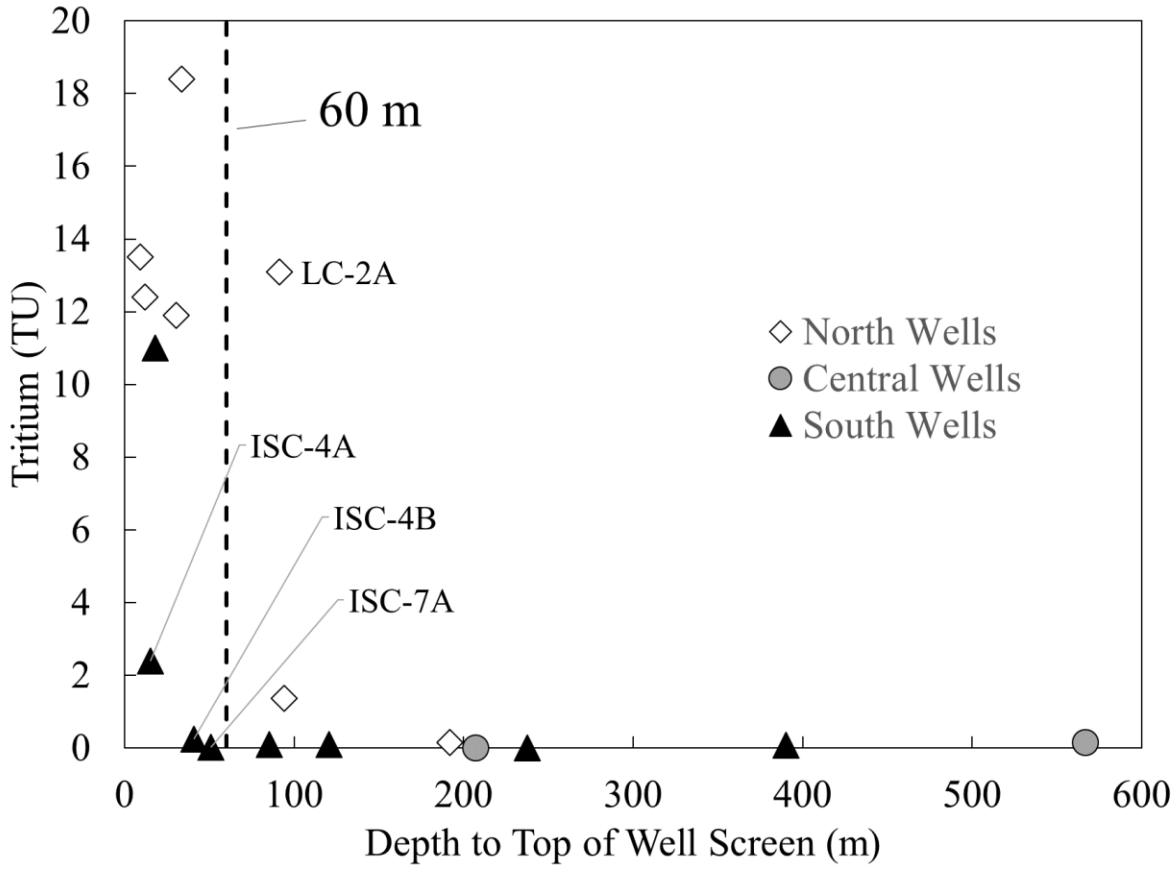

Figure 16. Diagram comparing tritium concentrations of groundwater samples compared to depth below land surface to the top of well screen. The dotted line indicates a depth below land surface to top of well screen of 60 m. Wells ISC-4A, ISC-4B and ISC-7A have particularly low amounts of tritium given their shallow screen depth suggesting mixing between older and younger waters. LC-2A is screened below 60 m yet has significant amounts of tritium, suggesting greater connectivity between the Rio Grande and the LC-2A well.

When depth to top of well screen is plotted against corrected ^{14}C concentrations (see Appendix C for short discussion of carbonate correction), salinity gradients between groundwater age and depth are apparent (Fig. 17). Salinity gradients between age and depth appear to be spatially dependent with higher salinity (>1,000 mg/L TDS) and relatively older groundwaters found at shallower depths throughout the southern Mesilla Valley. ^{14}C

concentrations in the northern and central Mesilla Valley are higher at shallow depths (relative to south wells) and have TDS values <1,000 mg/L. Old groundwater may not be a significant component in all southern wells as ISC-1D and ISC-1C have higher concentrations of ^{14}C even at depth and are lower in salinity (<1,000 mg/L TDS). Put simply, old groundwater does not equate to high salinity groundwaters in the Mesilla Valley, yet high salinity groundwaters are generally representative of old water.

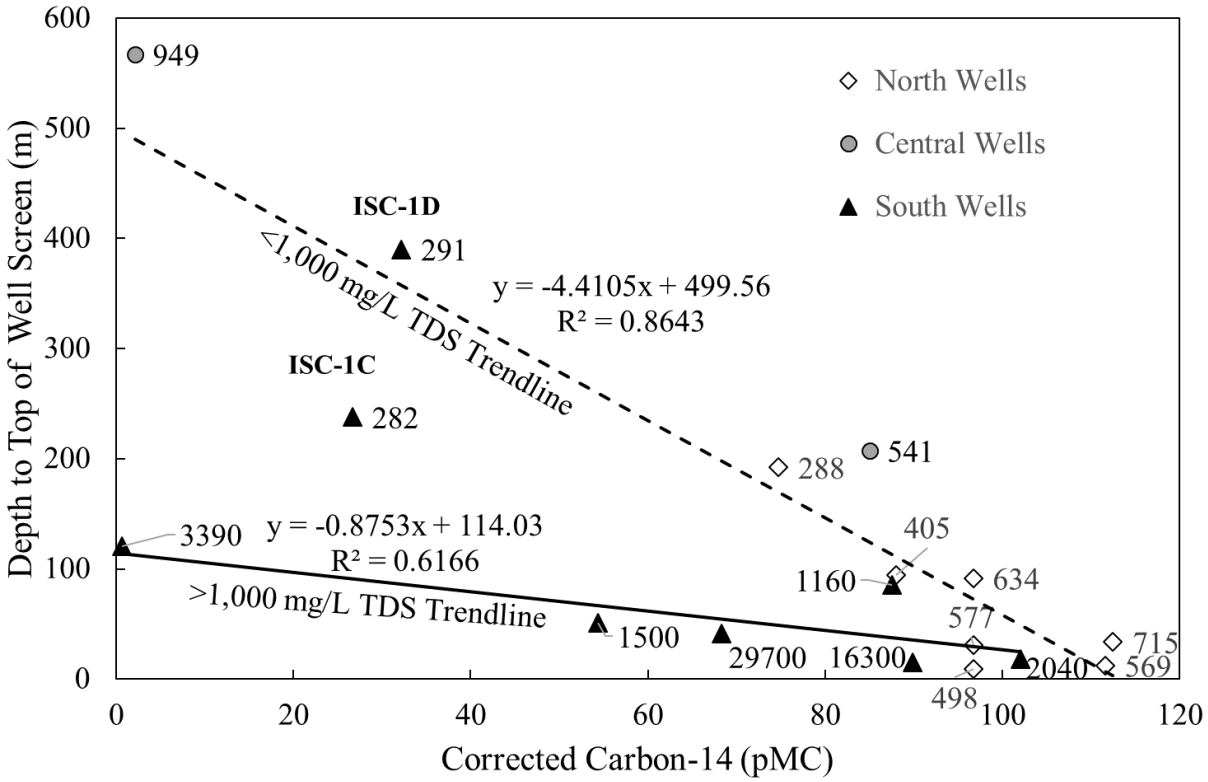

Figure 17. Diagram showing depth to top of well screen compared to corrected ^{14}C of groundwater samples throughout the Mesilla Valley. TDS values are shown next to data points. High salinity groundwaters tend to be older and found in the southern Mesilla Valley.

Similar to Fig. 17, salinity gradients between groundwater age and depth are observed when comparing ^{4}He with depth to top of well screen (Fig. 18). High salinity groundwaters in the southern Mesilla Valley tend to have higher concentrations of ^{4}He indicating a component of older groundwater (>1,000 years; Kendall and McDonnell, 1998). Northern and central Mesilla Valley wells have lower concentrations of ^{4}He at greater depths than southern wells and also are generally lower in salinity (<1,000 mg/L). South wells ISC-1D and ISC-1C are both lower in salinity (<1,000 mg/L) and lack significant concentrations of ^{4}He suggesting influence from old groundwater are negligible in some southern wells. Evidence from figures 17 and 18 support the hypothesis that high salinity groundwater is representative of old groundwater within the Mesilla Valley.

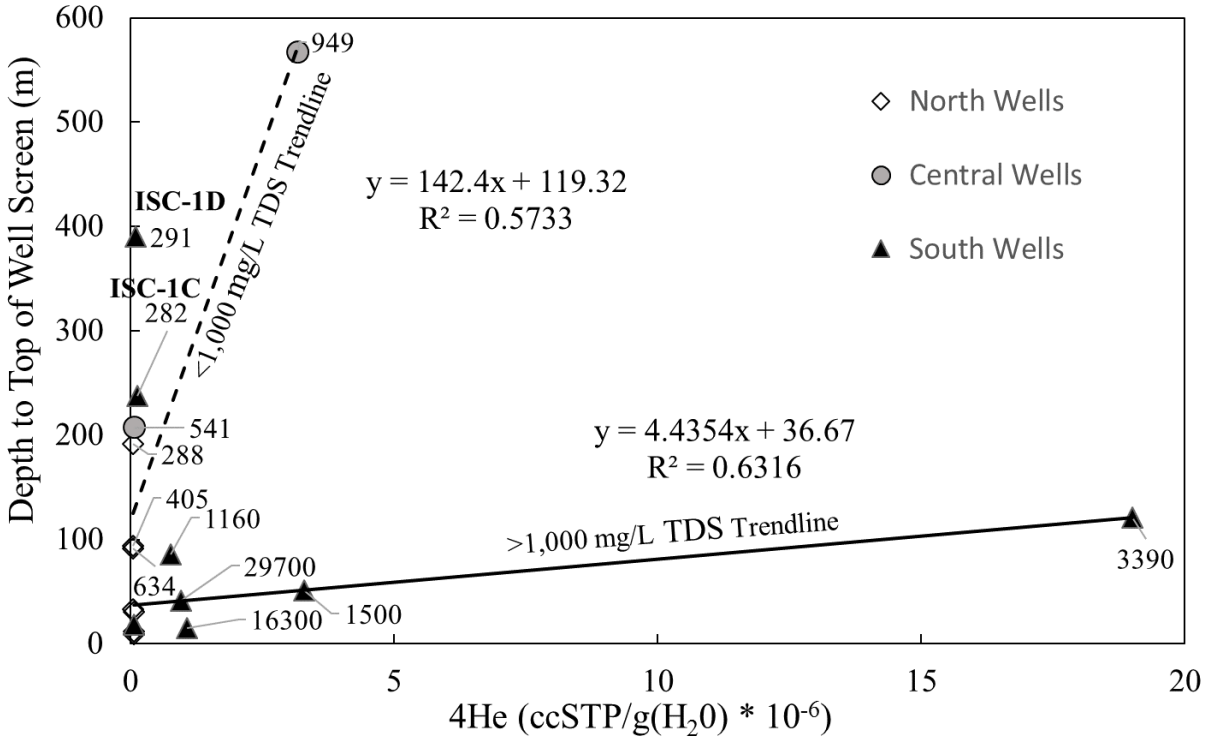

Figure 18. Diagram comparing depth to top of screen compared to ^{4}He of groundwater samples throughout the Mesilla Valley. TDS values are shown next to data points. High salinity groundwaters tend to be older and found in the southern Mesilla Valley.

Groundwater concentrations of ^{85}Kr were well below atmospheric concentrations suggesting most groundwater was recharged prior to 1950, although a modern signature can be observed in LC-2A (Table 3.; Kendall and McDonnell, 1998). Slight variation in ^{85}Kr reported values between University of Bern and Argonne National Laboratory can be attributed in variation in krypton separation processes between the two laboratories and did not alter our groundwater age data interpretation (Jake Zappala, Personal Communication, January 3, 2019). ^{81}Kr of groundwater was equal to atmospheric ratios suggesting groundwater older than 50,000 years, the earliest age ^{81}Kr decay can detect, was not present (Kendall and McDonnell, 1998).

Table 3. Age dating results of groundwater samples from wells throughout the Mesilla Valley.

Well Site	^{14}C, Water, Filtered, Non-Normalized (pMC)	^{14}C, modeled percent using revised Fontes/Garnier (pMC)	Tritium, Water, unfiltered (pCi/L)	^{85}Kr, U. of Bern (dpm/ccKr)	^{85}Kr, Argonne (dpm/ccKr)	^{39}Ar (pM)	$^{4}He\ 10^{-8}$ ccSTP/g(H2O)
ISC-1A	102.06		11				6.767
ISC-1B	11.02	87.58	0.1				76.29
ISC-1C	8.20	26.66	-0.03	2.6	1.01	55	12.94
ISC-1D	8.41	32.18	0.08		0.63	33	10.48
ISC-4A	89.85		2.39	1.9	0.55	134	107.9
ISC-4B	68.33		0.24		0.81	132	95.1
ISC-7A	0.89	54.39	0.02	4.6	2.54	74	330.0
ISC-7B	0.09	0.60	0.1				1,900
LC-2A	96.73		13.1	52.2		103	4.642
LC-2B	96.76		11.9				5.893
LC-2C	96.71		13.5				6.906
LC-2F	74.75		0.15	0.5		79	4.144
LMV-2A	15.31	85.02	-0.15	2	0.37	66	8.862
LMV-2B	0.18	2.10	0.16				318.9
M-2A	88.04		1.37				4.340
M-2B	112.50		18.4				5.095
M-2C	111.62		12.4				5.854

7.0 Discussion

The high salinity groundwater of the ISC-4 area (>9,000 mg/L TDS) is highly localized to a ~5 km long by ~2 km wide plume. The I-10 and the Three sisters' faults terminate within the plume suggesting that several conduits for upward flow of deep groundwater may be present. Above atmospheric concentrations of ^{39}Ar, elevated concentrations of ^{4}He, and lower concentrations of ^{14}C and tritium relative to the shallow screen depths of the ISC-4 wells support the hypothesis that "old" groundwater is discharging into the present aquifer in the southern Mesilla Valley. An andesite intrusion, if fractured, several kilometers north of the ISC-4 well

cluster may provide an additional input for deep high salinity groundwater to flow from Paleozoic units into the shallower alluvial aquifer. Sulfate $\delta^{34}S$ values from groundwater match Paleozoic units and are significantly enriched when compared to $\delta^{34}S$ values of Cretaceous units. Therefore, flow through the Cretaceous units is not indicated, which in turn requires upflow through fractures associated with faults. An additional possibility is gypsum was already equilibrium with groundwater prior to flowing through Cretaceous units which would prevent dissolution of Cretaceous gypsum into groundwater (Table 4. [1]).

Hawley and Kennedy (2004) note that a significant amount of paleo-recharge (pre-Holocene) may have been transported into the southern Mesilla Valley between Anthony, NM and the Paso Del Norte from ancestral Lake Palomas (Table 4. [2]). Research on Lake Palomas indicates that as late as the early Holocene, the floor of the Basin De Los Muertos was filled with a large lake with recharge that flowed northwest towards the Paso Del Norte (Hawley and Kennedy, 2004). This northwest flow gradient may have operated until the installment of the Conjeos-Medanos well field in the southern Mesilla basin/northern Mexico that has reversed any potential northwest flow (Hawley and Kennedy, 2004; CH2MHILL, 2013). Although possible, it seems unlikely that Lake Palomas is the source of the high salinity groundwater at ISC-4 site since groundwater water from the alluvial Conejos-Medanos aquifer of northern Mexico has an average salinity of ~2,000 mg/L, which is significantly lower than the observed TDS in the ISC-4 plume (IBWC, 2011). It is still unclear if a deeper regional flow path exists from the southwest.

An additional possible source of groundwater salinity within the ISC-4 plume is deep alluvial groundwater of the middle-lower Santa Fe Group dissolving gypsum throughout a regional flow path that discharges into the shallow alluvial aquifer due to uplifted Cretaceous bedrock, which rises to the land surface at the southern end of the Mesilla Valley (Table 4. [3]).

This scenario describes a topographically driven regional flow system where groundwater accumulates Ca and SO_4 ions from gypsum interbedded in the Hayner Ranch, Fort Hancock, and Rincon Valley formations of the middle and lower Santa Fe alluvial aquifer. Hiebing et al. (2018) suggested that Cl/Br ratios greater than 200, typical of geothermal waters in the region, in southern Mesilla Valley groundwaters was evidence for evaporite dissolution throughout the middle and lower Santa Fe. It seems plausible that the general changes in water type between the northern and central/southern Mesilla Valley may result from variations in gypsum and anhydrite deposition or presence in the middle and lower Santa Fe. Additionally, old groundwater signatures observed in high salinity southern Mesilla Valley groundwaters could be explained by deep, old groundwater being forced to the surface by uplifted bedrock. Yet, $\delta^{34}S$ in the ISC-4 wells and ISC-7 wells are greater than $\delta^{34}S$ values in the Rincon Valley Formation, which suggests the source of salinity to southern Mesilla Valley groundwater is not in lower or middle Santa Fe rocks. $\delta^{34}S$ and TDS also increase with decreasing depth difference between bedrock and well screens in the southern Mesilla Valley. These results suggest bedrock, as opposed to the Santa Fe Group rocks, are the main sources of groundwater salinity to the ISC-4 plume and the southern Mesilla Valley.

Evaporite beds formed in oxbows or wetlands have been suggested to be another possible source of high salinity groundwaters observed throughout the Mesilla basin (Table 4. [4]; Hiebing, 2018). The highly localized nature of the ISC-4 plume and elevated U concentrations in ISC-4B (Appendix A; Table 12.) wells suggest an ancestral oxbow or wetland may be present. In this scenario, surface water within an ancestral wetlands or oxbow would have evaporated resulting in a shallow deposit of evaporate minerals. In addition to evaporate minerals, reducing conditions of the wetlands or oxbows would have led to the precipitation of uranium bearing

minerals. If highly oxidized modern Rio Grande recharge were to flow though such deposits, uranium would become remobilized leading to elevated concentrations in groundwater (Culbert and Leighton, 1988). If an oxbow were present, XRD analysis would confirm the presence of gypsum throughout the Santa Fe group of the ISC-4B well cuttings and not just in the upper layers of Cretaceous bedrock. As noted earlier, common features of highly reduced environments such as H_2S production and SO_4 reduction were not observed in the ISC-4 wells. Additionally, the presence of old groundwater found at shallow depths in the southern ISC-4 and ISC-7 well clusters could not easily be explained in this proposed scenario.

Others have attributed high salinity groundwater in the ISC-4B area to seepage from irrigation (Table 4. [5]; Sheng, 2013). This appears to be an unlikely source of groundwater salinity in the ISC-4 area since sulfate $\delta^{34}S$ values do not match $\delta^{34}S$ signatures of fertilizers. Additionally, the TDS of the Rio Grande within the southern Mesilla Valley, the source of irrigation water, is ~1,000 mg/L, which is far less than the observed ~30,000 mg/L TDS in ISC-4B (CH2MHILL, 2013).

It has been previously speculated that the Montoya Drain or industrial waste from the Rio Grande Power plant may be the source of the high TDS groundwater in the ISC-4 plume (Table 4. [6,7]; CH2MHill, 2013). TDS measurements of the Montoya drain taken during the Winter between 1938-1990 never rose above 2,500 mg/L suggesting that these agricultural drains are not significant sources for groundwater salinity in the ISC-4 plume (CH2MHill, 2013). Additionally, discharge from the Rio Grande power plant river outfall was noted to have a maximum discharge of 5,800 mg/L TDS (CH2MHill, 2013), much lower than the ~30,000 mg/L TDS in ISC-4B. Measurements of salinity in the Rio Grande near at the Courchesne Bridge between 1938-2012 show River salinity is greatest during December with average salinity values of ~1,500 mg/L

(Table 4. [8]; Witcher et al., 2004), suggesting the reach of the Rio Grande adjacent to the ISC-4 plume is not the main source of groundwater salinity to the plume.

Table 4. Potential sources and flowpaths of high salinity southern Mesilla Valley groundwater.

Source of Salinity	**Mechanism of flow**
[1] Evaporate minerals located in Paleozoic Bedrock	Topographically driven regional flow (Hawley and Kennedy, 2004).
[2] Gypsum deposits located Lake Palomas (Mexico)	Topographically driven regional flow (Hawley and Kennedy, 2004).
[3] Gypsum deposits located in the middle and lower Santa Fe	Topographically driven regional flow (Hogan et al.,2007; Phillips et al., 2003).
[4] Ancestral Oxbow Playa	Recharge from the Rio Grande and agricultural drains (Hiebing et al., 2018).
[5] Fertilizer from Irrigation	Recharge in flood irrigated fields (Sheng et al., 2013).
[6] Agricultural Drains	Recharge along agricultural drains (Witcher et al., 2004).
[7] Industrial Waste	Discharge from power plants and nearby industry into the Rio Grande (CH2MHill, 2013).
[8] Rio Grande	Recharge from the Rio Grande along losing reaches (Sheng et al., 2013).

8.0 Conclusions and Recommendations

This project uses geochemical tracers in addition to lithological chemical analyses to improve groundwater flow information for salinity transfer and flow path mixing within the Mesilla Valley. $\delta^{18}O$ and $\delta^{2}D$ isotopes from groundwater samples support previous research that effectively shows groundwater in the Mesilla Valley is recharged primarily from the Rio Grande. Geochemical modeling indicates evaporate minerals are a significant source of groundwater

salinity to waters throughout the Mesilla Valley. Increasing TDS in groundwater along north to south flow paths in the Mesilla Valley were correlated with increasing groundwater ages and $\delta^{34}S$ groundwater signatures were comparable to Paleozoic units throughout southern New Mexico. Fractured andesite intrusions and faults in the southern Mesilla Valley likely provide preferential flow paths for transport of Paleozoic derived groundwater into the shallow alluvial aquifer. A plume of high salinity groundwater near the Paso Del Norte was shown to be the primary location of discharge of Paleozoic sourced groundwater along a regional flow path. Underlying volcanic and volcanoclastic formations in the central and northern Mesilla Valley, do not appear to contribute significantly to groundwater salinity in the central and northern alluvial aquifer. Instead, significant increases in groundwater salinity in the Mesilla Valley is dictated by proximity and connection to Paleozoic sedimentary units located in the southern Mesilla Valley. Variations in the age gradients for high salinity groundwater (>1,000 mg/L) and low salinity groundwater (<1,000 mg/L) were observed using both ^{4}He and corrected ^{14}C concentrations. These results suggest that groundwater salinity can be used as a tracer for groundwater age within the Mesilla Valley where high salinity groundwater contains an older component (>1,000 years).

Future workers in this area may drill several deeper wells (screened in Cretaceous/Paleozoic bedrock) within the ISC-4 plume to improve current understanding of groundwater flow and sources of salinity. If groundwater were derived from Paleozoic units along a regional flow path, an upwelling geothermal signature would likely be observed in one or several deeper wells. Additional research may also improve current understanding of the relationship between groundwater age signatures, which are often offset from one another. Such research could improve our current understanding of the relationship between groundwater age

and salinity in the Mesilla Valley, which appears to be correlated. This study illustrates how lithological analysis can be used in conjunction with water chemistry to characterize sources of salinity in a relatively homogenous aquifer system.

9.0 Appendix

9.1 Appendix A Data Tables

Table 5. Well site ID and well screen information.

Well Cluster	Well Site	Longitude	Latitude	Hole Depth (m)	Depth to top of screen interval (m)	Depth to bottom of screen interval (m)
ISC-1	ISC-1A	-106.623056	31.994444	30.48	18.29	24.38
	ISC-1B	-106.623056	31.994444	420.624	85.34	91.44
	ISC-1C	-106.623056	31.994444	420.62	237.74	243.84
	ISC-1D	-106.623056	31.994444	420.62	390.14	396.24
ISC-4	ISC-4A	-106.549989	31.804829	23.77	15.24	21.34
	ISC-4B	-106.549989	31.804829	54.86	41.06	47.15
ISC-7	ISC-7A	-106.635547	31.879271	152.4	50.96	57.059
	ISC-7B	-106.635547	31.879271	152.4	120.73	126.83
LC-2	LC-2A	-106.823061	32.295927	95.71	91.44	92.96
	LC-2B	-106.823061	32.295927	36.27	30.48	32.00
	LC-2C	-106.823061	32.295927	12.19	9.14	10.67
	LC-2F	-106.823061	32.296205	278.89	192.02	195.07
LMV-2	LMV-2A	-106.652216	32.028156	701.04	207.26	210.31
	LMV-2B	-106.652216	32.028156	701.04	566.93	569.98
M-2	M-2A	-106.771669	32.211485	97.54	94.18	95.71
	M-2B	-106.771669	32.211485	37.19	33.53	35.05
	M-2C	-106.771669	32.211485	15.85	12.19	13.72
None	ISC-2A	-106.6239	31.96508333	24.384	15.24	21.34
	Afton Power Plant Well (LRG-11409)	-106.845358	32.1152155	333.76	210.31	327.66
	Well 68 (322526106423101)	-106.708583	32.423833	313.94	Unknown	Unknown

Table 6. Temperature, pH, salinity, and pressure of groundwater samples.

Well Site	Temperature, water (degrees Celsius)	Barometric Pressure (mmHg)	pH, water, unfiltered, field (standard units)	Alkalinity, water, filtered, inflection-point method, field (mg/L as CaCO3)	TDS (mg/L)	Specific Conductance, field (uS/cm at 25 degrees Celsius)
ISC-1A	20.5	664	7.5	448	2040	3080
ISC-1B	23.5	665	7.4	283	1160	1980
ISC-1C	23.8	665	8.4	61	282	441
ISC-1D	24.5	664	8.5	70	291	470
ISC-4A	21.5	662	7.3	432	16300	22100
ISC-4B	21.5	662	7.3	194	29700	42600
ISC-7A	24.6	662	7.3	865	1500	2290
ISC-7B	30	664	7.1	816	3390	5550
LC-2A	20.2	664	7.5	173	634	1020
LC-2B	22.8	662	7.6	164	577	920
LC-2C	25	662	7.6	161	498	801
LC-2F	22.5	663	7.7	132	288	469
LMV-2A	20.3	664	8	227	541	815
LMV-2B	20.2		8.7	138	949	1640
M-2A	17.4	662	7.9	152	405	662
M-2B	19	662	7.5	191	715	1110
M-2C	21.2	656	7.8	165	569	906

Table 7. $^{87}Sr/^{86}Sr$, $\delta^{313}C$, $\delta^{34}S$ of groundwater samples. $\delta^{34}S$ data provided by Szynkiewcz et al. (2011).

Well Site	$^{87}Sr/^{86}Sr$, water, filtered	$\delta^{13}C$, water, unfiltered (per mil)	$\delta^{34}S$, water, filtered (per mil)	Sample date and time for $\delta^{34}S$ (m/d/y/t)
ISC-1A	0.7114	-13.55	2.28	02/09/2007 12:25
ISC-1B	0.71	-5.65	5.76	02/09/2007 14:35
ISC-1C	0.7105	-8.7	2.89	02/09/2007 16:45
ISC-1D	0.7105	-7.9	3.83	02/09/2007 13:20
ISC-4A	0.71	-13.74	12.36	02/13/2007 17:05
ISC-4B	0.7096	-11.58	12.46	02/13/2007 16:30
ISC-7A	0.7089	-3.88	8.01	02/12/2007 15:35
ISC-7B	0.7086	-6.35	9.52	02/12/2007 16:50
LC-2A	0.7098	-7.79		
LC-2B	0.7099	-7.81		
LC-2C	0.7105	-7.89		
LC-2F	0.7096	-7.3		
LMV-2A	0.7095	-6.45		
LMV-2B	0.7106	-4.73		
M-2A	0.7098	-9.61		
M-2B	0.7095	-8.67		
M-2C	0.7105	-7.6		

Table 8. Interpreted depth from bedrock and alluvial thickness of Mesilla Valley wells based off of Hawley (2018) cross-section.

Well Site	Depth Difference from bottom of Well Screen to Bedrock (m)	Alluvial Thickness (m)
ISC-1A	730	754
ISC-1B	663	754
ISC-1C	511	754
ISC-1D	358	754
ISC-4A	52	73
ISC-4B	26	73
ISC-7A	345	402
ISC-7B	276	402
LC-2A	486	579
LC-2B	547	579
LC-2C	568	579
LC-2F	384	579
LMV-2A	668	878
LMV-2B	308	878
M-2A	563	658
M-2B	623	658
M-2C	645	658

Table 9. Interpreted depth from bedrock and alluvial thickness of additional northern Mesilla Valley wells.

Well Site	Latitude	Longitude	Source	Depth Difference from Well Screen to Bedrock(m)	Alluvial Thickness (m)	TDS (mg/L)
Leasburg State Park Well	32.4917	-106.9184	Witcher et al. (2004)	40	12	2330
Fort Seldon State Park Well	32.4827	-106.9213	Witcher et al. (2004)	40	12	510
22S.01E.05.142	32.427	-106.865	USGS (2019)	220	134	529

Table 10. Sample locations of gypsum samples analyzed for $\delta^{34}S$.

Sample Formation	Latitude	Longitude	$\delta^{34}S$, Gypsum (VCDT)
Rincon Valley Formation	32.6773	-106.0734	7.9
Mesilla Valley Formation	31.795	-106.545	-24.1
Lake Lucero	32.6974	-106.4496	12.5

Table 11. $\delta^{18}O$, $\delta^{2}D$, Tritium, and ^{14}C of groundwater samples. Negative tritium values are a result of analytical error and are equivalent to zero pCi/L.

Well Site	δD, water, unfiltered (per mil)	$\delta^{18}O$, water, unfiltered (per mil)	^{14}C, non-normalized, water, filtered (pMC)	Tritium water, unfiltered (pCi/L)
ISC-1A	-69.27	-8.26	102.06	11
ISC-1B	-83.5	-11.08	11.01	0.1
ISC-1C	-84.19	-11.29	8.20	-0.03
ISC-1D	-84.83	-11.36	8.41	0.08
ISC-4A	-64.16	-8.06	89.85	2.39
ISC-4B	-68.76	-8.18	68.33	0.24
ISC-7A	-88.3	-11.96	0.89	0.02
ISC-7B	-72	-9.44	0.09	0.1
LC-2A	-65.87	-7.69	96.73	13.1
LC-2B	-65.46	-7.7	96.76	11.9
LC-2C	-68.41	-8.3	96.71	13.5
LC-2F	-89.25	-11.71	74.75	0.15
LMV-2A	-86.8	-11.32	15.31	-0.15
LMV-2B	-88.3	-11.83	0.18	0.16
M-2A	-87.4	-11.28	88.04	1.37
M-2B	-71.1	-8.47	112.50	18.4
M-2C	-67.9	-7.98	111.62	12.4

Table 12. U-Series of groundwater samples.

Well Site	^{238}U, water, filtered (pCi/L)	^{234}U, water, filtered (pCi/L)	^{235}U, water, filtered (pCi/L)	Uranium, water, filtered (ug/L)	^{234}U/^{238}U
ISC-1A	0.41	0.72	0.016	1.12	1.8
ISC-1B	0.65	1.94	0.053	2.08	3.0
ISC-1C	0.08	0.08	0.013	0.1	1
ISC-1D				0.11	
ISC-4A	1.46	2.4	0.12	4.65	1.6
ISC-4B	38	60	2.1	112	1.6
ISC-7A	6.2	9.5	0.31		1.5
ISC-7B	9.1	11.9	0.43		1.3
LC-2A	0.4	0.47	0.008	0.82	1.2
LC-2B	0.12	0.12	0.026	0.35	1
LC-2C	0.033	0.22	0.011	0.25	6.7
LC-2F	0.028	0.12	0.007	0.06	4.3
LMV-2A	0.08	0.32	0.007		4
LMV-2B	0.003	0.019	0.013		6.3
M-2A	0.73	2.1	0.05		2.9
M-2B	0.24	0.57	0.006		2.4
M-2C	0.1	0.22	0.017		2.2

Table 13. Noble gas concentrations of groundwater samples.

Well Site	Kr 10^{-8} ccSTP/g(H2O)	Xe 10^{-9} ccSTP/g(H2O)	N_2 10^{-2} ccSTP/g(H2O)	^{4}He 10^{-8} ccSTP/g(H2O)	Ne 10^{-7} ccSTP/g(H2O)	Ar 10^{-4} ccSTP/g(H2O)	CH_4
ISC-1A	6.797	8.962	1.897	6.767	2.015	3.105	BDL
ISC-1B	6.792	9.327	1.202	76.29	1.677	2.961	BDL
ISC-1C	7.022	9.621	1.153	12.94	1.701	3.029	BDL
ISC-1D	6.918	9.675	1.181	10.48	1.704	3.005	BDL
ISC-4A	6.192	8.271	CO2 interference	107.9	1.714	2.796	BDL
ISC-4B	5.663	7.380	1.087	95.1	1.578	2.524	BDL
ISC-7A	6.783	9.494	CO2 interference	330.0	1.814	3.039	BDL
ISC-7B	3.796	5.159	CO2 interference	1,900	1.088	1.803	BDL
LC-2A	6.357	8.483	1.271	4.642	1.868	2.890	BDL
LC-2B	6.789	8.749	1.349	5.893	2.309	3.224	BDL
LC-2C	6.633	8.624	1.380	6.906	2.600	3.179	BDL
LC-2F	7.129	9.829	1.252	4.144	1.664	3.049	BDL
LMV-2A	6.913	9.480	1.114	8.862	1.686	3.059	BDL
LMV-2B	6.961	9.431	1.220	318.9	1.778	3.094	BDL
M-2A	6.866	9.485	1.156	4.340	1.759	3.076	BDL
M-2B	7.138	9.639	1.574	5.095	2.068	3.294	BDL
M-2C	6.038	7.680	1.271	5.854	2.307	2.953	BDL

Table 14. Noble gas ratios of groundwater samples.

Well Site	R/Ra	$^{20}Ne/^{22}Ne$	$^{40}Ar/^{36}Ar$	$^{86}Kr/^{84}Kr$	$^{130}Xe/^{132}Xe$
ISC-1A	1.284	9.876	303.3	0.306	0.145
ISC-1B	1.759	9.795	296.2	0.304	0.146
ISC-1C	1.375	9.840	295.8	0.305	0.146
ISC-1D	1.264	9.799	296.5	0.305	0.146
ISC-4A	0.365	9.819	296.7	0.305	0.146
ISC-4B	0.246	9.776	295.5	0.306	0.145
ISC-7A	2.945	9.816	297.8	0.306	0.147
ISC-7B	2.917	9.913	319.9	0.305	0.151
LC-2A	1.093	9.842	296.7	0.306	0.147
LC-2B	1.026	9.790	296.2	0.306	0.148
LC-2C	0.988	9.805	296.1	0.304	0.146
LC-2F	1.210	9.793	296.0	0.305	0.147
LMV-2A	1.242	9.851	295.9	0.305	0.149
LMV-2B	0.263	9.845	296.6	0.306	0.150
M-2A	1.070	9.827	295.8	0.306	0.147
M-2B	2.929	9.822	296.2	0.305	0.149
M-2C	0.999	9.813	295.6	0.305	0.150

Table 15. Major cations of groundwater samples.

Well Site	Calcium, water, filtered (mg/L)	Magnesium, water, filtered (mg/L)	Sodium, water, filtered (mg/L)	Potassium, water, filtered (mg/L)
ISC-1A	113	46.5	536	23.7
ISC-1B	78.7	26.1	292	9.38
ISC-1C	13.4	0.573	76.8	2.84
ISC-1D	10.1	0.231	88.2	2.12
ISC-4A	593	288	4590	24.5
ISC-4B	987	805	8480	37
ISC-7A	27	42.6	487	8.25
ISC-7B	58.8	23.5	1190	6.98
LC-2A	86.1	13.1	110	4.98
LC-2B	69.6	11.8	109	5.27
LC-2C	62.1	11.9	86.9	7.6
LC-2F	42.1	6.71	45.8	2.9
LMV-2A	26.5	6.71	150	3.83
LMV-2B	7.72	0.912	332	3
M-2A	58.2	9.67	66.4	3.98
M-2B	121	18.3	89.4	5.12
M-2C	64	10.4	114	5.07

Table 16. Major anions of groundwater samples.

Well Site	Bicarbonate, water, filtered, inflection-point titration method, field (mg/L)	Chloride, water, filtered (mg/L)	Sulfate, water, filtered (mg/L)	Fluoride, water, filtered (mg/L)	Bromide, water, filtered (mg/L)
ISC-1A	540	393	614	0.46	0.456
ISC-1B	344	339	202	0.58	0.255
ISC-1C	73	44	72.6	0.82	0.064
ISC-1D	83	43.9	77	0.73	0.062
ISC-4A	523	5,390	5,090	0.25	3.78
ISC-4B	236	14,100	5,100	0.5	8.81
ISC-7A	1050	74.1	274	0.7	0.249
ISC-7B	992	703	854	0.65	0.64
LC-2A	210	109	178	0.41	0.211
LC-2B	199	97.8	157	0.51	0.145
LC-2C	195	68.1	140	0.71	0.127
LC-2F	160	38.4	46.9	0.45	0.058
LMV-2A	274	47.3	124	0.43	0.067
LMV-2B	160	240	259	4.85	0.274
M-2A	184	57	93	0.33	0.09
M-2B	231	117	223	0.32	0.195
M-2C	201	88.2	159	0.61	0.147

Table 17. Trace ions of groundwater samples.

Well Site	Thallium, water, filtered (ug/L)	Molybdenum, water, filtered (ug/L)	Vanadium, water, filtered (ug/L)	Selenium, water, filtered (ug/L)	Barium, water, filtered (ug/L)	Beryllium, water, filtered, (ug/L)	Boron, water, filtered (ug/L)	Cadmium, water, filtered (ug/L)	Chromium, water, filtered (ug/L)	Cobalt, water, filtered (ug/L)
ISC-1A	0.04	17	0.2	0.1	34	0.02	514	0.06	1	0.11
ISC-1B	0.06	17.9	0.3	0.15	27.9	0.03	297	0.09	1.5	0.36
ISC-1C	0.02	4.9	0.1	0.05	15.8	0.01	80	0.03	0.5	0.03
ISC-1D	0.02	5.7	0.1	0.05	3.83	0.01	86	0.03	0.5	0.04
ISC-4A	0.3	22.9	1.5	0.75	15.3	0.15	3070	0.45	7.5	0.45
ISC-4B	0.4	2.78	5.1	1	12.5	0.2	2810	0.6	10	0.68
ISC-7A							980			
ISC-7B										
LC-2A	0.06	7.35	0.3	0.15	130	0.03	213	0.09	1.5	0.09
LC-2B	0.06	7.24	0.3	0.15	111	0.03	200	0.09	1.5	0.38
LC-2C	0.06	6.84	0.3	0.15	98.6	0.03	138	0.09	1.5	0.09
LC-2F	0.02	3.19	0.1	0.05	89.7	0.01	75	0.3	0.5	0.03

Table 18. Trace ions of groundwater samples (continued).

Well Site	Copper, water, filtered (ug/L)	Iron, water, filtered (ug/L)	Lead, water, filtered (ug/L)	Mangangese, water, filtered (ug/L)	Nickel, water, filtered (ug/L)	Silver, water, filtered (ug/L)	Strontium, water, filtered (ug/L)	Zinc, water, filtered (ug/L)	Antimony, water, filtered (ug/L)	Aluminum, water, filtered (ug/L)	Lithium, water, filtered (ug/L)	Silica, water, filtered (mg/L as silica)
ISC-1A	0.4	437	0.04	370	0.83	2	2920	4.2	0.07	6	419	41.7
ISC-1B	0.6	68.6	0.06	31.8	0.6	3	2150	6	0.09	9	275	43.5
ISC-1C	0.2	8.5	0.02	7.51	0.2	1	174	2	0.04	3	33.2	34.3
ISC-1D	0.2	6.5	0.02	4.38	0.2	1	80.3	2	0.03	7.4	42.4	26
ISC-4A	3	2090	0.3	1760	3	15	16600	30	0.45	45	1340	41.2
ISC-4B	5.4	487	0.4	3030	5.8	20	24600	40	0.6	60	2280	16
ISC-7A		101		36.5							40.6	70.6
ISC-7B		224		26.6							1040	63.5
LC-2A	0.6	12.2	0.13	520	0.63	3	1030	6	0.09	9	88.4	26.6
LC-2B	0.6	7.2	0.06	463	1.3	3	803	6	0.09	9	91	25.6
LC-2C	0.6	412	0.06	383	0.6	3	771	6	0.09	9	97.7	22.7
LC-2F	0.2	50.1	0.02	102	0.2	1	412	2	0.03	3	71.1	24.3
LMV-2A		406		101							113	45.2
LMV-2B		334		119								18.8
M-2A		5		18.5							51.6	25
M-2B		11.2		385							67.8	25.4
M-2C		141		459							81.2	27.6

Table 19. ^{81}Kr, ^{85}Kr, and ^{39}Ar of groundwaters samples.

Date Sampled	Well Site	Argon (%)	Methane (%)	Nitrogen (%)	Carbon Dioxide (%)	Oxygen (%)	85Kr Bern (dpm/ccKr)	Error	85Kr Argonne (dpm/ccKr)	Error	39Ar (pM)	Error
Fall 2016	LC-2A	1.67	0.08	96.32	0.55	0.68	52.2	2.2			103	8
Fall 2016	LC-2F	2.08	0.29	97.04	0.20	0.38	0.5	0.2			79	15
8/30/2017	ISC-1C	1.65	0.1	97.37	0.03	0.85	2.6	0.3	1.01	0.22	55	7
10/26/2017	ISC-4A	1.39	0.15	97.12	0.63	0.72	1.9	0.4	0.55	0.12	134	12
1/10/2018	ISC-7A	1.48	0.11	95.14	1.35	1.92	4.6	0.4	2.54	0.29	74	9
1/10/2018	LMV-2A	1.74	0.21	97.3	0.13	0.62	2	0.4	0.37		66	9
6/5/2018	ISC-1D	1.7	0.1	98.03	0.03	0.14			0.63		33	6
6/6/2018	ISC-4B	1.51	0.09	97.72	0.44	0.24			0.81		132	13
8/1/2018	Afton Power Plant Well											
10/30/2018	Well 68											
10/30/2018	Well 68 (duplicate)											

Table 20. PHREEQC SI of groundwater samples.

Well Site	Percent error, 100*(Cat-|An|)/(Cat+|An|)	Anhydrite	Aragonite	Calcite	Chalcedony	Chrysotile	CO2(g)	Dolomite	Fluorite	Gypsum	H2S(g)
ISC-1A	1.81	-1.2	0.31	0.46	0.45	-3.46	-1.88	0.82	-1.75	-0.97	-67.31
ISC-1B	-0.12	-1.66	0.02	0.17	0.43	-4.08	-1.94	0.18	-1.59	-1.44	-67.19
ISC-1C	1.25	-2.56	-0.23	-0.08	0.31	-2.87	-3.56	-1.2	-1.83	-2.34	-77.5
ISC-1D	1.49	-2.67	-0.19	-0.05	0.17	-3.64	-3.6	-1.4	-2.08	-2.44	-78.58
ISC-4A	-2.7	-0.22	0.44	0.58	0.47	-2.97	-1.78	1.17	-2.14	0	-64.9
ISC-4B	-2.45	-0.16	0.28	0.43	0.1	-2.25	-2.18	1.11	-1.54	0.06	-65.07
ISC-7A	5.55	-2.06	-0.11	0.03	0.63	-3.66	-1.36	0.61	-1.99	-1.84	-66.24
ISC-7B	4.55	-1.43	-0.09	0.05	1.47	-3.59	-1.19	0.1	-1.95	-1.23	-64.63
LC-2A	1.25	-1.59	-0.04	0.11	0.25	-5.08	-2.26	-0.31	-1.72	-1.35	-67.69
LC-2B	0.81	-1.7	0	0.15	0.21	-4.3	-2.36	-0.15	-1.64	-1.47	-69.13
LC-2C	0.76	-1.77	-0.01	0.14	0.13	-4.09	-2.35	-0.1	-1.42	-1.55	-69.5
LC-2F	1.12	-2.31	-0.12	0.02	0.19	-4.29	-2.54	-0.43	-1.86	-2.08	-70.54
LMV-2A	0.68	-2.17	0.11	0.26	0.48	-2.43	-2.62	0.21	-2.15	-1.94	-72.8
LMV-2B	-0.58	-2.49	-0.05	0.1	0.08	-1.87	-3.57	-0.44	-0.68	-2.26	-79.49
M-2A	1.31	-1.95	0.16	0.31	0.26	-3.34	-2.71	0.09	-1.97	-1.7	-71.48
M-2B	0.15	-1.39	0.11	0.26	0.25	-4.89	-2.23	-0.04	-1.81	-1.15	-67.43
M-2C	0.51	-1.73	0.16	0.3	0.26	-3.4	-2.56	0.11	-1.5	-1.49	-70.87

Table 21. PHREEQC SI of groundwater samples (continued).

Well Site	Halite	O2(g)	Quartz	Sepiolite	Sepiolite(d)	SiO2(a)	Sulfur	Talc
ISC-1A	-5.32	-38.74	0.87	-1.6	-4.38	-0.41	-50.25	1.08
ISC-1B	-5.62	-38.1	0.84	-2.16	-5.02	-0.41	-50.29	0.46
ISC-1C	-7.03	-34	0.72	-1.57	-4.44	-0.54	-58.6	1.42
ISC-1D	-6.97	-33.36	0.58	-2.33	-5.22	-0.67	-59.47	0.4
ISC-4A	-3.4	-39.19	0.89	-1.29	-4.09	-0.38	-48.22	1.62
ISC-4B	-2.74	-39.2	0.52	-1.43	-4.24	-0.75	-48.39	1.6
ISC-7A	-6.08	-38.12	1.04	-1.59	-4.48	-0.21	-49.52	1.29
ISC-7B	-4.78	-37.13	1.86	-0.33	-3.36	0.65	-48.25	3.12
LC-2A	-6.51	-38.84	0.68	-3	-5.77	-0.6	-50.62	-0.94
LC-2B	-6.56	-37.54	0.62	-2.65	-5.5	-0.64	-51.83	-0.22
LC-2C	-6.81	-36.79	0.53	-2.73	-5.63	-0.71	-52.18	-0.14
LC-2F	-7.32	-37.24	0.6	-2.67	-5.5	-0.66	-53.05	-0.25
LMV-2A	-6.72	-36.81	0.9	-0.85	-3.63	-0.38	-54.73	2.17
LMV-2B	-5.7	-34.04	0.5	-1.15	-3.93	-0.78	-60.03	1.91
M-2A	-6.98	-38.23	0.69	-1.72	-4.42	-0.61	-53.65	0.77
M-2B	-6.57	-39.26	0.68	-2.83	-5.57	-0.61	-50.39	-0.78
M-2C	-6.58	-37.29	0.68	-1.91	-4.71	-0.6	-53.19	0.76

9.2 Appendix B Temperature Profiles. Plots and lithology provided by Dr. Shari Kelley (NMTech).

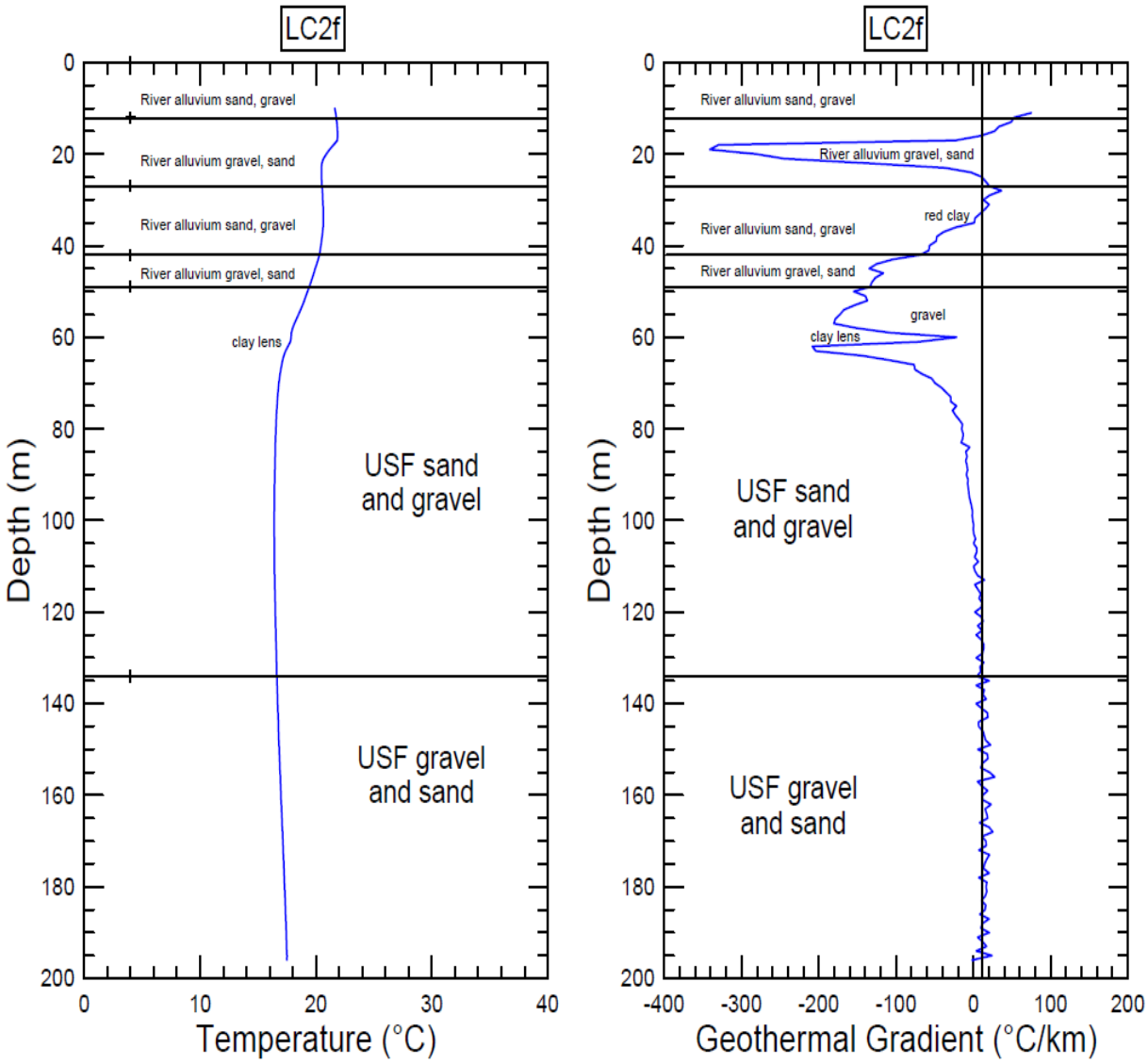

Figure 19. Temperature profile and temperature gradient of LC-2F.

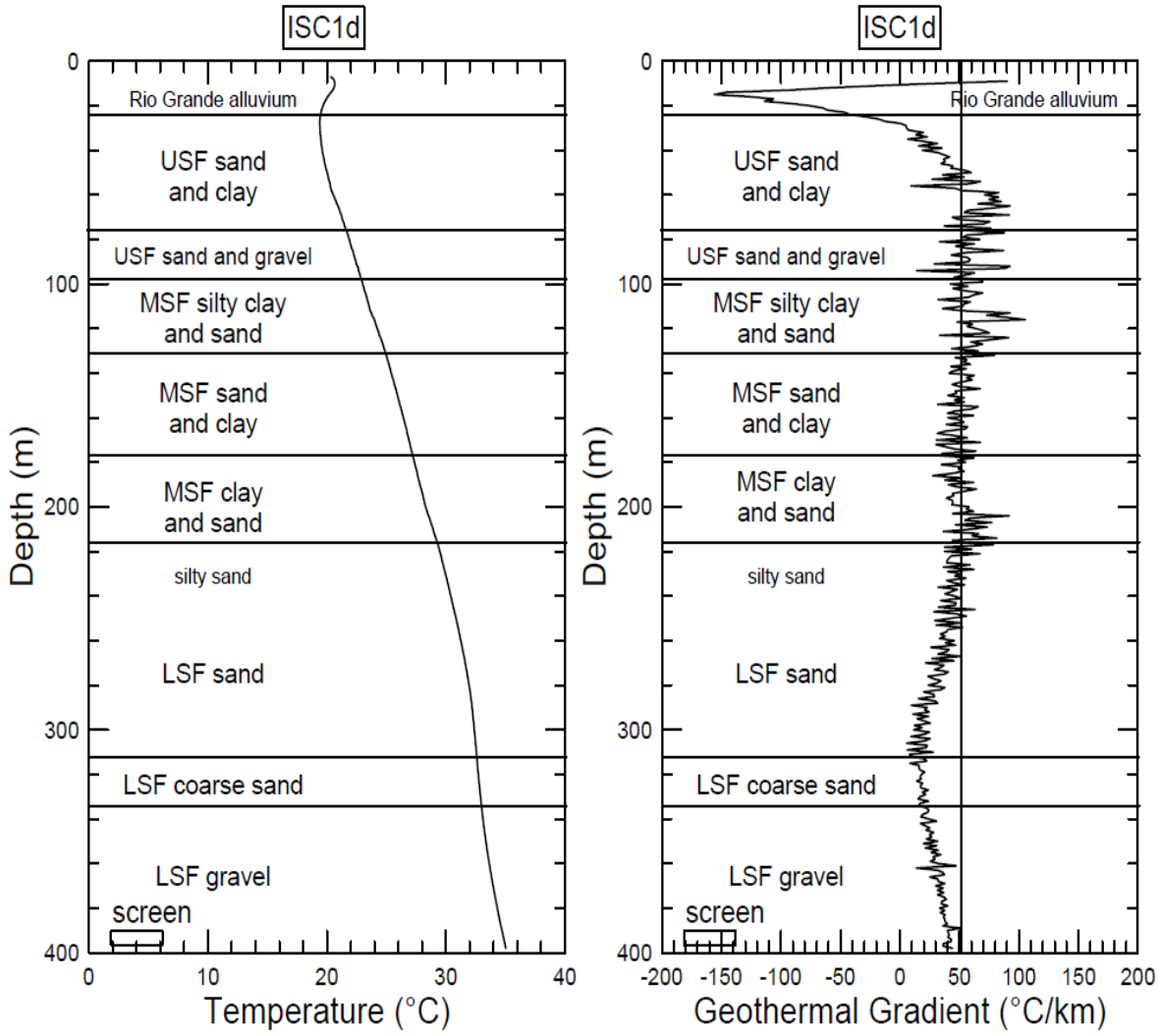

Figure 20. Temperature profile and temperature gradient of ISC-1D.

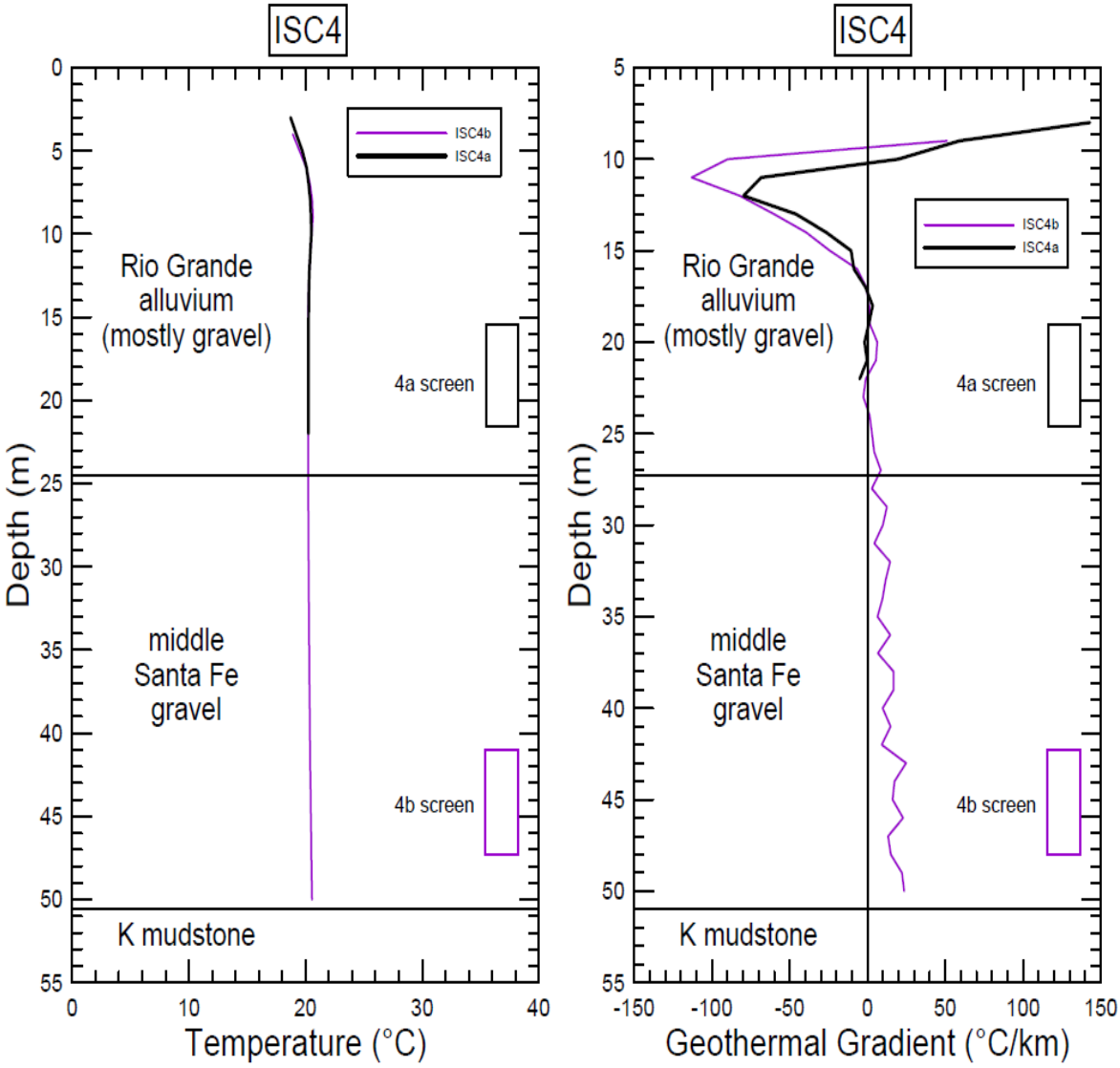

Figure 21. Temperature profile and temperature gradient of ISC-4A and ISC-4B.

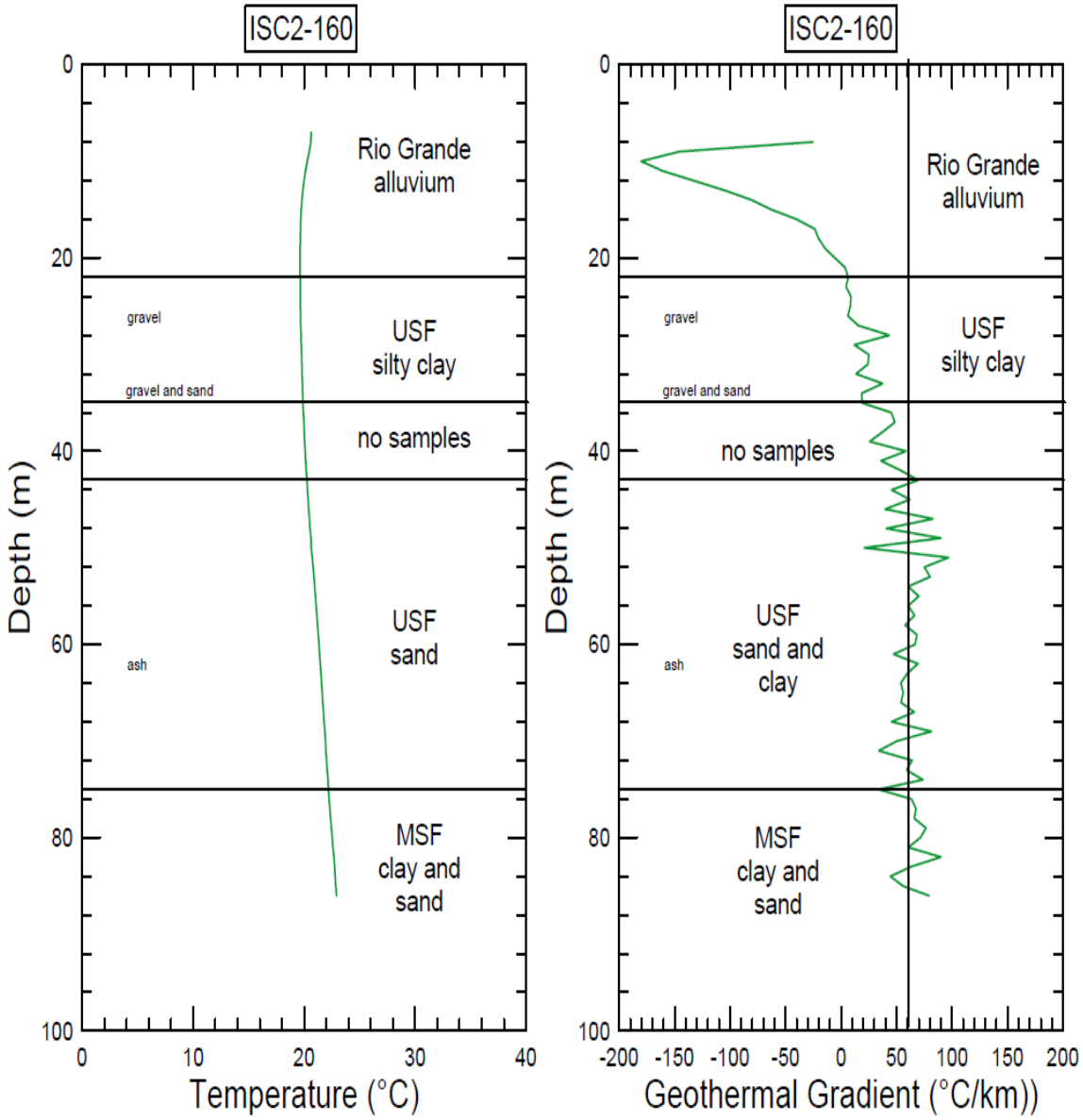

Figure 22. Temperature profile and temperature gradient of ISC-2A (also labeled 160).

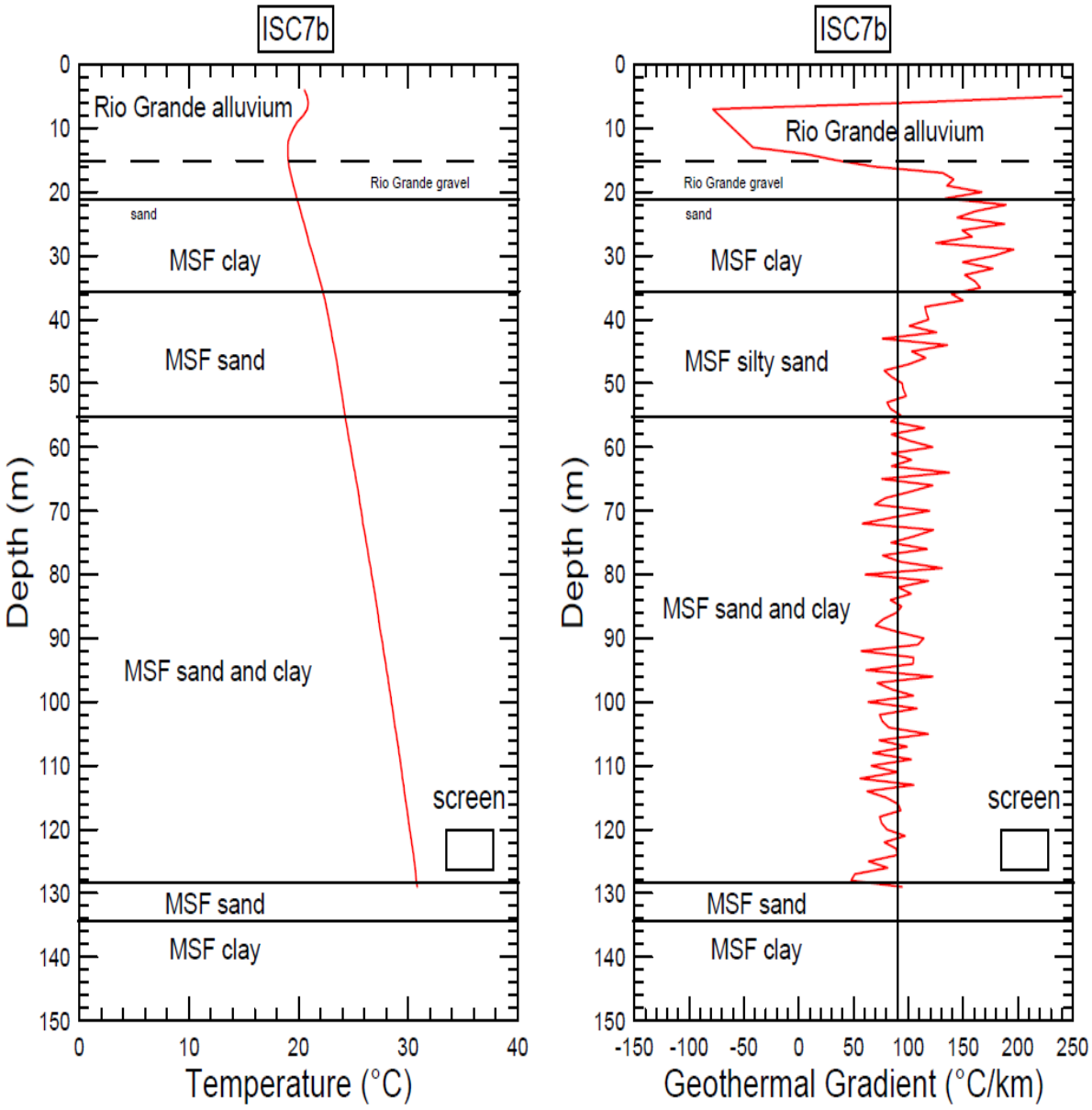

Figure 23. Temperature profile and temperature gradient of ISC-7B.

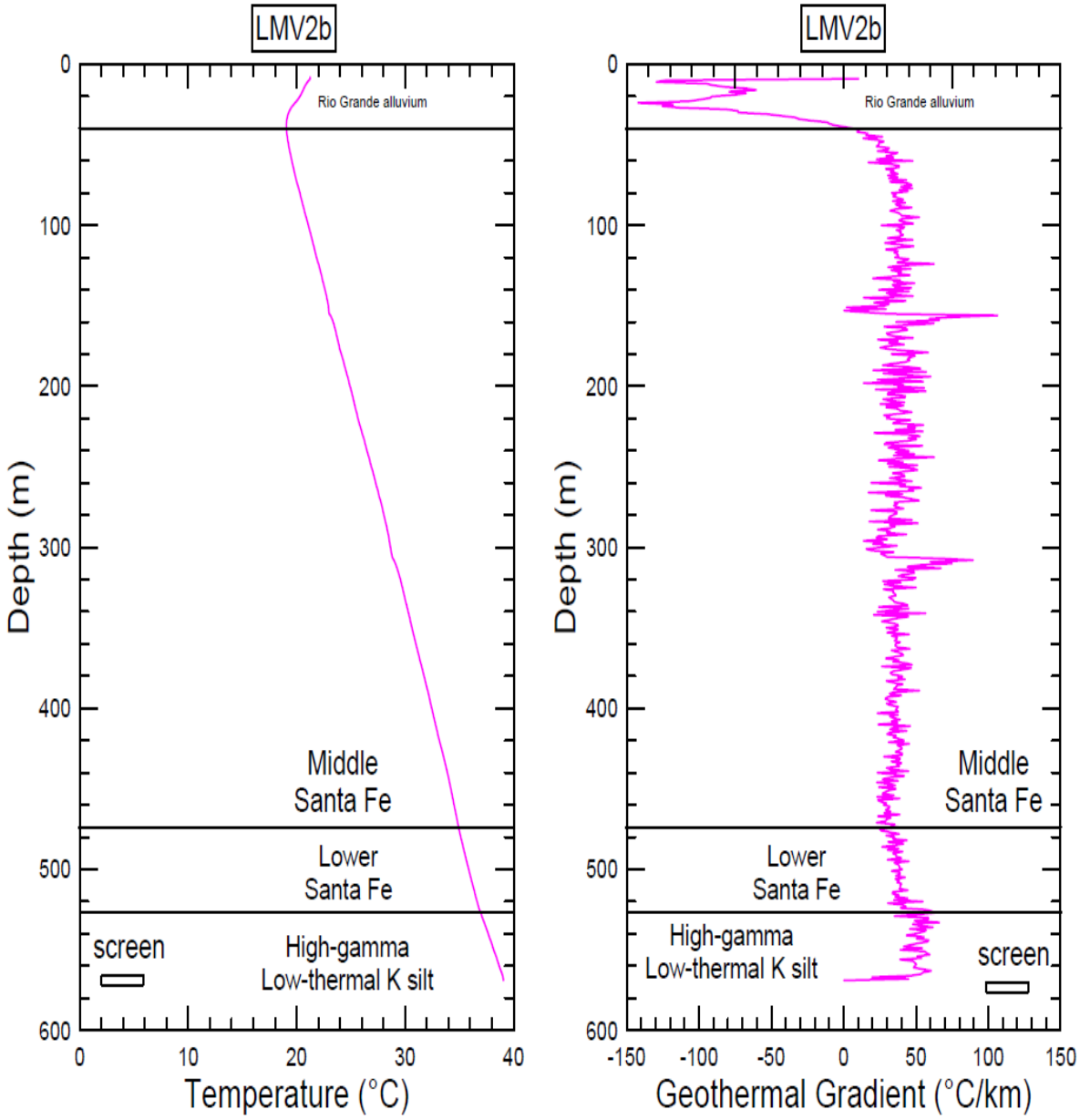

Figure 24. Temperature profile and temperature gradient of LMV-2B.

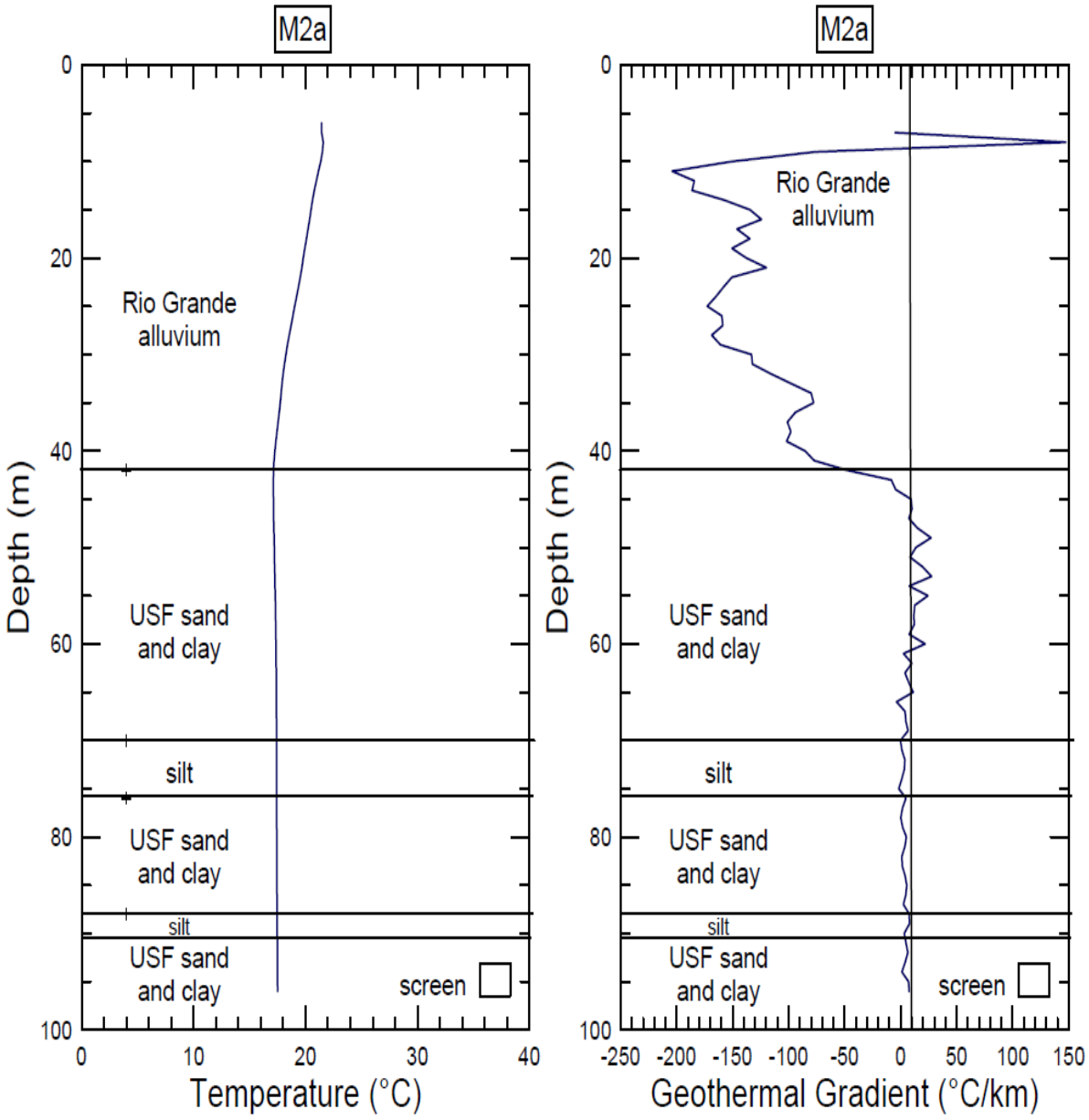

Figure 25. Temperature profile and temperature gradient of M-2A.

9.3 Appendix C Expanded Methodology

Between 2016 and 2018, standard USGS water quality parameters were measured in groundwater samples collected from various wells (Appendix A Table 5) throughout the Mesilla Valley, Mesilla basin, and the Jornada del Muerto (Fig. 1). The wells were used to obtain representative samples from different depths, zones, and lithologies of the inset Rio Grande fluvial deposits and Santa Fe group aquifers. Many of the wells were nested (with negligible lateral distance between boreholes and significant vertical variation between screen elevations; Appendix A Table 5). The nested monitor wells allow for vertical profiling at a few locations in the Basin interior near the Rio Grande where unconsolidated sediments have the greatest thicknesses (Hawley and Kennedy, 2004).

^{81}Kr, ^{85}Kr, and ^{39}Ar Groundwater Sampling and Analysis

Noble gas radioisotopes can provide complementary chronometric and geochemical source and mixing information to groundwater investigations (Yokochi et al., 2013). Because noble gases are inert, corrections for geochemical processes are generally not necessary (Clark and Fritz, 1997). The low abundance and solubility of the radioisotopes of krypton and argon, have required impractical sampling volumes in the past. With the advent of low-level analysis techniques such as Atom Trap Trace Analysis (ATTA; Chen et al., 1999) and Low-Level Counting (LLC; Oeschger and Wahlen, 1975), the noble gas isotopes krypton-81 (^{81}Kr), krypton-85 (^{85}Kr), and argon-39 (^{39}Ar) have become practical tracers for age-dating groundwater. The isotope ^{39}Ar is particularly valuable, as the argon system is the only isotopic system that will effectively bridge the groundwater age gap in the very important intermediate range of 50 to 1,000 years (Fig. 26).

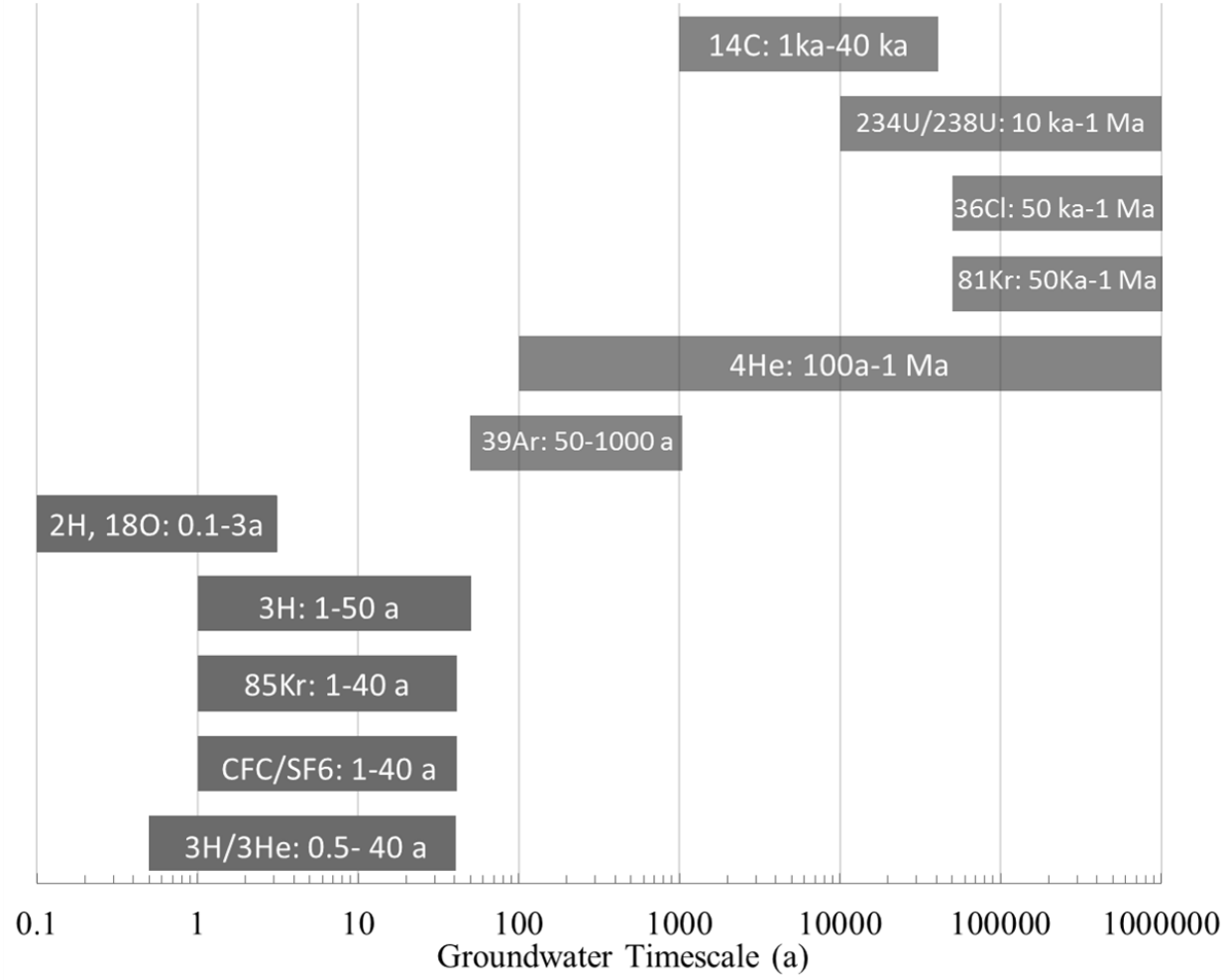

Figure 26. Isotope and chemical tracer groundwater age dating ranges (adapted from IAEA, 2013).

Dissolved gas samples were collected from various wells and then processed for Argon and Krypton gas at Argonne National Laboratory and the Radionuclides Laboratory at the University of Bern. Field sample collection of dissolved gas samples is as follows: Static water level was measured prior to pumping using a Solinst depth to water meter or "E-Tape". Measurements were made from a documented measuring point and recorded to the nearest 0.01 ft. At least three well volumes of water were purged from the well casing to remove resident water and allow sufficient replacement of groundwater prior to sample collection. Field water-quality

parameters, including water temperature, pH, specific conductance, alkalinity, turbidity, and dissolved oxygen were monitored during well purging and sampling (U.S. Geological Survey, variously dated). Water quality field parameters were monitored with an Exo YSI flow cell. Groundwater was pumped using an installed pump if present or a Grundfos portable submersible pump appropriately sized to the well dimensions. Once field parameters stabilized and three well volumes of groundwater had been purged, groundwater was then pumped into a gas separation apparatus (Fig. 27). Inside the gas separation apparatus, water was pumped through two American Plumber® W5P 5µm filters, and then drawn through two Liqui-Cel® Extra-Flow 2.5 X 8 (X40) membrane contactors which separated gas by means of a 115 V Dia-Vac® vacuum pump. Gas was then pumped into a 10.7 L N060 Luxfer Gas Cylinder fitted with a Luxfer CGA 346 valve, and compressed to a pressure between 50 and 65 psi. Once the sample cylinder had reached the appropriate pressure, the cylinder valve was closed and the cylinder was capped with a $3/4^{th}$ inch brass fitting. The pump was decontaminated by placing the pump in a carboy with 0.1% v/v Liquinox solution and flushed with a minimum of 5 gallons of Liquinox solution. The pump was then removed from the solution, rinsed with deionized water, then placed in a carboy with tap water and flushed with 5 gallons of tap water. Finally, the pump was rinsed and placed into a carboy with deionized water and flushed with 5 gallons of deionized water.

Dissolved gas samples were shipped to Argonne National Laboratory and the Radionuclides laboratory at the University of Bern, Switzerland to be analyzed for ^{39}Ar , ^{81}Kr, and ^{85}Kr. ^{81}K and ^{85}Kr were analyzed at Argonne national lab using the ATTA method. ^{39}Ar and ^{85}Kr were analyzed at the University of Bern Switzerland using LLC.

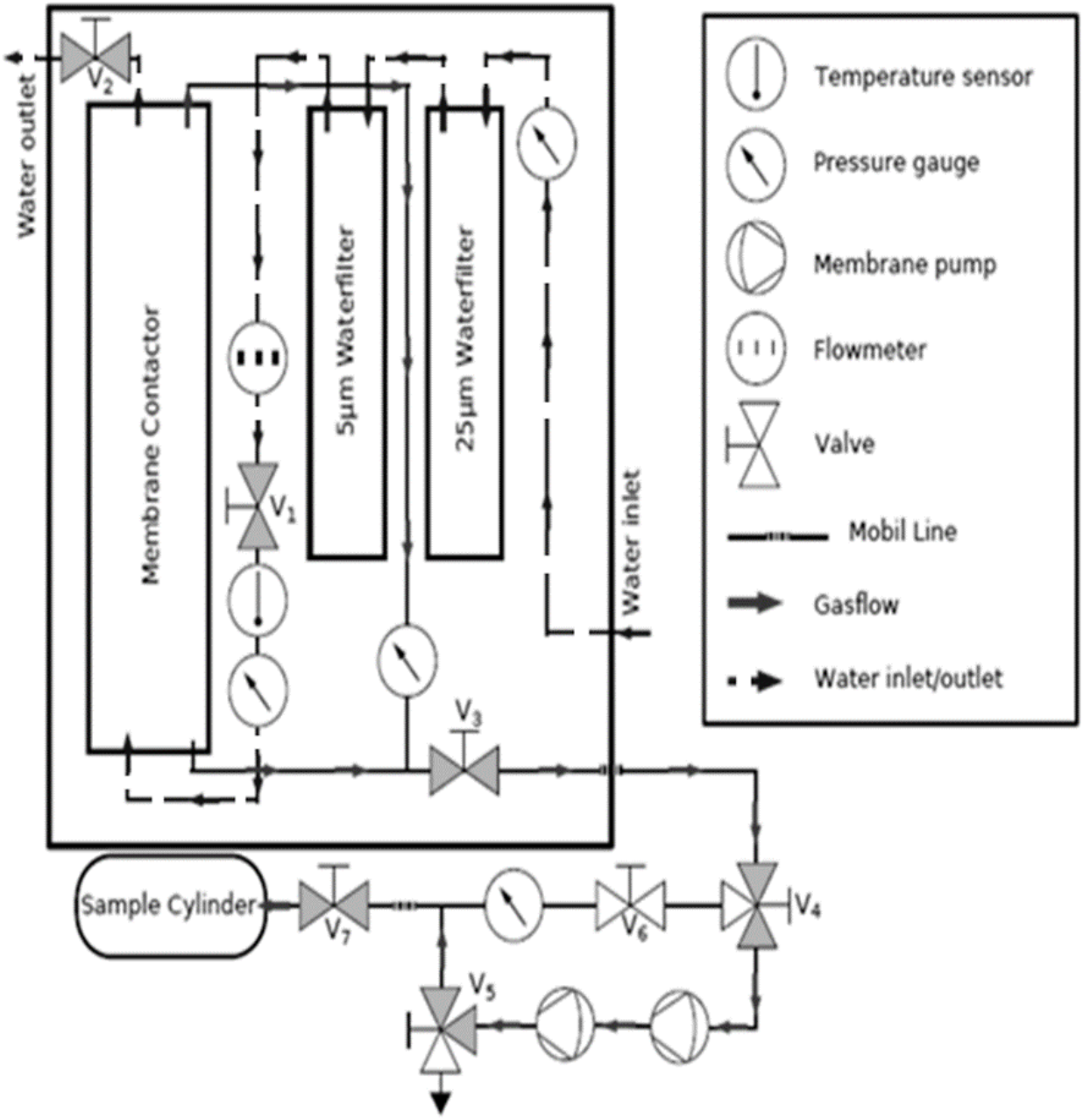

Figure 27. Schematic of dissolved gas sampling apparatus.

Groundwater Sulfur Isotope Sampling and Analysis

Approaches such as the use of sulfur isotopes for distinguishing between anthropogenic and geological sources of SO_4 have been effective in identifying sources of salt in other geochemical

investigations (Szynkiewcz et al., 2011; Miao et al., 2013). SO_4 is a major contributor of salt from both geological sources (e.g. gypsum ($CaSO_4$)) and fertilizers (e.g. H_2SO_4) found in irrigation waters (Szynkiewcz et al., 2011). To supplement aqueous geochemical data, we compared previously collected stable sulfate isotopes ($^{34}S/^{32}S$) of dissolved sulfate collected in 2007 by Szynkiewcz et al. (2011) to $\delta^{34}S$ of gypsum samples collected in this study (Appendix 10). $\delta^{34}S$ for groundwater samples was only collected from wells in the ISC-4, ISC-7, and ISC-1 well clusters by Szynkiewcz et al. (2011; Appendix A Table 7.).

Lithologic and Geophysical Sampling and Analysis

Well Cutting Sampling and Analysis

To evaluate if evaporite minerals were located in close proximity to well screens throughout the Mesilla Valley; seven well cutting samples were selected for XRD analysis of gypsum and halite. Two samples were selected from well cuttings of a central Mesilla Valley borehole (LMV-2), and five samples were selected from well cuttings from a southern Mesilla Valley well (ISC-4B).

To target well cuttings which were likely to test positive for halite and gypsum, individual well cuttings (bags of sediment collected for every ~3 m drilled) were analyzed for Cl, Ca, Na, and SO_4 concentrations. Microwave digestion (U.S. Environmental Protection Agency 3051A, 2007) was used to determine total Ca and Na, and a soil paste extract (Richards, 1954) was used to determine water extractable SO_4 and Cl. Chemical analysis was completed for each well cutting between 15.2 m and 55 m below the surface in ISC-4B and every well cutting between 27 m and 80 m below the surface for the LMV-2 borehole. Well cuttings from LMV-2 and ISC-4B were selected because of water elevation maps and well drilling logs (Nickerson et al. 2006; Tetra Tech, 2004)

indicating that the well cuttings selected were generally located along the same flow path in the Middle Santa Fe group (Hawley and Kennedy, 2004; Teeple, 2017).

Analysis for total Ca and Na was completed using a Perk Elmer Optima 4300 DV (Dual View) ICP-OES (Inductively Coupled Plasma- Optical Emission Spectrometer). Analysis for chloride concentration was completed on the Technicon AutoAnalyzer (Technicon Industrial Systems Tarrytown, NY USA). Analysis for SO_4 was completed using the Spec 20 Spectrophotometer (Thermo Spectronic Rochester, NY, USA).

Well cuttings that had total salinity concentrations ($Cl+Na+SO_4+Na$) greater than the 3rd quartile (75%) of all the samples were selected for XRD analysis. For ISC-4B the cuttings were 33.53 m to 36.58 m, 36.58 m to 39.62 m, 45.72 m to 48.77 m, and 48.77 m to 51.82 m below land surface elevation. For LMV-2 the cuttings were 57.91 m to 60.96 m, and 60.96 m to 64 m below land surface elevation.

For XRD analysis, samples were ground into a fine powder (similar to talcum powder) using a mortar and pestle and mounted into a silicon zero-background holder. Scans were conducted with step wise increases of 0.017°were between 6°and 69° 2θ positions on a Pananalytical X'Pert Pro X-Ray Diffraction diffractometer. Peak intensity and position were compared with diffractograms of gypsum and halite, the main constituents of evaporite deposits. The minimum detection for gypsum and halite was 2 percent by volume within the sample.

Temperature Log Sampling and Analysis

Temperature logs of unscreened or perforated wells can be used to determine the vertical rate of groundwater flow (Bredehoeft and Papadopulos, 1965; Haenel, 1988; Reiter, 2001; Reiter, 2005). The heat flow in the crust is usually low, thus a vertically flowing groundwater component may systematically change the conductive temperature gradient via convective heat

transport (Bredehoeft and Papadopulos, 1965). These changes in the natural temperature gradient can be observed and quantified to determine vertical groundwater flow component as upflow (discharge) or as downflow (recharge) and the vertical component of velocity (Fig. 28).

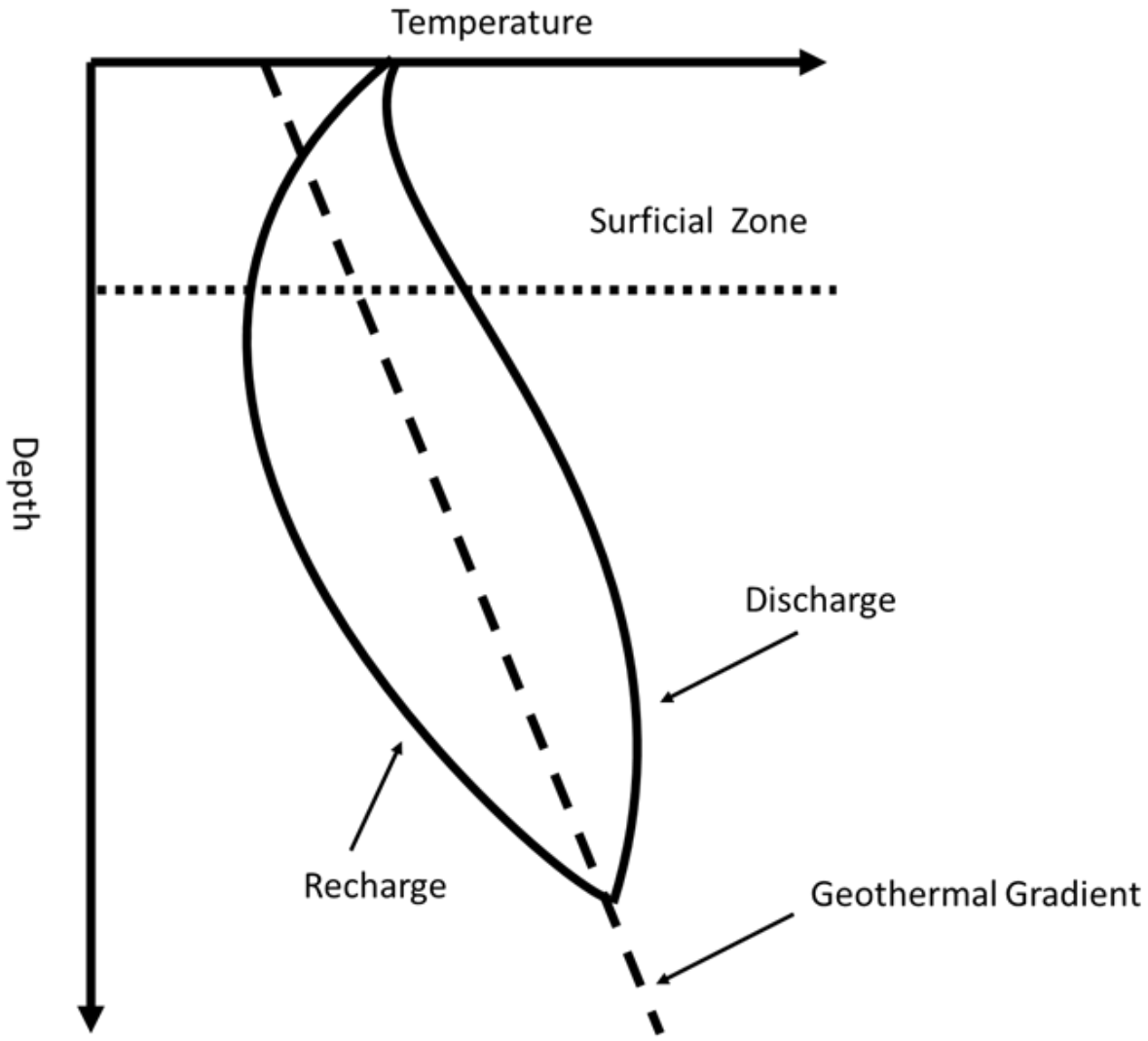

Figure 28. Temperature log schematic adapted from Anderson (2005).

In March 2018, eight temperature profiles were measured from the deepest well within the various well clusters and also ISC-2A (Fig. 1). Temperature profiles were measured by lowering a thermistor to the bottom of each well. A digital multimeter and a computer were

used to record resistance every meter at a 2 meters/minute rate. Resistance was then converted to temperature using a laboratory calibration derived from a platinum thermistor (Kelley et al., 2016). All wells were capped and cased and had not been pumped for at least two months prior to sampling.

Gypsum Mineral Sulfur Isotope Sampling and Analysis

To constrain geologic endmembers of groundwater $\delta^{34}S$, $\delta^{34}S$ of gypsum was analyzed from various rock formations in southern New Mexico. Gypsum samples were collected from an outcrop of the Mesilla Valley formation at Cerro De Cristo Rey, a roadcut of the Rincon Valley formation near Rincon, NM and Lake Lucero of White Sands, NM (Appendix A Table 10.). Gypsum samples were ground to a fine powder using a mortar and pestle and then poured into 250 mL – 450 mL of deionized water to dissolve. Solutions were stirred on low heat for five hours and then decanted into 1L HPDE bottles. Once prepared solutions were filtered and precipitated into ~1 g samples of $BaSO_4$ using methods outlined in Szynkiewicz et al. (2011; Table 1). Analysis for $\delta^{34}S$ was completed using methods outlined in Kelly et al. (2018) at Isotech Laboratories.

Data Analysis

Isometric Log Ratio Analysis

Conservative ions such as Cl, Br, B, and Li are highly soluble, biologically inert, and do not easily absorb onto clays (Clark and Fritz, 1997). For these reasons, Cl, Br, and Na ratios are common diagnostic tools for determining sources of salinity in sedimentary basins (Clark and Fritz, 1997). Common geological sources of solutes include: gypsum dissolution ($CaSO_4$:$2H_2O$), halite dissolution (NaCl), and weathering of feldspars and amphiboles (contribute Na, K, Ca, Mg and SiO_2; Witcher et al., 2004). If Ca concentrations in groundwater increase significantly enough,

calcite ($CaCO_3$) will precipitate, and buffer Ca concentrations in groundwater (Witcher et al., 2004).

Despite the widespread use of elemental concentration plots (Cl:Br) and elemental ratio plots (Cl/Br:Na/Br), these comparisons have been shown to result in spurious mathematical relationships (Engle and Rowan, 2012). Issue arises from the lack of independence between variables. For example, increasing the chloride concentration in groundwater will increase the solubility of other ions resulting in mixing relationships which may not exist; issues such as this are exacerbated in high salinity waters (Engle and Rowan, 2012; Engle et al., 2016). Engle and Rowan (2012) suggest adjusting molar concentration data using isometric log ratios, which lack the numerical issues associated with traditional methods.

In isometric log ratio plots concentrations are equally weighed within a coordinate system. For example, when plotting Na/Cl on an X axis using an isometric log ratio, a 1:1 ratio of Na/Cl would plot at zero. A Na/Cl ratio greater than one would plot positively and a Na/Cl ratio less than one would plot negatively, each direction in the coordinate is equally weighed. This allows for a better understanding of the balance between ions. For comparison, an elemental ratio plot of Na/Cl on an X axis has the following properties: an even ratio of Na/Cl is equal to 1, Na/Cl ratios greater than one are given an infinite amount of space to occupy, but Na/Cl ratios less than one 1 can only occupy space on the X coordinate between 1 and zero. The skew of the elemental concentration ratio grid can easily result in misinterpretation of data (Engle and Rowan, 2012).

Isometric log ratio balances were developed using sequential binary partitions. Sequential binary partitions are series of non-overlapping groups of parts (Engle, 2016). Once concentrations are converted into isometric log ratios, they can be interpreted in standard

Euclidean geometry (Engle et al., 2016). Previously reported balances were used to interpret halite (NaCl) dissolution and gypsum ($CaSO_4$) dissolution in high salinity groundwaters (Engle and Rowan, 2012; Engle et al., 2016).

Geochemical Modeling Analysis and Mapping

The geochemical software PHREEQC version 3.3.12 (Parkhurst and Appelo, 2013) was used to calculate saturation indices for selected mineral which is relative comparison to the thermodynamic dissolve precipitation equilibrium between water solutions and solid minerals. A positive saturation index indicates oversaturation which leads to precipitation, a negative value indicates undersaturation which indicates potential for dissolution of a mineral, and a value of zero marks equilibrium between water and a mineral (Parkhurst and Appelo, 2013). Water sample chemistry from all wells was input into the program with common rock forming minerals selected for comparison.

A previously published dataset from Hiebing et al. (2018) was used to create a total dissolved solids contour map using the program *Surfer® 14 from Golden Software, LLC (www.goldensoftware.com)*. Kriging was used to contour maximum TDS for each point location. Faults and dikes reported in Sweetkind (2017) were overlaid onto the map using the program QGIS (QGIS, 2015).

Corrections for ^{14}C ages of groundwater are often necessary (Clark and Fritz, 1997). Processes which can affect ^{14}C ages include calcite dissolution, dolomite dissolution, exchange with the aquifer matrix, oxidation of organics, and diffusion of ^{14}C into the aquifer matrix (Clark and Fritz, 1997). $\delta^{13}C$ has been shown to be an effective tracer for determining how open or closed a system is along a groundwater flow path (Clark and Fritz, 1997). When a system is open, exchange with the atmosphere occurs, resulting in young ^{14}C ages and $\delta^{13}C$ comparable to soil

CO_2. When a system is closed ^{14}C ages will be older and the degree of carbonate dissolution may be determined by how closely groundwater $\delta^{13}C$ signatures resemble carbonates in the subsurface and the molality of dissolved carbonate species in groundwater. To correct for carbonate dissolution, the predominant cause of shifted ^{14}C ages in most aquifers, a revised Fontes and Garnier model was used (Clark and Fritz, 1997; Han and Plummer, 2013). This simplified model requires inputs for $\delta^{13}C$ of both soil and carbonates in the subsurface. Input parameter for soil CO_2 were -20 $\delta^{13}C$ and -2.73 $\delta^{13}C$ for calcite/carbonates; these values were based off $\delta^{13}C$ values reported by Witcher et al. (2004) of southern New Mexico calcite/carbonate (-2.2 to -5.5) and organic carbon (-15.7 to -25). The assigned pMc (percent modern carbon) of soil CO_2 was 100 and 0 for calcite/carbonate; these values are standardly used to represent the transition between an open and closed system in most aquifers (Han and Plummer, 2013). Required inputs for estimating the corrected ^{14}C age of a groundwater sample are molality of carbonate species, observed ^{14}C concentration, $\delta^{13}C$ signature, and temperature. Model corrections were only applied to groundwaters with an initial concentration of less than 50 pMC; groundwaters with concentrations less than 50 pMC are assumed to exist in a closed system where $\delta^{13}C$ signatures of groundwater are dictated solely by reactions between calcite and soil CO_2 (Han and Plummer, 2013). Additionally, corrections of groundwater in the unsaturated zone would likely be inaccurate due to influences from surface caliche layers which are enriched in $\delta^{13}C$ (-0.6 to -11; Witcher et al., 2004). The revised Fontes and Garnier model has been used in other southwestern basins with success (Hagedorn, 2015).

9.0 References

Anderholm, S.K., 1992, Water quality and geochemistry of the Mesilla Basin, in Frenzel, P.F., and Kaehler, C.A., 1992, Geohydrology and simulation of ground-water flow in the Mesilla Basin, Doña Ana County, New Mexico and El Paso County, Texas: U.S. Geological Survey Professional Paper 1407–C, p. 64-73.

Anderson, M.P., Heat as a groundwater tracer: Groundwater, v. 43, no. 6, p. 951-968.

Bredehoeft, J.D., and Papadopulos, I.S., 1965, Rates of vertical groundwater movement estimated from the earth's thermal profile: Water Resources Research, v. 1, p. 325–328.

CH2MHill, 2013, Distal Mesilla conceptual site model prepared for the United States Army Corps of Engineers:Techical Report, 224 p.

Chen, C., Li, Y., Bailey, K., O'Connor, T., Young, L., and Lu, Z.-T., 1999, Ultrasensitive isotope trace analyses with a magneto-optical trap: Science, v. 286, no. 5442, p. 1139-1141.

Clark, I.D., and Fritz, Peter, 1997, Environmental Isotopes in Hydrogeology: Boca Raton, Fla., Lewis Publishers, 328 p.

Craig, Harmon, 1961, Isotopic variations in meteoric waters: Science, v. 133, p. 1702–1703.

Culbert, R., and Leighton, D., 1988, Young uranium: Ore Geology Reviews, v. 3, no. 1-3, p. 313-330.

Davis, S.N., Whittemore, D.O., and Fabryka-Martin, 1998, Uses of chloride/bromide ratios in studies of potable water: Groundwater v. 36, no. 2, p. 338–350.

Donahue, D.J., Linick, T.W., and Jull, A.J.T., 1990, Isotope ratio and background corrections for accelerator mass spectrometry radiocarbon measurements: Radiocarbon, v. 32, book 2, p. 135–142.

Doremus, Dale, and Michelsen, A.M., 2008, Rio Grande salinity management—First steps towards interstate solutions, in proceedings of the 53rd Annual NewMexico Surface Water Conference, Suface Water Opportunities in New Mexico, New Mexico Water Resources Research Institute, 8 p.

Du, X., Purtschert, R., Bailey, K., Lehmann, R., Lorenzo, R., Lu, Z.T., Mueller, P., O'conner, T.P., Sturchio, N.C., Young, L., 2003, A new method of measuring 81Kr and 85Kr abundances in environmental samples: Geophysical Research Letters, v. 30, 20 p.

Engle, M.A., and Rowan, E.L., 2012, Interpretation of Na–Cl–Br systematics in sedimentary basin brines: comparison of concentration, element ratio, and isometric log-ratio approaches: Mathematical Geosciences, v. 45, no. 1, p. 87-101.

Engle, M.A., Reyes, F.R., Varonka, M.S., Orem, W.H., Ma, L., Ianno, A.J., Schell, T.M., Xu, P., and Carroll, K.C., 2016, Geochemistry of formation waters from the Wolfcamp and "Cline" shales: Insights into brine origin, reservoir connectivity, and fluid flow in the Permian Basin, USA: Chemical Geology, v. 425, p. 76-92.

Faure, Gunter, 1986, Principles of Isotope Geology: New York, Wiley, 589 p.

Fishman, M.J., 1993, Methods of analysis by the U.S. Geological Survey National Water Quality Laboratory— Determination of inorganic and organic constituents in water and fluvial sediments: U.S. Geological Survey Open-File Report 93–125, 217 p.

Fishman, M.J., and Friedman, L.C., 1989, Methods for determination of inorganic substances in water and fluvial sediments: U.S. Geological Survey Techniques of Water-Resources Investigations, book 5, chap. A1, 545 p.

Frenzel, P.F., and Kaehler, C.A., 1992, Geohydrology and simulation of ground water flow in the Mesilla Basin, Doña Ana County, New Mexico and El Paso County, Texas: U.S. Geological Survey Professional Paper 1407–C, 114 p.

Garbarino, J.R., 1999, Methods of analysis by the U.S. Geological Survey National Water Quality Laboratory— Determination of dissolved arsenic, boron, lithium, selenium, strontium, thallium, and vanadium using inductivelycoupled plasma-mass spectrometry: U.S. Geological Survey Open-File Report 99–093, 31 p.

Garbarino, J.R., Kanagy, L.K., and Cree, M.E., 2006, Determination of elements in natural-water, biota, sediment and soil samples using collision/reaction cell inductively coupled plasma-mass spectrometry: U.S. Geological Survey Techniques and Methods, book 5, sec. B, chap. 1, 88 p.

Gu, A., 2005, Stable isotope geochemistry of sulfate in groundwater of southern Arizona: Implications for groundwater flow, sulfate sources, and environmental significance: Tuscon, Arizona, University of Arizona, PhD Dissertation, 256 p.

Haenel, R., Rybach, L., and Stegena, L., 1988, Fundamentals of Geothermics, Handbook of Terrestrial Heat-Flow Density Determination: Springer, p. 9-57.

Hagedorn, B., 2015, Hydrochemical and ^{14}C constraints on groundwater recharge and interbasin flow in an arid watershed: Tule Desert, Nevada: Journal of Hydrology, v. 523, p. 297-308.

Han, L.-F., and Plummer, L.N., 2013, Revision of Fontes & Garnier's model for the initial ^{14}C content of dissolved inorganic carbon used in groundwater dating: Chemical Geology, v. 351, p. 105-114.

Hawley, J.W., Kennedy, J.F., and Creel, B.J., 2001, The Mesilla basin aquifer system of New Mexico, west Texas and Chihuahua—An overview of its hydrogeologic framework and related aspects of groundwater flow and chemistry, in Mace, R.E., and Angle, E.S., Aquifers of West Texas: Texas Water Development Board Report 356, chap. 7, p. 76–99.

Hawley, J.W., and Kennedy, J.F., 2004, Creation of a digital hydrogeologic framework model of the Mesilla Basin and southern Jornada del Muerto Basin: Las Cruces, New Mexico Water Resources Research Institute, New Mexico State University, WRRI Technical Completion Report no. 332, 105 p.

Hawley, J.W., and Lozinsky, R.P., 1992, Hydrogeologic framework of the Mesilla Basin in New Mexico and western Texas: New Mexico Bureau of Mines and Mineral Resources Open File Report 323, 55 p.

Hawley, J.W., 1984, Hydrologic cross sections of the Mesilla Bolson area, Doña Ana County, New Mexico, and El Paso County, Texas: Socorro, New Mexico Bureau of Mines and Mineral Resources Open-File Report v. 190, p. 8.

Hawley, J.W., Swanson, B.H., Walker, J.S., Glaze, S.H., 2018, Hydrogeologic framework of the Mesilla Basin region of New Mexico, Texas, And Chihuahua (Mexico)- Advances in conceptual and digital model development: New Mexico Water Resources Research Institute Report 363, Technical Completion Report (draft), p. 162.

Hiebing, M., Doser, D.I., Avila, V.M., and Ma, L., 2018, Geophysical studies of fault and bedrock control on groundwater geochemistry within the southern Mesilla Basin, western Texas and southern New Mexico: Geosphere, v. 14, no. 4, p. 1912-1934.

Hill, C.A., 2000, Overview of the geologic history of cave development in the Guadalupe Mountains, New Mexico: Journal of Cave and Karst Studies, v. 62, no. 2, p. 60-71.

Hogan, J.F., Phillips, F.M., Mills, S.K., Hendrickx, J.M.H., Ruiz, Joaquin, Chelsey, J.T., and Asmerom, Yamane, 2007, Geologic origins of salinization in a semi arid river—The role of sedimentary basin brines: Geology, v. 35, p. 1063-1066.

Hunt, A.G., 2015. US Geological Survey Noble Gas Laboratory's standard operating procedures for the measurement of dissolved gas in water samples Book 5, Laboratory Analysis: US Geological Survey, 21 p.

International Atomic Energy Agency, 2013, Isotopes Methods For Dating Old Groundwater: Guidebook, Vienna, 357 p.

International Boundary and Water Commission, 2011, Hydrogeological activities in the Conejos- Medanos/ Mesilla Basin Aquifer, Chihuahua Phase I: New Mexico Water Resources Research Institute, Transboundary Assessment Program Report p. 104.

Jiang, W., Bailey, K., Lu, Z.-T., Mueller, P., O'Connor, T., Cheng, C.-F., Hu, S.-M., Purtschert, R., Sturchio, N., and Sun, Y., 2012, An atom counter for measuring ^{81}Kr and ^{85}Kr in environmental samples: Geochimica et Cosmochimica Acta, v. 91, p. 1-6.

Kelley, S., Folsom, M., Keller, S., and Jiracek, G., 2016, Preliminary analysis of complex subsurface temperature variations in the Buckman well field, Santa Fe County, New Mexico, SEG Technical Program Expanded Abstracts 2016: Society of Exploration Geophysicists, p. 4941-4945.

Kelly, W., Panno, S., Hackley, K., Hadley, D., and Mannix, D., 2018, Paleohydrogeology of a Paleozoic sandstone aquifer within an intracratonic basin: Geochemical and structural controls: Journal of Hydrology, v. 565, p. 805-818.

Kendall, Carol, and McDonnell, J.J., 1998, Isotope Tracers In Catchment Hydrology: Elsevier Science B.V., Amsterdam, 839 p.

King, W., and Hawley, J., 1975, Geology and ground-water resources of the Las Cruces area: New Mexico Geological Society 26th Annual Field Conference, p. 195-204.

Kirkland, D.W., 1982, Origin of gypsum deposits in Carlsbad Caverns, New Mexico: New Mexico Geology, v. 4, no. 2, p. 20-21.

Kirkland, D.W., Denison, R.E., and Dean, W.E., 2000, Parent brine of the Castile evaporites (Upper Permian), Texas and New Mexico: Journal of Sedimentary Research, v. 70, p. 749–761.

Kottlowski, F.E., Flower, R.H., Thompson, M.L., Foster, R.W., 1956, Stratigraphic studies of the San Andres Mountains, New Mexico, State Bureau of Mines and Mineral Resources: Memoir 1, New Mexico Institute of Mining and Technology, p. 132.

Land, L., 2016, Overview of Fresh and Brackish Water Quality in New Mexico: New Mexico Bureau of Geology, Open-file Report 583, 49 p.

Larsen, D., Waldron, B., Schoefernacker, S., Gallo, H., Koban, J., and Bradshaw, E., 2016, Application of environmental tracers in the memphis aquifer and implication for sustainability of groundwater resources in the Memphis metropolitan area, Tennessee: Journal of Contemporary Water Research & Education, v. 159, no. 1, p. 78-104.

Lee, W.T., 1907, Water Resources of the Rio Grande Valley in New Mexico, United States Geological Survey: Water Supply Paper 188, 59 p.

Loosli, H., 1983, A dating method with ^{39}Ar: Earth and Planetary Science Letters, v. 63, no. 1, p. 51-62.

Loosli, H.H, Lehmann, B.E, and Däppen, G., 1991, 4. Dating by Radionuclides, Applied Isotope Hydrology, A case study in Northern Switzerland: Studies In Environmental Science, v. 43, Elsevier, Amsterdam, p. 153-174.

Lovejoy, E.M.P, 1976, Geology of Cerro de Cristo Rey Uplift, Chihuahua and New Mexico: New Mexico Bureau of Mines & Mineral Resources Memoir 31, 84 p.

Lucas, S.G., Krainer, K., Spielmann, J.A., and Durney, K., 2010, Cretaceous stratigraphy, paleontology, petrography, depositional environments, and cycle stratigraphy at Cerro de Cristo Rey, Doña Ana County, New Mexico: New Mexico Geology, v. 32, no. 4, p. 103-130.

Mace, E., Aalseth, C., Brandenberger, J., Day, A., Hoppe, E., Humble, P., Keillor, M., Kulongoski, J., Overman, C., and Panisko, M., 2017, Methods for using argon-39 to age-date groundwater using ultra-low-background proportional counting: Applied Radiation and Isotopes, v. 126, p. 9-12.

Medville, D.M., 2018, Speleogenesis of caves in a Cretaceous shale: Bighorn Basin, Wyoming: Journal of Cave and Karst Studies, v. 80, no. 2, p. 66-80.

Mei, D.-M., Yin, Z.-B., Spaans, J., Koppang, M., Hime, A., Keller, C., & Gehman, V. (2010). Prediction of underground argon content for dark matter experiments: Physical Review C, v. 81, 7 p.

Miao, Z., 2013, Application of stable isotopes and geochemical analysis to characterize sulfate, nitrate, and trace element contamination of groundwater and its remediation at a former uranium mining site: Tucson, University of Arizona, M.S. thesis, 168 p.

Moyer, D.L., Anderholm, S.K., Hogan, J.F., Phillips, F.M., Hibbs, B.J., Witcher, J.C., Matherne, A.M., and Falk, S.E., 2013, Knowledge and understanding of dissolved solids in the Rio Grande–San Acacia, New Mexico, to Fort Quitman, Texas, and plan for future studies and monitoring: U.S. Geological Survey Open-File Report 2013–1190, 55 p.

Nickerson, E.L., 2006, Description of piezometers and ground-water-quality characteristics at three new sites in the lower Mesilla Valley, Texas, and New Mexico: United States Geological Survey Scientific Investigations Report 2005-5248, 27 p.

Nickerson, E.L., 1986, Selected geohydrologic data for the Mesilla basin, Doña Ana County, New Mexico and El Paso County, Texas: U.S. Geological Survey Open-File Report 86–75, 59 p.

Nickerson, E.L., and Myers, R.G., 1993, Geohydrology of the Mesilla ground-water basin, Doña Ana County, New Mexico, and El Paso County, Texas: U.S. Geological Survey Water-Resources Investigations Report 92–4156, 96 p.

Oeschger, H., and Wahlen, M., 1975, Low level counting techniques: Annual Review of Nuclear Science, v. 25, no. 1, p. 423-463.

Östlund, H., Dorsey, H.G., and Rooth, C.G., 1974, GEOSECS North Atlantic radiocarbon and tritium results: Earth and Planetary Science Letters, v. 23, no. 1, p. 69-86.

Östlund, H.G., Rinkel, M.O., and Rooth, C., 1969, Tritium in the equatorial Atlantic current system: Journal of Geophysical Research, v. 74, no. 18, p. 4535-4543.

Parkhurst, D.L, Appelo, C.A.J, 2013, PHREEQC Version 3: A Computer Program for Speciation, Batch-reaction, One dimensional Transport, and Inverse Geochemical Calculations, U.S. Geological Survey, Denver, Colorado.

Phillips, F.M., Hogan, J.F., Mills, S.K., and Hendrickx, J.M.H., 2003, Environmental tracers applied to quantifying causes of salinity in arid-region rivers Preliminary results from the Rio Grande, southwestern USA, in Alsharhan, A.S., and Wood, W.W., eds., Water Resources Perspectives— Evaluation, Management, and Policy: Amsterdam, Elsevier, Developments in Water Science, v. 50, p. 327–334.

Piper, A.M., 1944, A graphic procedure in the geochemical interpretation of water analyses: Transactions, American Geophysical Union, v. 25, p. 914–923.

Plummer, L.N., Bexfield, L.M., Anderholm, S.K., Sanford, W.E., and Busenberg, Eurybiades, 2004, Geochemical characterization of ground-water flow in the Santa Fe Group aquifer system, Middle Rio Grande Basin, New Mexico: U.S. Geological Survey Water Resources Investigation Report 03–4131, 414 p.

QGIS Development Team, 2019, QGIS Geographic Information System: Open Source Geopspatial Foundation. http://qgis.osgeo.org

Reiter, M., 2001, Using precision temperature logs to estimate horizontal and vertical groundwater flow components: Water Resources Research, v. 37, no. 3, p. 663-674.

Reiter, M., 2005, Possible ambiguities in subsurface temperature logs: Consideration of ground-water flow and ground surface temperature change: Pure and Applied Geophysics, v. 162, no. 2, p. 343-355.

Révész, Kinga, and Coplen, T.B., 2008A, Determination of the δ^2H of water: RSIL lab code 1574, chap. C1 of Révész, Kinga, and Coplen, T.B., eds., Methods of the Reston Stable Isotope Laboratory: U.S. Geological Survey Techniques and Methods, book 10, chap. C1, 27 p.

Révész, Kinga, and Coplen, T.B., 2008B, Determination of the $\delta^{18}O$ of water: RSIL lab code 489, chap. C2 of Révész, Kinga, and Coplen, T.B., eds., Methods of the Reston Stable Isotope Laboratory: U.S. Geological Survey Techniques and Methods, book 10, chap. C2, 28 p.

Richards, L.A., ed., 1954, Diagnosis and improvement of saline and alkali soils: U.S. Department of Agriculture, Agriculture Handbook 60, 160 p.

Roberts, M.L., Burton, J.R., Elder, K.L., Longsworth, B.E., McIntyre, C.P., von Renden, K.F., Han, B.X., Rosensheim, B.E., Jenkins, W.J., Galutschek, E., and McNichol, A.P., 2010, A high-performance ^{14}C accelerator mass spectrometry system: Radiocarbon, v. 52, p. 228–235.

Sheng, Z., 2013, Impacts of groundwater pumping and climate variability on groundwater availability in the Rio Grande Basin: Ecosphere, v. 4, no. 1, p. 1-25.

Šrámek, O., Stevens, L., McDonough, W. F., Mukhopadhyay, S., & Peterson, R. J., 2017. Subterranean production of neutrons, 39Ar and 21Ne: Rates and uncertainties. *Geochimica et Cosmochimica Acta*,v. *196*, p.370-387.

Sweetkind, D.S., 2017, Three-dimensional hydrogeologic framework model of the Rio Grande transboundary region of New Mexico and Texas, USA, and northern Chihuahua, Mexico: U.S. Geological Survey Scientific Investigations Report 2017-5060, 49 p.

Szynkiewicz, A., Borrok, D.M., Ganjegunte, G.K., Skrzypek, G., Ma, L., Rearick, M.S., and Perkins, G.B., 2015, Isotopic studies of the Upper and Middle Rio Grande. Part 2—Salt loads and human impacts in south New Mexico and west Texas: Chemical Geology, v. 411, p. 336-350.

Szynkiewicz, A., Ewing, R.C., Moore, C.H., Glamoclija, M., Bustos, D., and Pratt, L.M., 2010, Origin of terrestrial gypsum dunes—Implications for Martian gypsum-rich dunes of Olympia Undae: Geomorphology, v. 121, no. 1-2, p. 69-83.

Szynkiewicz, A., Newton, B.T., Timmons, S.S., and Borrok, D.M., 2012, The sources and budget for dissolved sulfate in a fractured carbonate aquifer, southern Sacramento Mountains, New Mexico, USA: Applied geochemistry, v. 27, no. 8, p. 1451-1462.

Szynkiewicz, A., Witcher, J.C., Modelska, M., Borrok, D.M., and Pratt, L.M., 2011, Anthropogenic sulfate loads in the Rio Grande, New Mexico (USA): Chemical Geology, v. 283, no. 3-4, p. 194-209.

Tetra Tech EM Inc., 2004, Final Report for Well Installation Activities Within the Mesilla Valley Lower Rio Grande Basin: Consultant's report for New Mexico Interstate Stream Commission, 8 p.

Teeple, A.P., 2017, Geophysics- and geochemistry-based assessment of the geochemical characteristics and groundwater-flow system of the U.S. part of the Mesilla Basin/Conejos-Médanos aquifer system in Doña Ana County, New Mexico, and El Paso County, Texas, 2010–12: U.S. Geological Survey Scientific Investigations Report 2017 5028, 183 p.

Tucker, B.J., and Workman, S.M., 2013, Evaluation of Uranium Measurements in Water by Various Methods-13571:Waste Management Symposia, Tempe, AZ, 11 p.

U.S. Geological Survey, variously dated, National field manual for the collection of water-quality data: U.S. Geological Survey Techniques of Water-Resources Investigations, book 9, chaps. A1–A9.

United States Environmental Protection Agency, 2007, Method 3051A Microwave Assisted Acid Digestion of Sediments, Sludges, Soils, and Oils, p. 30.

Vogel, J.S., Nelson, D.E., and Southon, J.R., 1987, ^{14}C background levels in an accelerator mass spectrometry system: Radiocarbon, v. 29, book 3, p. 323-333.

Williams, A.J., Crossey, L.J., Karlstrom, K.E., Newell, D., Person, M., and Woolsey, E., 2013, Hydrogeochemistry of the Middle Rio Grande aquifer system—Fluid mixing and salinization of the Rio Grande due to fault inputs: Chemical Geology, v. 351, p. 281-298.

Williams, R.T., Goodwin, L.B., Mozley, P.S., Beard, B.L., and Johnson, C.M., 2015, Tectonic controls on fault zone flow pathways in the Rio Grande rift, New Mexico, USA: Geology, v. 43, no. 8, p. 723-726.

Wilson, C.A., White, R.R., Orr, B.R., and Roybal, R.G., 1981, Water resources of the Rincon and Mesilla Valleys and adjacent areas: New Mexico State Engineer Technical Report 43, 514 p.

Witcher, J.C., King, J.P., Hawley, J.W., Kennedy, J.F., Williams, J., Cleary, M., and Bothern, L.R., 2004, Sources of salinity in the Rio Grande and Mesilla Basin groundwater: New Mexico Water Resources Research Institute Technical Completion Report 330, 184 p.

Yokochi, R., Sturchio, N., Purtschert, R., Jiang, W., Lu, Z.-T., Mueller, P., Yang, G.-M., Kennedy, B., and Kharaka, Y., 2013, Noble gas radionuclides in Yellowstone geothermal gas emissions: A reconnaissance: Chemical Geology, v. 339, p. 43-51.

Zappala, J.C., 2017, Atom Trap Trace Analysis: Developments & Applications: Chicago, IL, The University of Chicago, PhD Dissertation, 173 p.

Zappala, J.C., 2019, Email Correspondance regarding krypton seperation methodology, Argonne National Laboratory.